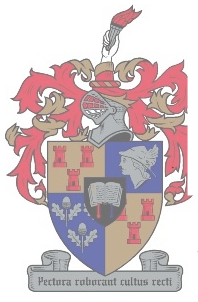

Low Earth Orbit Satellite Propagators

JAF du Plessis

Thesis presented in fulfilment of the requirements for the degree of
Master of Engineering
at the
University of Stellenbosch
Department of Electrical and Electronic Engineering.

Study leader: Prof. J.J. du Plessis

5th December 1999

Declaration

I, the undersigned, hereby declare that the work contained in this thesis is my own, unless stated otherwise, and has not previously been submitted at any university for a degree.

Abstract

The objective of this study was to implement an orbital propagation algorithm, which could be used for the purpose of mission planning and hardware-in-the-loop simulations for the SUNSAT microsatellite. Different propagation algorithms were investigated in order to find one for which the initial conditions for the propagator was freely obtainable and that satisfied the accuracy specification as determined by the onboard activities. The SGP4 analytical algorithm was selected for this purpose.

Along with the propagation of the position of the satellite in its orbit, different models were investigated and implemented for modelling the space environment as the sensors observe it onboard the satellite. A conceptual study was performed on methods to improve the quality of the orbital predictions by the combination of sensor measurements with an orbital propagation algorithm in an extended Kalman filter.

Knowledge was gained and documented in the field of astrodynamics and it was applied in a practical situation during the launch and operation of SUNSAT.

Opsomming

Die doelwit van hierdie studie was die implementering van 'n wentelbaan voorspellings-algoritme wat gebruik kon word vir missie-beplanning en apparatuur-in-die-lus simulasie van die SUNSAT mikrosatelliet. Verskeie voorspellings algoritmes is ondersoek in 'n poging om 'n algoritme te vind waarvan die begintoestande algemeen beskikbaar is en wat aan die vereistes vir akkuraatheid, soos bepaal deur die aktiwiteite aan boord van die satelliet, voldoen. Die SGP4 analitiese voorspellings-algoritme is gekies vir hierdie doel.

Saam met die voorspelling van die posisie van die satelliet in die wentelbaan is verskeie modelle wat die ruimte omgewing beskryf soos wat dit deur die sensore waargeneem word, ondersoek en geïmplementeer. 'n Ondersoek in beginsel is ingestel na metodes wat gebruik kan word om die kwaliteit van die wentelbaan-voorspellings te verbeter deur sensor-lesings en 'n voorspellingsalgoritme te kombineer in 'n uitgebreide Kalman-filter.

Kennis is versamel en gedokumenteer in die studieveld van ruimte-dinamika en hierdie kennis is prakties toegepas tydens die lansering en bedryf van SUNSAT.

Acknowledgements

I would like to thank the following people for their contribution to the success of my research:

- My wife, Marelize, for the support, love and patience she had with me for the duration of my research. I really appreciate it.
- Prof. Jan du Plessis who provided me with more than simply intellectual advice. He also showed me what it means to really think and provided me with advice that will last for the rest of my life.
- My parents and family, who are always interested in what I do.
- My heavenly Father, who has shown me what it means to be free and to enjoy every moment of my life.

Contents

List of Symbols viii
List of Acronyms x
List of Figures xii
List of Tables xiii

1 Introduction **1**
1.1 Problem Definition 2
1.1.1 Mission phases 2
1.1.2 Objectives 3
1.1.3 Simulation Software Framework 5
1.2 Overview of chapters 6

2 Performance criteria **9**
2.1 Propagator Accuracy Specification 10
2.2 Internal Sensor Modelling Specifications 11

3 Orbit Propagation **13**
3.1 Modelling Satellite Position 13
3.1.1 Orbital Models 14
3.1.2 Evaluation of Propagation Techniques 22
3.2 Modelling the space environment 25
3.2.1 Modelling the Sun Position 25
3.2.2 Horizon 28
3.2.3 Magnetic Field 29
3.2.4 Terminator 31
3.2.5 Modelling the Stellar Positions 32
3.3 Combining Propagations with Sensors 32
3.3.1 Improvement of Predictions 32
3.3.2 Validation of Sensors 36

4 Simulation Environment for Satellites **37**
4.1 Software Architecture 37
4.2 Software Structure 39
4.2.1 Client Component 40
4.2.2 Server Component 40
4.3 Evaluation 41
4.3.1 Comparison with GPS data 43
4.3.2 Comparison with TLE 45
4.3.3 Comparison with STK 46

5 Conclusions and Recommendations **47**
5.1 Summary of Research 47
5.2 The future 49
5.3 Conclusion 50

A Spacecraft Systems Overview **56**
A.1 ADCS 56
A.1.1 Star Sensors 56
A.1.2 Two-Axis Horizon Sensor 57
A.1.3 Sun Sensors 57
A.1.4 Reaction Wheels 58
A.1.5 Magneto Torque Coil 58
A.1.6 Three-Axis Fluxgate Magnetometer 58
A.1.7 Tip Mass and Boom 58
A.2 Communications Subsystem 58
A.3 Telecommand (TCMD) 59
A.4 TLMS 60
A.5 OBC's 60
A.6 SPS 60
A.7 Payloads 60
A.7.1 Pushbroom Imager 60
A.7.2 GPS 61
A.7.3 Amateur Packet Radio Services 61
A.7.4 School Experiments 61

B Reference systems **63**
B.1 Coordinate Systems 63
B.1.1 Earth Centred Inertial (ECI) 64
B.1.2 ECEF Coordinate System 67
B.1.3 Perifocal Coordinate System, PQW 68
B.1.4 Topocentric Horizon Coordinate System, SEZ 69

B.2 Time 70
B.2.1 Precession and Nutation 71
B.2.2 Solar Time 73
B.2.3 Sidereal Time 75
B.2.4 Dynamical and Atomical Time 76
B.3 Coordinate Transformations 76
B.3.1 Classical Orbital elements to ECI 76
B.3.2 ECI to Classical Orbital Elements 79
B.3.3 ECI and ECEF 81
B.3.4 ECEF, Geocentric and Geodetic Coordinates 81
B.3.5 ECI and SEZ 84
B.3.6 ECI Rectangular and ECI Spherical 85

C Orbital mechanics **87**
C.1 Historical background 87
C.2 Orbital motion 88
C.2.1 Basic parameters 88
C.2.2 Two-body motion 90
C.2.3 Satellite orbital state representation 95

D Orbital perturbations **103**
D.1 Introduction to Perturbations 104
D.1.1 Earth's Oblateness 106
D.1.2 Aerodynamic Drag 109
D.1.3 Third-Body Attractions 111
D.1.4 Solar Radiation Pressure 112
D.2 Mathematical Foundations of Perturbations 113
D.2.1 General Perturbations 114
D.2.2 Special Perturbations 125

E IGRF Magnetic Field Modelling **129**

F The SGP4 model **132**
F.1 The SGP4 model 132
F.2 Users guide, constants and symbols 137

G Orbital elements in practice **140**
G.1 Orbital element formats 140
G.2 Explanation of Two-line Elements 142
G.3 Initial conditions of Orbital Elements 144

List of Symbols

ϵ	Obliquity of the ecliptic
Υ	The direction of the vernal equinox
α	Right ascension
δ	Declination
$\vec{r}$	Position vector
r	Radial distance / magnitude of position vector
$\vec{v}$	Velocity vector
v	Magnitude of velocity vector
V	Inertial speed
ϕ_{fpa}	Flight-path angle
Az	Azimuth angle
ϕ'	Geocentric latitude
ϕ	Geodetic latitude
λ	Longitude
ρ	Radial distance / Atmospheric density
h	Geodetic height
$\Delta\psi$	Nutation in longitude
$\Delta\epsilon$	Nutation in Obliquity
ϵ_0	Mean obliquity of the ecliptic
θ_{MST}	Mean Sidereal Time
θ_{AST}	Apparent Sidereal Time
θ_{GST}	Apparent Sidereal Time at the Greenwich meridian
$\vec{h}$	Angular momentum vector
$\vec{e}$	Eccentricity vector
a	Semimajor axis
b	Semiminor axis
e	Eccentricity
G	Gravitational constant
μ	Gravitational parameter of the Earth
p	semi-parameter / semilatus rectum
P	Period of orbital motion

n	Mean motion
i	Inclination
Ω	Right ascension of the ascending node
ω	Argument of perigee
ν	True anomaly
M	Mean anomaly
E	Eccentric anomaly
t	Time
$\vec{a}_p$	Perturbative accelerations
R	Disturbing function
U	Potential function
J_{nm}	Gravitational harmonic coefficients
P_n	Legendre functions
a_e	Mean equatorial radius of the Earth
$\vec{B}$	Magnetic field vector

List of Acronyms

ADCS	Attitude Determination and Control System
AMSAT	The Radio Amateur Satellite Corporation
AU	Astronomical Units
CCD	Charge Coupled Device
DSST	Draper Semianalytical Satellite Theory
ECI	Earth Centered Inertial coordinate system
ECEF	Earth Centered Earth Fixed coordinate system
EKF	Extended Kalman Filter
GEM	Goddard Earth Model
GPS	Global Positioning System
GUI	Graphical Users Interface
HIL	Hardware-in-the-loop
IGRF	International Geomagnetic Reference Field
JD	Julian days
JGM	Joint Gravitational Model
JPL	Jet Propulsion Laboratory
LEO	Low Earth Orbit
NASA	National Aeronautics and Space Administration
NORAD	North American Aerospace Defense Command
PQW	Perifocal coordinate system
SEZ	Topocentric horizon coordinate system
SGP	Simplified General Perturbations
SUNSAT	Stellenbosch University Satellite
T	Julian centuries
TCP/IP	Transmission Control Protocol/Internet Protocol
TLE	Two-line Element
UTC	Coordinated Universal Time
VOP	Variation of Parameters
WGS	World Geodetic Survey

List of Figures

1.1 Block diagram representation of the framework within which the study was performed. 4
1.2 Block diagram representation indicating the connection between the orbit propagator, environmental models and the HIL simulation. 6

3.1 Propagator accuracy for satellites in low Earth orbit. 23

4.1 The initial architecture considered for distributing the orbital data. 38
4.2 The client-server architecture which was implemented for distributing the orbital data. 38
4.3 The functional layout of the client component software. 41
4.4 The functional layout of the propagator thread. 42
4.5 The functional layout of the server component software. 43
4.6 A comparison between the predicted position of the satellite with a SGP4 propagator and GPS measurements. 44
4.7 A comparison between the SGP4-predicted position of the satellite and the position predicted with new TLE's. 45
4.8 A comparison between the SGP4-predicted position of the satellite and STK predictions. 46

A.1 SUNSAT Satellite - Configuration before boom deployment . . 57

B.1 The Cartesian ECI coordinate system. 65
B.2 The spherical ECI coordinate system. 66
B.3 The difference between the geodetic and geocentric coordinate systems. 68
B.4 The perifocal (PQW) coordinate system. 69
B.5 The topocentric horizon coordinate system. 70
B.6 Precession and nutation of the Earth's rotational axis. 71
B.7 The measurement of Solar and Sidereal time. 74

B.8 The position and velocity vectors in the perifocal coordinate system. 77
B.9 The relationship between the ECI and the PQW coordinate systems. 78
B.10 The relationship between the ECI and the ECEF coordinate systems. 82

C.1 The most important properties of elliptical orbits. 89
C.2 The classical orbital elements. 97
C.3 The relationship between the true anomaly and the eccentric anomaly. 99

D.1 The effect of perturbative forces on the orbital elements of a satellite. 105
D.2 Nodal regression. 107
D.3 Apsidal rotation. 108
D.4 The decay of an orbit under the influence of drag. 109

List of Tables

3.1 Error in the prediction of the position of the Sun. 28
3.2 A summary of sensors used to improve the accuracy of the orbital predictions. 33

D.1 Two examples of real orbital data for SUNSAT. 108

G.1 An examples of a TLE-file for SUNSAT. 142
G.2 The format of the second line of data in the two-line element file. 143
G.3 The format of the third line of data in the two-line element file. 144

Chapter 1

Introduction

The advent of the space age in the latter part of the twentieth century has seen the evolution of a number of new fields of research. One of these fields consisted of the determination of the orbit and the prediction of the position of a satellite at some moment in the future by using knowledge of the orbit. Initially methods used to predict the future position of satellites was borrowed form the astronomical community, which used these methods to predict the position of the celestial bodies. The flaws in the astronomical methods applied to satellite orbit predictions soon became evident. Perturbative forces, which are unique to satellite orbits, caused major deviations from predictions made with the existing methods. Along with the propagation algorithms, orbit determination algorithms were required which could be used to find the initial positions of satellites for use in the prediction algorithms. The shortcomings of the astronomical prediction and orbit determination algorithms necessitated scientists and engineers to develop new prediction algorithms. It was customised for satellites in Earth orbit in that it modelled forces and effects unique to orbits around Earth.

Knowledge of the position and orbit of a spacecraft is required for all missions to outer space. Knowledge of the orbit is required, as the position of the satellite is a function of the shape and orientation of the orbit in space. The position of the satellite at a future moment in time is primarily required to ensure that communication with the satellite is established from a groundstation. This task is only possible during times when the satellite is in view of a groundstation. Other tasks that require knowledge concerning the future position of the satellite are onboard operations such as remote sensing and observation of the Earth and the space environment near the Earth, which need to be planned and scheduled beforehand.

The research presented in this document consisted of an investigation into orbit prediction algorithms to be used for orbit and mission analysis and

planning activities related to the Stellenboch University Satellite (SUNSAT). Low accuracy prediction algorithms were considered sufficient for use during planning and analysis, but high precision predictions were required for the daily operation of the satellite.

SUNSAT was built at the University of Stellenbosch and was launched in February 1999 into a near-circular polar orbit with an altitude ranging from 650 km to 870 km. The primary mission objectives were to successfully test, manage and operate the full payload of the satellite. The high-resolution pushbroom imager can be considered the most important part of the payload. Secondary objectives were the testing of new orientation-control software on the Attitude Determination and Control System (ADCS) hardware, the testing of functional software for implementation on the on-board computers and a variety of experiments involving the amateur radio community. An overview of all the sub-systems on the satellite is provided in appendix A.

1.1 Problem Definition

1.1.1 Mission phases

The lifespan of a satellite is divided into different phases [27]. These phases—usually applicable to satellites in geostationary orbit—include

- pre-launch
- LEOP (Launch and Early Orbit Phase)
- spacecraft commissioning and subsystem calibration
- main mission phase
- EOL (End Of Life)

The pre-launch phase in itself consists of different phases. On the level of the spacecraft, it includes the development of the different subsystems, the testing of the satellite on component level, the integration and environmental testing of the spacecraft and the testing of the complete system as an integrated unit. During this phase the interface between the spacecraft and the launch vehicle have to be provided and the launch and launch-procedures have to be finalised. A preliminary flight operations plan for the initial part of the orbit has to be decided on.

The LEOP phase is very critical in terms of the stability and safety of the satellite. It is very important that the spacecraft is stabilised as soon as

possible after the launch in order to protect delicate sensors from exposure to direct sunlight and ensure that over-heating of one side of the spacecraft does not occur. The major objective of this phase and the commissioning and calibration phase is to establish the spacecraft correctly in its operational configuration and to produce evidence that it is performing according to its predefined requirements.

The main mission phase can begin after it has been verified that the satellite support structure—communication links, ADCS, Onboard Computers (OBC's) and power system—is healthy and able to support the operations of the main payload. This part of the overall mission is in itself divided into separate missions which has to be executed on a day-to-day basis. During this phase of the mission, the activities onboard the satellite and those at the groundstation have to be coordinated in such a way to ensure that every mission objective is met in a time and energy optimal way. Muraoka et al. [105] achieved this objective with an autonomous mission planning scheduler for the Aster satellite.

For SUNSAT, the EOL phase will be initiated when the Nickel-Cadmium batteries which provide the power for the satellite, start to fail. It is expected that this stage of the mission will be reached approximately 4 to 5 years after the launch. During this phase no more missions for the main payload will be scheduled and spacecraft activities will be downscaled to basic telemetry and telecommand. This will continue until the spacecraft is no longer able to support these most basic activities.

1.1.2 Objectives

The research in this document was performed from the point of view presented in the previous section. The groundstation support describing the orbital motion of the satellite was required to ensure the successful execution of the various onboard activities and mission objectives. The last four mission phases depend heavily on accurate predictions of the satellite's position. Onboard operations and communication between the satellite and the groundstation need to be scheduled during the productive part of the mission. During the EOL phase of the mission, the orbital predictions could sometimes be necessary to predict the time of re-entry of the satellite into the atmosphere.

The framework within which this groundstation support was provided can best be explained at the hand of figure 1.1. The top part of this figure describes the motion of an Earth orbiting satellite in its orbit. The orbital motion of a satellite is primarily determined by the equations of motion, but is greatly influenced by various perturbative forces. The combination of these

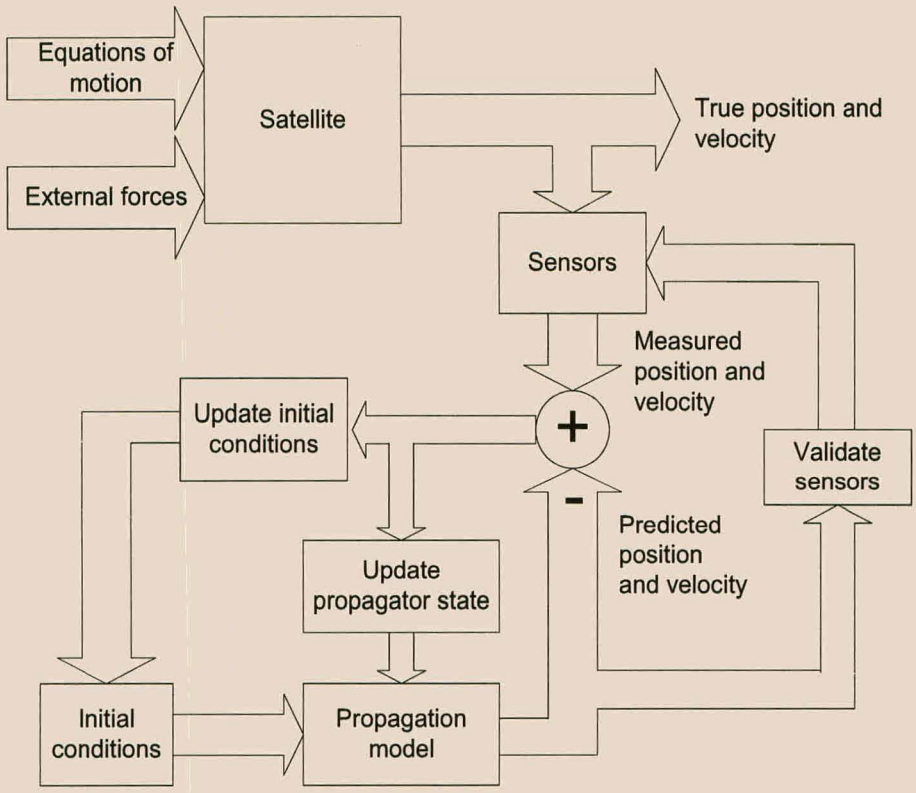

Figure 1.1: Block diagram representation of the framework within which the study was performed.

forces determines the position and velocity of the satellite at a particular moment in time. For some satellites the orbital motion of the satellite can be controlled by using thrusters, but for SUNSAT this was not the case as no thrusting mechanism is available onboard the satellite.

The bottom part of the figure describes the methods which are used to predict the position and velocity of the satellite. The propagation model consists of a mathematical description of the motion of the satellite and the forces influencing it. This model uses initial conditions defined at a particular moment as input to the propagation algorithm. The initial conditions are required as they describe the position and velocity of the satellite for a specific moment—which is known as an epoch—at which the prediction commences. Due to the complexity of describing the exact motion of the satellite, the propagation model can only predict the satellite's position and velocity accurately for a limited period. New initial conditions—defined at a new epoch—are then required. This will again provide an accurate prediction of the satellite's position, provided that the initial conditions are accurate.

The sensors in figure 1.1 can be used to improve the predictions of the propagation model. The sensors can be divided into two groups. The one group consists of sensor-systems that are used to create updated initial condition of the satellite for use in the propagator. These sensors usually are Earth-based. The other group of sensors consists of sensors onboard the satellite that can be used to improve the predicted position and velocity of the satellite.

The predicted position of the satellite is not only useful for activities surrounding the satellite, it is also possible to validate sensors by determining when a particular sensor is able to provide valid data. This could improve the quality of the prediction even more by eliminating the possibility of using invalid data in the propagator. An example of this can be found with the use of the Sun sensors to obtain orientation information of the satellite. These sensors can only provide data concerning the position of the Sun relative to the satellite when the Sun is visible to the satellite. By predicting the times when the satellite would be eclipsed by the Earth, the periods during which valid sensor data are available can be determined.

This study was primarily concerned with the various propagation models used to predict the position of the satellite from a set of initial conditions. A thorough study was performed to gain knowledge of the available propagation models and the ways in which these models are used. Existing algorithms and techniques used in the practical implementation of these algorithms were studied in order to developed a propagation algorithm which could be used for the mission planning onboard SUNSAT and to perform hardware-in-the-loop (HIL) simulations of the ADCS on an engineering model of the satellite. The use of sensors to improve the predictions of the propagation algorithm and methods of orbit determination were only studied in concept and can be considered as the logical next step for an extension of this research.

A block diagram presentation of the connection between the orbit propagator, environmental models and the HIL simulation is presented in figure 1.2). Engelbrecht [15] presents a study of the HIL simulation for SUNSAT.

1.1.3 Simulation Software Framework

As defined above, the developed propagation algorithm were to be used in a HIL simulation of the control system and for mission planning activities. The following framework was specified within which the development of the software, which was used to fulfil these objectives, occurred. It was extracted from the preliminary study conducted by Du Plessis and Engelbrecht [13].

- It was required that the software should to be able to operate in a multi-

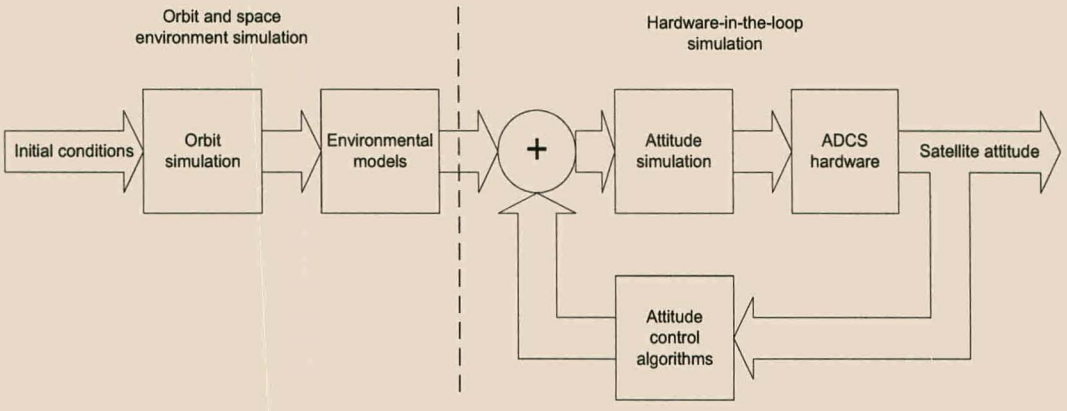

Figure 1.2: Block diagram representation indicating the connection between the orbit propagator, environmental models and the HIL simulation.

computer setup by providing the output data via a network (TCP/IP) connection to user applications.

- The nature and format of the output data had to be representative of the sensor data of the ADCS system of the SUNSAT micro-satellite for it to be used in a HIL simulation.
- The software needed to be modular in order to be transparent to new users. Modularity was required to ease future developments or changes to the source code.
- It had to provide a user-friendly Graphical Users Interface for ease of operation by a new user.

By combining the above stated specifications with the overall objective of the study, it can be seen that the selected software structure and architecture needed to satisfy the immediate requirements of the study while still being well suited to changes and upgrades of the software.

1.2 Overview of chapters

The document is structured so that it can be used effectively by both newcomers to the field of astrodynamics and by persons with a good knowledge of the field. The main part of the document are presented with the assumption that the reader is familiar with the field of research. The appendices present the additional information to supplement the main part. It is recommended

that newcomers should first familiarise themselves with the contents of the appendices before the main part of the document is read.

The main text consists of the following chapters:

- Chapter 2 introduces the guidelines and criteria used in the research performed throughout the rest of this study.
- Chapter 3 constitutes the most important part of this study and consists of a discussion of various propagation and space environmental models and their implementation. Whenever possible, an evaluation of the applicable models is performed. An indication is given as to where the propagation and environmental models would fit into future research.
- Chapter 4 provides an overview of the software environment developed for the implementation of the propagation and environmental models and the accuracy of predictions that was performed by the developed software, is evaluated.
- Chapter 5 consists of a conclusion and recommendations for further research.

As stated above, the appendices consist of information which is supplementary to the research, with some of the appendices explaining subjects which make up an integral part of the field of astrodynamics.

- Appendix A presents a short overview of the SUNSAT microsatellite, the subsystems onboard the satellite and the basic functionality of these subsystems.
- Appendix B consists of a discussion of different coordinate and time systems used throughout the document and presents methods of conversion between the different coordinate systems.
- Appendix C introduces the equations of motion modelling the motion of a satellite in its orbit. Various descriptions of the shape, orientation and size of the orbit and the position of the satellite within the orbit are presented.
- Appendix D describes the perturbative forces influencing the motion of a satellite in its orbit. This appendix consists of two parts. In the first part a general description of perturbations is provided in order to provide the reader with an overview of the effect that perturbations have

on the orbit. The second part of this appendix provides a mathematical description of the perturbative forces for inclusion into propagation algorithms.

- In appendix E the mathematical algorithm of the International Geomagnetic Reference Field (IGRF) for calculating the magnetic field vector is presented.
- Appendix F presents the algorithm for the SGP4 analytical propagation algorithm.
- Appendix G discusses various practicalities involved with the use of orbital elements in propagation algorithms. The different formats in which the elements are presented, an interpretation of the two-line element format and a discussion on initial conditions is provided.

Chapter 2

Performance criteria

In this chapter the criteria is formulated for the development of a kinematic orbit simulation environment[1] for use in the hardware-in-the-loop (HIL) simulation of the ADCS of the SUNSAT satellite and for mission planning activities. The measurement accuracy of the respective sensor subsystems and the hardware environment into which this simulation environment had to be embedded, are investigated in order to formulate the required accuracy and design specifications of the simulation software.

The development of the simulation environment occurred at the hand of the following objectives:

- it had to accurately propagate the position of the satellite in the orbit. This means that an appropriate propagation model[2] to accurately determine the position of the satellite in relation to the space environment as a function of time, was required.
- it had to simulate the measurements made by the ADCS sensors by using accurate models of the space environment.
- The output data of the above mentioned simulations needed to be provided in a number of coordinate systems which corresponded with the measurement systems of the actual sensors.
- the simulated data had to be available to users on other computers.
- the simulation environment was required for mission planning operations.

[1] Refer to De Villiers [12] for previous research on this subject.

[2] The full significance of "an appropriate propagation model "will become clear in chapter 3.

The remainder of this chapter will translate these requirements into practical design-specifications.

The accuracy of the mathematical models used in the simulation was determined by the activities and measurement accuracy of the sensors on board the satellite. As the simulation environment was to be used during actual mission planning operations, the highest possible simulation accuracy was required in order to model the actual position and derive the orientation of the satellite. This section will stipulate the specifications for the mathematical models used to simulate the motion of the satellite and the space environment seen by the internal sensors.

2.1 Propagator Accuracy Specification

The HIL simulation of the ADCS consists of the simulation of all the activities that require the use of the control system. Steyn [33] provides the specifications for the attitude control of the SUNSAT satellite. One of the specifications states that "*the imager boresight position had to be determined better than 1 km close to the sub-satellite point ...*". This specification defines the required accuracy of the propagator that is used to simulate the position of the satellite in the orbit. The prediction accuracy of the sub-satellite point had to be better than the 1 km accuracy needed for the imager. When it is compared to sampling (the spatial equivalent of the Nyquist criteria), the predicted position of the sub-satellite point had to be closer than 0.3 km to its true value to ensure that the specified imager-accuracy is achieved[3]. In theory a modelling accuracy of 0.5 km is necessary for a measurement accuracy of 1 km.

The 0.3 km accuracy can be transformed into an angular specification: when the Earth is taken as a perfect sphere with a diameter of 6378.14 km, it has a circumference of 40075 km. When a great circle of the Earth (the equator) is divided by 360°, the 0.3 km specification is equivalent to an angular accuracy of 0.047 mrad (0.0027°). This means that the simulated position of the satellite has to be within a geocentric angle of approximately 0.05 mrad from the true sub-satellite point.

[3]All subsequent modelling accuracy specifications will be three times more accurate than the measurement accuracy of the sensor.

2.2 Internal Sensor Modelling Specifications

Each one of the ADCS sensors is related to a different aspect of the space environment. The modelling accuracy required for every environment is determined by the measurement accuracy of the sensor that measures the relevant environment. For each one of the following sensors the required modelling accuracy will be specified.

- The 3-axis magnetometer is used to measure the geomagnetic field vector of the Earth. This measured data is filtered through a Kalman filter and the resulting vector is compared to a geomagnetic field model of the Earth to determine the attitude of the satellite. Since the vector can be determined with an accuracy of 1° per axis after Kalman filtering and referred to the geomagnetic field model, the geomagnetic field needed to be modelled to an accuracy of at least 0.3° along all the axis.

- The 2-axis horizon sensor measures the pitch and roll attitude angles to an accuracy of 0.5 mrad (0.029°). The horizon sensors [32] use the position of the Sun and the flattening of the Earth to make a measurement with the position of the satellite as reference. Since these sensors measure the position of the sunlit horizon, the position of the horizon has to be modelled to a higher accuracy than what the sensor can measure. The pixel resolution in these sensors is 0.25 mrad. To ensure that the simulated measurement is as accurate as possible, the modelling of the position of the horizon in terms of the angle between the sub-satellite point and the horizon need to be at least 0.08 mrad accurate.

- The fine Sun sensor has an angular resolution of 2 mrad (0.117°) when it measures the position of the Sun relative to the satellite. This sensor has a narrow slit[4] which is used to focus the sun on a CCD. The slit ensures that the focused image of the Sun on the CCD is a point-source representation of the Sun. This sensor is used to obtain high accuracy yaw orientation data of the satellite. The CCD-type sensors usually has a pixel resolution that is twice the required measuring accuracy obtained from the sensor, which means that it has a pixel resolution of 1 mrad. In order to simulate the measurement of the position of the Sun accurately (the Sun is modelled as a single point source) within the 1 mrad resolution, the position of the Sun need to be modelled more accurate than the sensor pixel resolution. When the three times

[4]Refer to Beuche [6] for a discussion on diffraction.

over-sampling specification is taken into consideration, the position of the Sun needs to be modelled to an accuracy of 0.3 mrad (0.019°).

- The coarse Sun sensors are used to determine rough roll, pitch and yaw attitude information of the satellite. Since these sensors consume almost no power and are very reliable, they were used immediately after launch to determine the unstabilised satellite's attitude relative to the Sun. As the name specifies, these sensors do not have high measurement accuracy. It measures the position of the Sun relative to the satellite with an angular resolution of 5°. Since these sensors have lower measurement accuracy than the fine Sun sensors, the required modelling accuracy for the position of the Sun was determined by the fine Sun sensors and not by these coarse sensors.

- Unlike the other ADCS sensors, the star sensor is a largely independent sub-system that does not supply the ADCS with raw measurements. This sensor interprets the measurements and provides processed orientation data. The star sensor can determine the 3-axis orientation of the satellite with an accuracy of 0.5 mrad (Steyn [33]). The environment that should be simulated when testing this sensor is a complete rotating image of the sky at nighttime. Since this is a complex task, which falls outside the scope of this study, it was not attempted. The other option was to simulate the orientation data that will be supplied to the ADCS by the star sensor. As this would require knowledge about the attitude of the satellite, it was again not attempted.

Chapter 3

Orbit Propagation

This chapter will discuss some of the mathematical models available for modelling the space environment as viewed from a satellite. The models applicable to every aspect of the space environment will be presented and evaluated. SUNSAT and the sensors onboard this particular satellite were used to determine which aspects of the space environment would be modelled.

It is assumed that the reader has some background knowledge on the fundamentals of orbital motion, coordinate systems and transformations between coordinate systems. These topics are covered in the appendices and it is recommended that the reader should be familiar with the contents of the appendices before reading this chapter.

3.1 Modelling Satellite Position

This section will handle the problem of predicting the state (position and velocity) of a satellite in orbit at a given time, t, given the state at some reference time, t_0. The problem which will be addressed here is historically known as ***Kepler's problem*** or simply as ***orbital propagation***. Different solutions to the problem of orbital propagation exist depending on the intended application and the required accuracy of prediction. The simplified case where no perturbations are taken into account in the prediction of the satellite's motion is commonly known as ***Keplerian motion*** and a solution can be obtained via the two-body propagator. It can be extended to include some perturbative effects, but is of limited use due to its short-term accuracy. When the perturbations[1] to the orbit is taken into account, the motion of the satellite is known as ***non-Keplerian motion*** with solutions of a higher

[1]Refer to appendix refOrbitalPerturbations for a discussion of orbital perturbations and the underlying mathematics.

complexity than the basic two-body propagator. The solutions available for this problem can be divided into two categories viz. analytical propagators and numerical propagators.

3.1.1 Orbital Models

Two-body Propagator

The ***two-body propagator*** is the most basic of all propagational algorithms with its main disadvantage being that it does not consider the perturbations. However, because of its simplicity, it is a good starting point for describing the motion of the satellite in its orbit[2], something which is not always easy to grasp when a complex propagational algorithm is used. The two-body propagator is often used for rough calculations and analysis during mission planning phases when high accuracy is not required. Combined with the simplified descriptions for the perturbative forces, it is a useful tool during the mission planning phase or when basic orbital analysis is performed. For the daily operation of the satellite, high accuracy predictions are required to accurately determine the access times of the satellite from the groundstation.

The basic two-body equation of motion was the first method used by Kepler himself to find a solution to what is known today as Kepler's problem. He defined the problem by expressing the position of the satellite in terms of the classical or Keplerian orbital elements as defined in appendix C. The solution starts with the six classical elements a, e, i, ω, Ω and M_0 defined at a particular epoch. The parameter M_0 is often substituted with the true anomaly, ν, or the eccentric anomaly, E. When the assumption is made that no perturbative forces are present, the values of the first five classical elements stay constant, but the value of M changes linearly with time via the equation

$$M = M_0 + n\Delta t \tag{3.1}$$

In this equation Δt is the time since epoch and n is the mean motion of the satellite defined by

$$n = \sqrt{\frac{\mu}{a^3}} \tag{3.2}$$

From this, the eccentric anomaly can be determined. It is obtained from the algorithm known as Kepler's equation

$$M = E - e \sin E \tag{3.3}$$

[2]Refer to Brown [7] for a discussion on the basic two-body motion and its applications.

Since this is a transcendental equation, it cannot be inverted directly to obtain E from M. It is usually solved through an iterative method such as the Newton-Rhapson technique with the initial value taken as $E = M$. The true anomaly, ν, can be calculated from the eccentric anomaly from the equations

$$\begin{aligned} \sin\nu &= \frac{\sqrt{1-e^2}\sin E}{1-e\cos E} \\ \cos\nu &= \frac{\cos E - e}{1-e\cos E} \\ \nu &= \tan^{-1}\frac{\sin\nu}{\cos\nu} \end{aligned} \tag{3.4}$$

The result obtained from equation 3.4 presents the position of the satellite as a function of time in terms of the classical orbital elements. This format of presenting the satellite state is not very suitable for the purposes of analysing its motion relative to a rotating Earth or comparing its position with the celestial bodies. For this reason, the position of the satellite is usually transformed[3] to another coordinate system in which it is easier to analyse the state of the satellite. These transformations include conversion to the ECI coordinate system for comparison with celestial bodies, conversion to the SEZ coordinate system for tracking purposes or representing the ground-track of the satellite in terms of geodetic latitude and longitude.

Analytical Theories

Analytical theories of orbital propagation consist of an analytical description of the motion of a satellite under the influence of the perturbative forces. These theories are of historical significance as they were the first propagational theories that were developed. They are also of practical significance as they provide fast and computationally efficient desriptions of a satellite's motion and give some insight into the influence of the perturbations on the orbit.

Methods of Kozai and Brouwer In October 1959 two outstanding articles on the influence of perturbations on Low Earth Orbit satellites were published in the same issue of the *Astronomical Journal*. The authors of the two articles were Yoshihide Kozai and Dirk Brouwer. The theories presented by these two articles were so outstanding that numerous advanced propagational theories are still based on it today. Kozai and Brouwer had the same ideas, but they had different approaches to solving the problem.

[3]Refer to section B.3 for a discussion of coordinate transformations.

Kozai: Kozai's approach was to use LaGrange's variation of parameters[4] to describe the effect of an oblate Earth on the motion of a satellite. His original theory did not consider atmospheric drag. The influence of the perturbative forces was separated into secular, short-periodic and long-periodic variations. These variations were combined to find the position of the satellite. The process followed and the results obtained in appendix D for the analytical modelling of the oblate Earth, was the exact process followed and results obtained by Kozai. As indicated, he used an averaging technique to determine the mean variations in the elements. As this technique is unique to Kozai's theory, only variations in the elements that was determined with Kozai's averaging process can be used in his propagation theory.

Kozai's theory is described by the following equations:

$$
\begin{aligned}
a &= \bar{a} + \Delta a_{SP} \\
\bar{a} &= a_0 \left\{ 1 - \frac{3a_e^2 J_2 \sqrt{1-e_0^2}}{4p^2} (2 - 3\sin^2(i_0)) \right\} \\
e &= e_0 + \Delta e_{LP} + \Delta e_{SP} \\
i &= i_0 + \Delta i_{LP} + \Delta i_{SP} \\
\omega &= \omega_0 + \dot{\omega}\Delta t + \Delta\omega_{LP} + \Delta\omega_{SP} \\
\Omega &= \Omega_0 + \dot{\Omega}\Delta t + \Delta\Omega_{LP} + \Delta\Omega_{SP} \\
M &= M_0 + \bar{n}\Delta t + \Delta M_{SP} \\
\bar{n} &= n_0 \left\{ 1 + \frac{3a_e^2 J_2 \sqrt{1-e_0^2}}{4p^2} (2 - 3\sin^2(i_0)) \right\} \\
n_0 &= \sqrt{\frac{\mu}{a_0^3}}
\end{aligned}
\tag{3.5}
$$

where overbars indicate "mean" values and the subscripts "SP" and "LP" indicate short-periodic and long-periodic variations, respectively. The Δt indicate the time that has passed since the epoch of the elements, $\dot{\Omega}$ and $\dot{\omega}$

[4]The variation of parameters technique is discussed in appendix D.

are the secular variations in the respective elements and the "*0*" subscript indicate the initial mean values of the elements.

The new classical element set calculated from equation 3.5 is used with the two-body propagator presented in the previous section to determine the position of the satellite. Every time the position of the satellite is calculated, equation 3.5 must be used to update the classical elements.

The equations presented above present the full theory of Kozai, but are sometimes used in part as a perturbed two-body propagator theory. Escobal [16] describes such a case where only the dominating perturbative effects are considered for propagation.

The accuracy of the perturbation theory depends on the number of terms included in the series expansion for each perturbative effect. For simplifications, the periodic terms are often ignored and only the secular terms are included. This results in the propagation of the "mean" position of the satellite.

Brouwer: Kozai developed his theory for the variations in the classical elements while Brouwer developed his for the variations in the Delauney[5] elements. His theory modelled the same perturbations as that of Kozai—oblate Earth without drag modelling—but his calculation of the variations in the elements due to perturbative forces differed from that of Kozai. The updated set of classical elements determined from Brouwer's theory is similar to that presented by Kozai and is found from

$$
\begin{aligned}
a &= \bar{a} + \Delta a_{LP} + \Delta a_{SP} \\
e &= e_0 + \Delta e_{LP} + \Delta e_{SP} \\
i &= i_0 + \Delta i_{LP} + \Delta i_{SP} \\
\omega &= \omega_0 + \dot{\omega}\Delta t + \Delta\omega_{LP} + \Delta\omega_{SP} \\
\Omega &= \Omega_0 + \dot{\Omega}\Delta t + \Delta\Omega_{LP} + \Delta\Omega_{SP} \\
M &= M_0 + \bar{n}\Delta t + \Delta M_{LP} + \Delta M_{SP}
\end{aligned}
$$

[5]Refer to Vallado [35] for a discussion of Delauney variables.

$$n_0 = \sqrt{\frac{\mu}{a_0^3}} \tag{3.6}$$

Brouwer also refer to the initial orbital elements as mean elements, but they differ from those defined by Kozai as their derivation was based on different assumptions concerning the perturbations. The expressions for the short periodic variations are the same in both the theories of Brouwer and Kozai, but the expressions for the long-periodic and secular variation differ considerably.

Simplified General Perturbation Methods The analytical theories introduced by Kozai and Brouwer in 1959 had significant shortcomings in that both theories only modelled the perturbative effects of an oblate Earth. It soon became apparent that atmospheric drag greatly influences the motion of satellites in Low Earth Orbit and that the perturbative effect of drag needed to be included in the propagations. This lead to the extension of the above mentioned theories to include the effect of drag on the orbit.

Kozai's theory was used as the basis for the first operational, analytical propagation technique. A simplified version of his gravitational model was combined with a drag model that expresses the influence of drag on the mean anomaly as linear with time. In the 1970's, the U.S. Air Force conducted a survey to determine what theories were available and in order to obtain a measure of configuration control over all the theories that were in circulation. They published the results of this investigation in the *Spacetrack Report No.3* [103]. The propagation model derived from the theory of Kozai was published in this report as the ***Simplified General Perturbation*** (SGP) technique. The North American Aerospace Defence Command (NORAD) started to distribute orbital element sets that were compatible with the SGP in that it presented the Kozai mean values for the elements. Due to their format, these element sets quickly became known as *two-line element* sets or TLE. TLE's are the format of orbital elements most commonly available today. NORAD provides TLE's for over 9000 objects orbiting the Earth.

Brouwer developed his theory with the perturbations being presented in a canonical format, which, due to its ease of use when implementing new perturbations, became very popular. This theory was also extended to include the effect of atmospheric drag on the orbit with a power density function being used as an atmospheric model. The most widely used form of this extension to the work of Brouwer was published in the *Spacetrack Report No.3* [103] and became known as the ***SGP4*** algorithm. The SGP4 algorithm was developed in such a way that the same TLE's could be used in any of the propagational theories presented in the Spacetrack Report. This

was achieved by changing the interpretation of some of the parameters in the TLE, such as the derivatives of the mean motion and the drag parameter, depending on the propagational algorithm that is used. As stated above, the theories of Brouwer and Kozai are based on different assumptions concerning the mean values of the elements. In order to maintain generality in the composition of the TLE's, the SGP4 algorithm transforms the Kozai mean values presented in the TLE to osculating values which are compatible with the theory of Brouwer.

Semianalytical Theories

Analytical propagation theories dominated numerical theories for many years due to its faster speed of execution. With the use of modern computers, high accuracy propagation predictions using numerical methods can be computed quicker than previously, but it still requires a lot of computational time and power. This opened the door for the use of semianalytical techniques which includes the best of both worlds in that it executes almost as fast as analytical theories while it has the accuracy of numerical methods. As previously mentioned, the increased accuracy of the numerical methods results from the numerical calculation of the influence of perturbative forces on the orbit. The idea is to separate the short-periodic variations in the orbit from the secular and long-periodic variations. The high frequency in variation of the short-periodics usually requires a very small integration step size that slows the propagation process. By removing the short-periodics, the long-periodics and secular variations can be numerically integrated with large step sizes (on the order of a day). At the integration step times the contributions from the short-periodics—which is modelled as Fourier series in the 2π periodic fast varying true anomaly—can be combined to determine the osculating motion of the satellite.

The ***Draper Semianalytical Satellite Theory*** (DSST) was developed by Paul Cefola and his colleagues at the C.S. Draper Laboratory based on the above-mentioned idea. It is a very high accuracy propagation method that is flexible enough for most orbit geometries and which contains complete models for all the major perturbative forces. The operation of DSST can be described by referring to figure D.1. The secular variations in the orbit are numerically integrated with large integration step sizes with the periodic terms being calculated at the integration step times.

Brouwer's theory became the basis for numerous extensions in the analytical theories of orbital propagation. The SGP4 algorithm was extended to the SDP4 algorithm for use with satellites above Low Earth Orbit—considered as *deep* space . The algorithm uses numerical integration techniques to model

some of the perturbations above low Earth orbit.

Numerical propagators

Numerical propagators predict the motion of a satellite by numerically integrating the perturbed equation of motion:

$$\vec{a} = -\frac{\mu}{r^3}\vec{r} + \vec{a}_p \tag{3.7}$$

With the inclusion of the most important perturbations for low Earth orbit, this expression can be written as

$$\vec{a} = -\frac{\mu}{r^3}\vec{r} + \vec{a}_{nonspherical} + \vec{a}_{drag} + \vec{a}_{3-body} + \vec{a}_{SR} \tag{3.8}$$

where the perturbative accelerations result from the nonspherical Earth, atmospheric drag, third body attractions and solar radiation pressure, respectively. Expressions for the numerical calculation of the perturbative accelerations are supplied in appendix D.2.2. The perturbative accelerations can also be calculated from the direct numerical integration of the variation of parameter equations of Gauss and Lagrange[6]. The advantage of using equation 3.8 is that all the secular and periodic variations is automatically included into the computation of the satellite motion via the formulation of the perturbing forces. When all the perturbative forces are included to the highest possible order, the propagation made with the numerical integration of equation 3.8 is of a superior accuracy compared to analytical techniques.

Unlike analytical solutions (general perturbations), no complete numerical propagation theory exists. Complete high accuracy implementations of the special perturbation theory do exist, but the computer source-code is usually not available for general use. The numerical technique that is required for a particular application usually needs to be developed from first principles. By considering the specified accuracy, the degree of accuracy to which the perturbative accelerations need to be calculated can be determined. The solution of equation 3.8 becomes quite a complex process when all the different methods of solution and perturbative models are considered to a significant degree of accuracy.

The two numerical methods that are commonly used are Encke's method and Cowell's method. These two theories are presented in appendix D.2.2. When the first numerical techniques were implemented, Encke's method was preferred over that of Cowell as it was computationally much more efficient for implementation on the limited capability computers available at that

[6]Refer to appendix D.2.1.

time. The increase in the computational power and speed of modern computers combined with the simplicity in the formulation of Cowell's method cause it to be the preferred numerical method. A variety of numerical integration techniques exists for the solution of Cowell's method and it is not always easy to determine what technique should be used. Vallado [35] discusses some of the more important numerical integration techniques used and provides an indication of the integration step size that should be selected for different applications. The integration step size is one of the most important parameters in the numerical propagation algorithm as it influences both the execution speed and the accuracy of the propagation.

The following passage will summarise three independent implementations of the special perturbations techniques.

- Barker et al. [3] used a high accuracy numerical propagation technique to compare the accuracy of various analytical and semianalytical propagation theories. This numerical propagator used a 12^{th} order summed Cowell/Adams Predict-Partial Correct integrator. The perturbations were modelled as follows: the gravitational field of the Earth used a 21×21 Goddard Earth Model (GEM), drag was modelled using the Jacchia 70 dynamic atmosphere model, lunar and solar gravitational attraction were included and the direct solar radiation pressure was used. The accuracy of the system was stated as classified.

- Shum et al. [31] developed an extremely high accuracy numerical propagator for use in the calibration of the sensors of the Space Surveillance Network (SSN). The integration technique is not stated, but the particular perturbation models used and the accuracy of the predictions are presented. The gravitational field of the Earth was modelled with the 70×70 JGM-3 gravitational model. The positions of the Sun and the Moon were obtained from the high precision DE-200 ephemeris supplied by the Jet Propulsion Laboratory (JPL). Atmospheric drag was modelled with the Drag Temperature Model (DTM). The other perturbations that were modelled included the solid Earth tides (deformations in the Earth due to the perturbing forces), the ocean tides, solar radiation pressure and the Earth radiation pressure—solar radiation reflecting off the Earth. In order to ensure the maximum accuracy, all measurements, calculations and positions of the sensor sites were referred to the same J2000 mean equinox and mean equator reference frame. With this complete numerical technique, the following prediction accuracy was obtained: the orbits of Lageos-1 and Lageos-2 which is at 6000 km altitude were 50 m accurate over a 14 month time

span and the 1300 km TOPEX/Poseidon orbit was predicted 1500 m accurate over a 40-day time span.

- Du Toit [14] required a relatively high accuracy propagation of the orbit for the evaluation of constellation control procedures using drag. As it was a conceptual investigation, absolute accuracy was not required, but the inclusion of drag and all the major perturbative effects were essential. The propagations performed lasted only for a few days and for this reason no long-term high accuracy predictions were needed. He used a 4^{th} order Runge-Kutta numerical integration algorithm with a step size of 28 seconds. The step size meant that the position of the satellite would be updated 200 times per orbit. It was expected that the small step size would maintain the maximum accuracy over the short period under consideration. The perturbations were modelled as follows: a modified exponentially varying drag model was used with the modifications representing the variations due to solar flares and the day-night variations, the gravitational model only included the J_2 zonal harmonics, the third-body model used simplified orbits for the Sun and the Moon and solar radiation pressure was modelled as a constant value.

It is significant to note that the accuracy of each implementation in the above case study depended purely on the application for which it was needed. In the first two cases the numerical technique was selected due to its superior accuracy, but for the third case the numeric solution was selected over a general perturbations method due to its superior accuracy over the short term and the ease with which it could be included in the simulation environment of the particular application.

3.1.2 Evaluation of Propagation Techniques

Barker et al. [3] performed a study to determine the accuracy of several general perturbations and semianalytical theories. The general perturbations theories which were evaluated included SGP, SGP4 and the Hoots Analytic Dynamic Ephemeris (HANDE). The semianalytic theories included the Semianalytic Liu Theory (SALT), which was developed specifically as an improvement to SGP4 for high drag and/or high eccentricity orbits, and DSST. These theories were evaluated against a high accuracy special perturbations technique. In order to perform a comprehensive evaluation of the propagation theories, a variety of orbits representative of the entire orbit geometries were required. These orbits were grouped into different categories for evaluation purposes. The evaluation which is of importance to this study is that

performed on the category of orbits with eccentricity smaller than 0.05 (circular orbits) and altitude between 575 km and 1000 km. Figure 3.1 shows the propagation accuracy of the different theories compared to the special perturbations theory for this category of orbits. The values presented in the graph are the root mean square (RMS) values of the position magnitudes relative to the special perturbations theory. The RMS values were computed form the equation

$$RMS = \sqrt{\bar{x}^2 + \left(\frac{n-1}{n}\right)\sigma^2} \tag{3.9}$$

where $\bar{x}$ represents the mean value and σ the standard deviation of a data sample and n represents the number op data points.

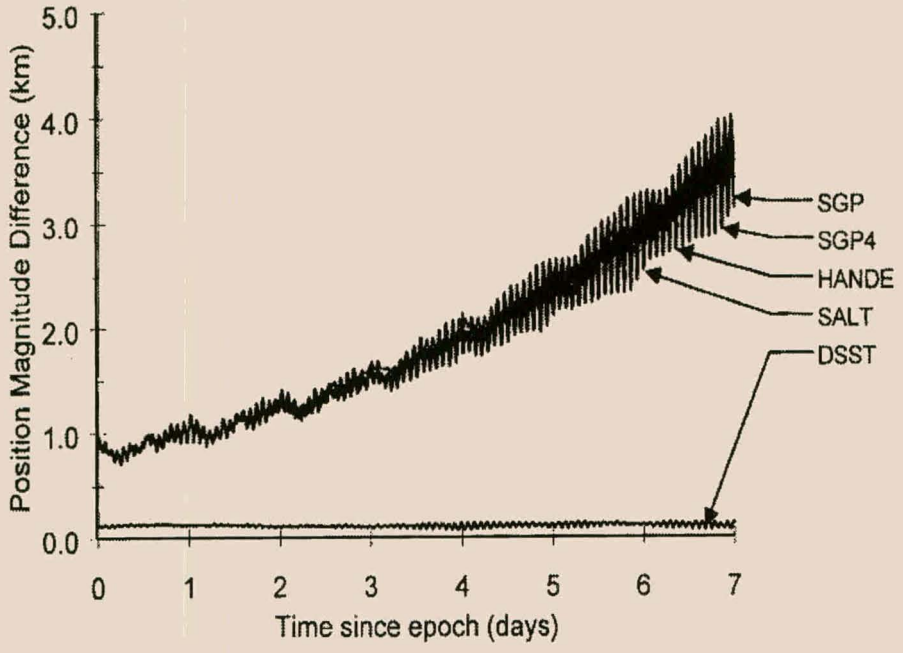

Figure 3.1: Propagator accuracy for satellites in low Earth orbit.

Satellites in the orbit category under investigation experience moderate quantities of drag with the major perturbation effect being that of the oblate Earth. This becomes apparent from figure[7] 3.1 where the unmodelled gravitational harmonics in all the theories except DSST and the special perturbations theory caused short periodic and longer periodic variations (on the

[7]Image taken from Barker et al. [3].

order of a day). The high accuracy predictions were obtained from DSST by using an 8×8 gravitational model with the inclusion of some higher order harmonics.

In chapter 2 it is stated that the required accuracy of the propagation algorithm should be approximately 0.3 km when projected onto the surface of the Earth. Figure 3.1 presents the RMS magnitude of the error in the position vector for the various propagation theories and not the projection onto the surface of the Earth. When the value is interpreted as a projection onto the surface of the Earth, it can be seen that the projected accuracy will at least be of the same magnitude as the RMS position magnitude, but probably better than that presented in figure 3.1. From Jones [19] it can be seen that the major part of this error represents an along-track displacement from the true position of the satellite.

From the study performed by Barker et al. it became apparent that three possibilities existed from which a propagator had to be selected for use during this study. The three methods were SGP4, DSST and a special perturbations technique. SGP4 was considered due to the availability of the computer code for the algorithm and the availability of orbital elements that are used with this theory for all Earth orbiting satellites. DSST was considered due to the accuracy of the propagator, its speed of computation and the ease with which it could be customised to a variety of orbital geometries. The special perturbations technique was considered due to its supreme accuracy of propagation. From figure 3.1 it can be seen that DSST has a propagation accuracy of approximately 150 m. From the study of Shum et al. [31] it was found that a high quality special perturbations technique such as used by Barker et al. could be considered as absolutely accurate for this study. SGP4 has an initial propagation accuracy of approximately 1 km that translates to a projection error that falls on the boundary of the above specified accuracy.

When the accuracy of the propagators are compared, an important factor, which should be taken into consideration, is the accuracy of the initial conditions, which is discussed in appendix G. The TLE files generated by NORAD and distributed via the Internet are generated by means of a differential correction process by using the SGP4 algorithm, which has an initial accuracy of only 1 km. DSST can use the TLE data as initial conditions, but osculating orbital data for the special perturbations method are not generally available. The best substitution is the use of GPS measurements made onboard the satellite, but this is not generally available. When the data in the TLE is used as initial conditions in the special perturbations technique and DSST, the accuracy of the propagations will degrade. DSST will continue the propagation with the 1 km accuracy of the TLE, but the accuracy of the special perturbations technique cannot be predicted.

When the problem with the initial conditions is taken into consideration, it is clear that a special perturbations technique could not be used for this study. The computer code for the DSST algorithm could not be obtained which left SGP4 as the only option available for implementation. In evaluating SGP4 from figure 3.1, it is found that the accuracy specification for the propagation algorithm will either be marginally satisfied or not be satisfied at all. In order to maintain propagation accuracy close to the theoretical accuracy of the theory, the orbital elements should be updated as frequently as possible and at least once a week. When high accuracy ephemerides is required, the propagation should be performed close to the epoch of the element set in order to use the inherent accuracy of the TLE for propagations performed close to the epoch.

An important feature of propagation theories which became apparent from the study performed by Barker et al. [3] and which should be noted is that a propagation theory does not perform equally effective for all orbital geometries. Some of the theories—such as SALT and HANDE—were developed to model high eccentricity orbits and therefore they perform well for this type of orbits. However, these same two theories delivered an average performance for the medium drag circular orbits under consideration in the Barker-study. Vallado [35] compares the accuracy of a simplified numerical propagator to a very high accuracy numerical propagator for various orbits. It is clear that perturbations that are of importance are different for each orbit considered. The accuracy of a propagation technique will be different for different types of orbits as the influence of perturbations on the orbit depends on the altitude, eccentricity and inclination of the orbit.

3.2 Modelling the space environment

3.2.1 Modelling the Sun Position

Sun Prediction Models

The position of the Sun and the Moon can be determined from high accuracy numerically integrated ephemerides or from analytical algorithms. The high accuracy ephemerides are calculated at the Jet Propulsion Laboratory and supplied in the annual *Astronomical Almanac*. A variety of analytical theories exist and it is usually more convenient to use an analytical algorithm in a computer program than the list of numerically determined ephemerides.

For this particular study, the position of the Moon was not required. Meeus [22] presents a low accuracy and a high accuracy analytical algorithm for calculation of ephemeris for the Sun. The low accuracy algorithm has

an 0.01° accuracy which is better than the accuracy that was specified in chapter 2.

The assumption is made that the Earth follows a purely elliptical orbit. It means that the perturbations to the orbit of the Earth due to the gravitation of the Moon and other planets can be ignored. In the first instance the number of Julian centuries from J2000, T, need to be calculated from equation B.6. The geometric mean longitude of the Sun referred to the mean equinox of date is calculated from

$$L_0 = 280.46645^\circ + 36000.76983^\circ\ T + 0.0003032^\circ\ T^2 \tag{3.10}$$

The mean anomaly of the Sun is

$$\begin{aligned} M &= 357.52910^\circ + 35999.05030^\circ\ T - 0.0001559^\circ\ T^2 \\ &\quad -0.00000048^\circ\ T^3 \end{aligned} \tag{3.11}$$

The eccentricity of the Earth's orbit around the Sun is

$$e = 0.016708617 - 0.000042037\ T - 0.0000001236\ T^2 \tag{3.12}$$

The equation for the center of the Sun is

$$\begin{aligned} C &= (1.914600^\circ - 0.004817^\circ\ T - 0.000014^\circ\ T^2) \sin M \\ &\quad +(0.019993^\circ - 0.000101^\circ\ T) \sin 2M \\ &\quad +0.000290 \sin 3M \end{aligned} \tag{3.13}$$

From these equations the true longitude of the Sun follows as

$$\Theta = L_0 + C \tag{3.14}$$

For the calculation of the apparent longitude, λ, of the Sun, Θ needs to be corrected for the nutation and the aberration[8]. For this particular low accuracy algorithm, this correction is calculated as follows

$$\Omega = 125.04^\circ - 1934.136^\circ\ T \tag{3.15}$$

$$\lambda = \Theta - 0.00569^\circ - 0.00478^\circ \sin \Omega \tag{3.16}$$

For the calculation of the apparent position of the Sun, the above defined expressions must be used with the value for the apparent obliquity of the

[8]Seidelmann [30] defines aberration as: "the apparent angular displacement of the observed position of a celestial object from its geometric position, caused by the finite velocity of light in combination with the motions of the observer and the observed object."

ecliptic, ϵ. This value is determined by correcting the mean obliquity of the ecliptic, ϵ_0, defined by equation B.4 to obtain the quantity

$$\epsilon = \epsilon_0 + 0.00256^\circ \cos\Omega$$

The right ascension and declination of the Sun can then be determined as

$$\tan\alpha = \frac{\cos\epsilon \sin\Theta}{\cos\Theta} \tag{3.17}$$

$$\sin\delta = \sin\epsilon \tan\Theta \tag{3.18}$$

These values of right ascension and declination are combined with the magnitude of the Sun's radius vector, $r_\odot$,expressed in astronomical units (AU)[9], as

$$r_\odot = \frac{1.000001018(1-e^2)}{1+e\cos(\nu)}\text{AU} \tag{3.19}$$

to determine the components of the Sun's radius vector in the ECI coordinate system as

$$\vec{r}_\odot = \begin{bmatrix} r_\odot \cos(\alpha)\cos(\delta) \\ r_\odot \sin(\alpha)\cos(\delta) \\ r_\odot \sin(\delta) \end{bmatrix} \tag{3.20}$$

Evaluation of Sun Prediction Model

The low-accuracy model presented by Meeus [22] was selected for modelling the position of the Sun. Meeus states the accuracy as being approximately 0.01°. This could only be evaluated by comparison with the true position of the Sun. The most accurate ephemeris available for the Sun is the DE200 numerically integrated ephemeris from JPL that is presented in the Astronomical Almanac [1]. When the ephemeris for a particular time is required, the on-line computation of the position of the Sun can be used. The on-line calculation is performed by the software known as MICA[10] (Multiyear Interactive Computer Almanac) which uses the same DE200 ephemeris as is used for the calculations presented in the Astronomical Almanac. These ephemerides were the most accurate data available for evaluating the model of the Sun and therefore it was considered to be representative of the true position of the Sun.

[9] 1 AU = 1.4959787×10^{11} m

[10] http://aa.usno.navy.mil/AA/

The Astronomical Almanac presents the position of the Sun in terms of right ascension, declination and radial distance. By using the conversion methods presented in appendix B.3.6, it can be converted to Cartesian ECI coordinates. This is the most useful reference frame for comparison between the data from MICA and the implemented model of Meeus. By using vector algebra, the angular separation between the two position vectors can be determined. The angular separation between the true position of the Sun and the modelled position of the Sun is presented in table 3.1. It was calculated at four evenly spaced moments throughout the duration of the year in order to eliminate biases in the model.

Date	Time (UTC)	Error (°)
1 Jan 1999	00:00:00	0.00575
1 Apr 1999	00:00:00	0.00343
1 Jul 1999	00:00:00	0.00118
1 Oct 1999	00:00:00	0.00423

Table 3.1: Error in the prediction of the position of the Sun.

It is clear that the error in the model never exceeds the specified 0.019° modelling accuracy. Therefore, the model can be considered as a satisfactory accurate model.

3.2.2 Horizon

Modelling the Horizon

The true shape of the Earth is not a perfect sphere. It can be represented by a variety of models that differ in complexity. The more complex models define the shape of the Earth by means of an expansion of the gravitational potential in terms of the spherical harmonics as presented in equation D.9. Wertz [36] presents a way to model the horizon of the Earth as seen from space where it is assumed that the shape of the Earth can be modelled as an ellipsoid with flattening $f = 1/298.257$. He defines the distance from the center of the Earth to the subsatellite point as

$$R = \frac{a_e(1-f)}{\sqrt{1-(2-f)f\cos^2\lambda}} \tag{3.21}$$

where a_e is the Earth's equatorial radius and λ, in this case, refer to the geocentric latitude. The angular radius of the horizon of the Earth as a

function of the azimuth angle of the horizon vector is defined as

$$\rho = \cot^{-1}\left\{\left[\frac{(d^2-R^2)}{a_e^2}\left(1+\frac{(2-f)fR^2\cos^2\lambda}{(1-f)^2a_e^2}\sin^2\Psi\right)\right]^{1/2} + \frac{(2-f)fR^2\sin 2\lambda}{2(1-f)^2a_e^2}\sin\Psi\right\} \tag{3.22}$$

where λ is the geocentric latitude of the subsatellite point, d is the radial distance of the satellite from the center of the Earth and Ψ is the azimuth angle of the horizon vector measured counterclockwise from east.

Equations 3.21 and 3.22 can be used to determine the loci of points describing the position of the horizon as seen from the satellite, or it can be used to determine the angular separation from the subsatellite point to the horizon for a particular sensor. For this to be achieved, it is necessary to know the attitude of the satellite, as the orientation of the body-mounted sensors is determined from the attitude of the satellite.

Evaluation of Horizon Model

Wertz [36] indicates that the ellipsoid defined above is a *good* approximation to the true shape of the Earth. Vallado [35] also refers to the ellipsoid as being a *good* approximation to the mean surface height of the Earth, but no real verification of the accuracy of the model was found.

The modelling specification which was laid down in chapter 2 used the measurement accuracy of the horizon sensors to specify the accuracy required in modelling the horizon, but as no model was found which satisfied the specifications, the unverified model was used.

3.2.3 Magnetic Field

Modelling the Magnetic Field

The magnetic field of the Earth is predominantly a dipole field with the Sun being the primary source of perturbations to the dipole field. The South Pole of the field is located in the Northern Hemisphere and the North Pole is located in the Southern Hemisphere. The magnitude of the field is the strongest over the magnetic poles and the weakest over the magnetic equator. The magnetic field can be modelled as the gradient of a scalar potential function with the potential function being expanded in terms of the Gaussian coefficients. The International Geomagnetic Reference Field (IGRF) model is the empirical representation of the Earth's magnetic field recommended for

scientific use by the International Association of Geomagnetism and Aeronomy (IAGA). This model represents the main (core) field without external sources. As the magnetic field rotates with the Earth, the IGRF model employs the spherical harmonics expansion of the scalar potential in ECEF coordinates. The objective of the 10^{th} order IGRF model is to empirically determine the Gaussian coefficients by doing a least squares fit based on all available data sources. It includes geomagnetic measurements from observatories, ships, aircraft and satellites. The magnetic field model is presented as an analytical theory that is well suited for implementation on a computer.

Appendix E contains the mathematical expressions describing the algorithm and proposals presented in Wertz [36] to make the algorithm computationally more efficient. The coefficient sets[11] for the IGRF model are available in steps of 5 years (1990, 1995, 2000 ...) with the coefficients and the first time derivatives of the coefficients being included in the coefficient sets. For a thorough discussion on the Earth's magnetic field, refer to Wertz [36] and the *ESA Space Environments and Effects Analysis Section* [102].

Evaluation of Magnetic Field Model

As it was indicated in the previous section, the IGRF magnetic field model is an empirical representation of the magnetic field of the Earth derived from measurement of the magnetic field. Unpredictable time-varying solar activities cause a varying intensity in the solar wind that distorts the magnetic field. The time-varying intensity of the solar wind has a major influence on the model of the magnetic field. Measurements, which were used to derive an empirical model of the averaged field, may be biased or may have been obtained during times of extreme solar activity. The majority of these measurements were taken from sites on or over the continents with almost no measurements being made over the oceans or in space. The lack of accurate measurements over certain areas of the Earth resulted in the available measurements being extrapolated to obtain a model that represents the complete magnetic field. As it can be expected, the accuracy of this model derived from extrapolated data, will be less accurate over areas of low measurement concentrations. The result is that the IGRF model is exactly what its name indicates it to be—a *model* of the field which does not necessarily represent the true magnitude and orientation of the field at a particular time.

Wertz [36] indicates that the magnitude of the dipole field determined from the IGRF model on the magnetic equator at an altitude of 445 km is approximately 25 μT. At this altitude the maximum error in the magnitude

[11]The coefficients for the IGRF model can be obtained via the Internet from *ftp://nssdc.gsfc.nasa.gov/models/geomagnetic/igrf/*.

of the IGRF model is 0.54 μT and the RMS error in the magnitude of the IGRF model is 0.18 μT. He also indicates that the maximum errors in the IGRF model for the other components of the field—the azimuthal and coelevation components—are approximately 1 μT. When the influence of the solar wind on the intensity of the components of the field is taken into consideration, it should be clear that even the indications of modelling accuracy presented by Wertz, could be far from the truth for certain conditions of solar activity.

The IGRF model was the only model available for implementation into the simulation environment. As this is the model which was used to determine the attitude of the satellite from the magnetometer measurements, the attitude obtained from Kalman filtering will be, at best, as accurate as the IGRF model. Therefore, the specification for the implementation accuracy of the magnetic field model could not be fulfilled. The errors in the model exceed the measurement accuracy of the magnetometer. This modelling error is recognised by control system engineers and therefore the data derived from magnetometer readings—even if it is very accurate—cannot be considered as high accuracy attitude or position information.

3.2.4 Terminator

Modelling the Terminator

Wertz [36] defines the terminator as "*the boundary between the day and the night on a planet or a planetary satellite which forms an approximate great circle* 90° *from the subsolar point*". It is defined as "*approximate*" as this boundary does not appear as a well-defined line on the surface of the Earth, but rather as a fuzzy transition from light to dark regions. The reason for modelling the terminator is that it is used to determine the validity of some of the sensors on board a satellite. The fuzzy appearance of the terminator prevents it to be used for the direct triggering of sensor measurements, but knowing the location of the terminator, it can be used to determine whether the horizon sensors see a sun-lit or a dark horizon. These sensors determine the location of the horizon in the optical part of the spectrum and are enabled only when a sun-lit horizon is visible. Another reason for modelling the terminator is that orientation of the Sun with respect to the satellite, is determined in the calculation of the position of the terminator. The Sun orientation obtained from the terminator calculation is used to determine the validity of the measurements from the Sun sensors.

Steyn [32] models the terminator by using the Earth centred angle between the sub-satellite and subsolar points. The direction of motion of the

satellite is determined by constructing a great circle through the current sub-satellite point and a point delayed by 18° in the orbit plane from the current sub-satellite point. The Earth is assumed to be perfectly spherical and by using spherical trigonometry, the Earth centred angle between the sub-satellite and subsolar points and the azimuth angle—measured counter clockwise from the negative direction of motion—of the Sun is determined.

Evaluation of Terminator Model

As indicated above, the position of the terminator was only required to determine the validity of some of the sensors on the satellite. Therefore the vague definition of the position of the terminator could be tolerated and the modelling accuracy specified in chapter 2 did not have to be verified.

3.2.5 Modelling the Stellar Positions

As mentioned in chapter 2, the modelling of the stellar positions was not considered part of this study. Refer to Wertz [36], Meeus [22], Seidelmann [30], Jacobs [18] or The Astronomical Almanac [1] for information on modelling the position of the stars as seen by the satellite.

3.3 Combining Propagations with Sensors

This section will provide a more thorough discussion than chapter 1 on certain aspects of figure 1.1. The topics discussed in this section was not researched in detail and was not implemented, but the inclusion of the conceptual study which will be presented in the following paragraphs was considered necessary as it should indicate to the reader where the researched topics fit into the total field of study.

3.3.1 Improvement of Predictions

It is possible to improve the accuracy of the predictions made with a propagation algorithm by using the input from a number of sensors. These sensors can be divided into two groups that consist of internal or onboard sensors and external sensors. When it is compared to the classical model of an estimator[12], the internal sensors are used to update the states of the estimator—in this case the orbital states of the propagator—and the external sensors are

[12]Refer to Franklin et al. [17] for a discussion on estimation techniques.

used to update the initial conditions of the estimator—in this case the initial conditions of the propagation algorithm. Table 3.2 indicate the different types of sensors used to improve the accuracy of the orbital predictions.

Internal sensors	External sensors	Hybrid sensors
Sun sensor	Radar	GPS
Magnetometer	Satellite Laser Ranging	
Horizon sensors	Optical sensors	
Star sensor	RF tracking antennae	

Table 3.2: A summary of sensors used to improve the accuracy of the orbital predictions.

Internal Sensors

Internal sensors include the magnetometer, horizon sensors, Sun sensor and star sensor. GPS can be considered as a hybrid sensor as it uses external sources to obtain its data, but as its measurements are available onboard the satellite, it will be considered as an internal sensor.

By using sensors onboard the satellite, it is possible to improve the accuracy of a propagation algorithm through comparison with the true measured position of the satellite. The improvement of the propagation accuracy usually consists of the implementation of an Extended Kalman Filter (EKF) along with the measurements. When implemented onboard a satellite, the use of an EKF with sensor data to predict the orbit of a satellite is usually known as an autonomous orbit determination system. The measurements made onboard the satellite can also be used at the groundstation to improve the accuracy of the orbit propagation algorithms at the groundstation.

The best results from a combination of internal sensors with an EKF will be obtained when a high accuracy propagation algorithm is used to propagate the orbital state of the satellite. Most reasonably accurate analytical algorithms require mean orbital elements as initial conditions. The disadvantage of mean elements is that the generation of the orbital elements is quite a complex process and the elements have a limited accuracy. Numerical algorithms require the osculating state of the satellite as initial conditions. These algorithms are very well suited for implementation in an EKF as the osculating orbital state of the satellite is usually quite easily derived from the measurements. The increased accuracy obtained from the combination of a numerical algorithm with appropriate force models also has the added benefit

that the time intervals between updates of the EKF with sensor measurements can be increased as the predictions would stay accurate for a longer period of time.

Magnetometer Measurements made with a magnetometer are probably the most general and most easily obtainable position data available onboard the majority of satellites. By comparing magnetometer measurements with the IGRF model, a rough estimate of the position of the satellite can be obtained. When this comparison is performed with an EKF, it is possible to make reasonably accurate—on the order of 1 km to 10 km—predictions of the position of the satellite. Jordaan [20], Psiaki [28], [29] and Bar-Itzhack and Shorshi [2] investigated the use of a magnetometer for orbit determination and prediction. Two basic methods were followed for doing orbit prediction with magnetometer data. The first method consisted of using the magnitude of the magnetic field measurement as measurement inputs to the EKF. This resulted in predicted accuracy on the order of tens of kilometres. The improved method consisted of using attitude information to improve the quality of the measurement data used as input to the EKF. By using attitude information, the components of the magnetic field vector could be used as measurement inputs that provides three measuring points instead of one for every update of the EKF.

Star sensor The star sensor is the highest accuracy sensor onboard SUNSAT and is used to accurately determine the orientation of the satellite in all three axis of orientation. The camera cannot be used autonomously for orbit determination, but, as indicated by Psiaki [29], the accuracy of the orbit prediction made with other sensors such as the magnetometer, can be improved by using attitude information obtained from the star sensor.

Sun sensor Measurements obtained from the fine Sun sensor for SUNSAT are almost ten times more accurate than direct measurements obtained from the magnetometer. Psiaki [29] presents a method to combine the magnitude of the measurements obtained from the magnetometer with the angle between the magnetic field vector and the Sun vector in such a way that high accuracy orbital predictions are obtained without the need for attitude information. The advantage of this proposal is that, instead of using the relatively complex and expensive star sensor, the Sun sensor, which is less expensive and functionally less complex than the star sensor, can be used for improving the orbital predictions.

Horizon sensor Two types of horizon sensors are generally used onboard satellites. The two types are CCD sensors, such as are used onboard SUNSAT, and conical scan horizon scanners[13]. Nagarajan et al. [26] presents a method to use scanner type horizon sensors along with attitude information in an EKF to obtain 2 km accurate orbital predictions. The angular radius of the Earth as seen by the satellite and the radial distance from the satellite to the Earth is obtained from the sensor measurements. This information is combined with attitude information in the EKF to estimate the orbital state of the satellite.

GPS GPS measurements performed onboard a satellite contains high accuracy position and velocity information of the satellite. GPS measurements performed onboard SUNSAT are approximately 50 m accurate with the possibility to improve the accuracy of the measurements to sub-meter level with some processing of the data. As GPS measurements provide the orbital state vector of the satellite in terms of position and velocity vectors, these measurements are well suited for inclusion in an orbit prediction EKF as indicated by Psiaki [29] and by Jordaan [20]. The disadvantage of using GPS measurements—as highlighted by Psiaki—is that it is not truly autonomous as it depends on obtaining data from the constellation of GPS satellites. Availability of these data can be affected by political factors which result is satellite designers usually not relying solely on GPS measurements for position information. Another disadvantage is that GPS receivers that are currently used onboard satellites consumes excessive amounts of power which result in the receivers being operated only for short periods of time.

The advantage of using GPS data is the accuracy of the data. When combined with a high accuracy propagation algorithm in an EKF, the improved propagation accuracy should enable the increase of the time between measurement updates of the EKF. The increased interval between measurement updates would eliminate the drawback that the power consumption of the receiver has on the availability of data. Therefore, the receiver would not need to be operated continuously.

External Sensors

External sensors consist of radar measurements, Satellite Laser Ranging (SLR), optical sensors and measurement data derived from tracking antennae. Vallado [35] provides some information on these sensors, where the sensors are situated and how the data is used. Except for data derived

[13]Refer to Wertz [36] for a discussion on different types of horizon sensors.

from tracking antennae at the local groundstation and GPS measurements, the measurements of the external sensors are not available for general use. The measurements made with external sensors are used to update the initial conditions[14] used as input for the propagation algorithms. As discussed in appendix G, initial conditions for analytical propagators are available on the Internet where as the initial conditions for numerical propagators are not available for general use. By combining GPS measurements or the angular measurements obtained from a tracking antenna in a Kalman filter or least squares process, initial conditions for numerical algorithms can be generated. For the best results in both analytical and numerical propagators, the initial conditions need to be updated as frequently as possible.

3.3.2 Validation of Sensors

Some of the sensors such as the horizon and Sun sensors can only be used under certain conditions. The Sun sensor can only provide valid data when the satellite is not eclipsed and the horizon sensor can only be used when the satellite is in view of a sunlit horizon and the terminator is not in view. For the best estimation results the predicted position of the satellite should be combined with the modelled position of the Sun to ensure that the data from the horizon and Sun sensors are only used when valid.

[14] Appendix G contains a short discussion on the way initial conditions are derived.

Chapter 4

Simulation Environment for Satellites

The two most important specifications stipulated for the project stated that

1. the satellite position and the space environment had to be modelled and

2. the output of the simulation needed to be distributed to its area of application via a TCP/IP network.

The mathematical models for the space environment and the orbital propagation algorithms are presented in chapter 3. By considering these models as fixed, what remained was to decide upon the format in which these models would be incorporated into the software environment.

The specifications for the simulation software are stipulated in section 1.1.3. This chapter will discuss the decisions made to satisfy these specifications and present an evaluation of the quality of the predictions obtained from the implemented model.

4.1 Software Architecture

The specification stated that the data of the satellite position and the space environment needed to be generated on one computer and transmitted to the system involved in the hardware-in-the-loop simulation via a TCP/IP network. Two basic architectures were considered for the distributed application.

The first and least complex architecture that was considered involved a simple pipeline structure between only two users. It is illustrated in figure

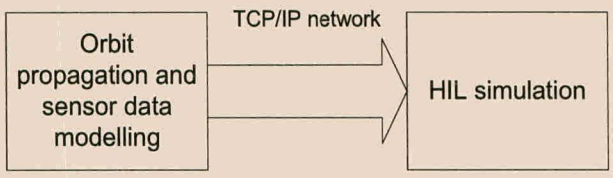

Figure 4.1: The initial architecture considered for distributing the orbital data.

4.1. A single connection is established between the orbit simulation and the computer involved in the hardware simulation with data flowing in one direction from the orbit simulation to the hardware simulation computer. The receiving computer would simply require an interface that could be used to capture the data transmitted form the orbital simulation computer. All the propagation algorithms and models for the space environment would be located on the orbital simulation computer. In this implementation, only these two systems would be involved without any third party being able to obtain data for another application.

The second architecture that was considered was the basic client-server model (Tanenbaum [34]) which is illustrated in figure 4.2. It is the natural

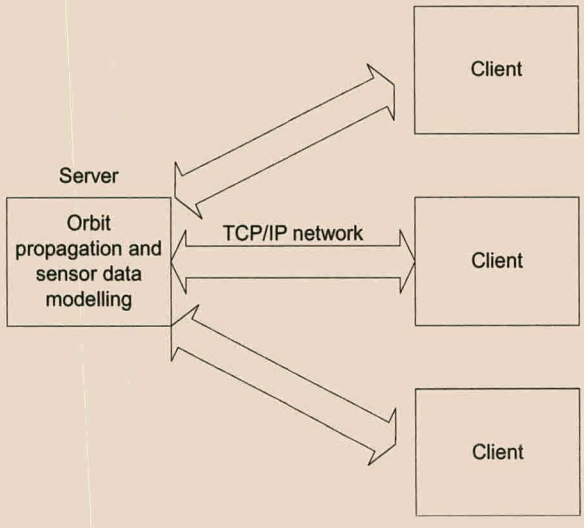

Figure 4.2: The client-server architecture which was implemented for distributing the orbital data.

extension of the pipelined architecture and can be considered as a more general architecture in which more that one user can obtain simulation data

at the same time. In this architecture, the server contains almost all the functionality of the application. The client has the minimum functionality required and connects to the server via a TCP/IP network. The advantage of this architecture is that more than one application can obtain data from the server at the same time.

The client-server architecture was selected as the basis for the development of the software. By using this architecture, it was possible to make the software less application specific. The possibility was created for the server to be used by other applications to generate orbital ephemerides while it was involved in the HIL simulation. The immediate objective of this study was to master the field of orbit propagation and to model the space environment for the purpose of hardware-in-the-loop simulation. Therefore, the client-server model was selected for implementation as it provided the maximum flexibility in the software without taking up too much developing time.

4.2 Software Structure

Delphi 4 was selected for the development of the software as it is generally used in the laboratory and well known to the author. The selected environment was well suited to the implementation of the above mentioned specifications for the structure of the software code. The well-defined TCP/IP components provided by Delphi 4 significantly reduced the time spent on developing the network interface for data distribution. These components could be used as "black boxes" without the user requiring expert knowledge of the network protocol. The Delphi Visual Component Library was a handy tool in developing the GUI.

The software for the propagation algorithms and some of the environmental models that were used, were based on Pascal code developed by Kelso [104] and Steyn [32], [33]. Kelso's software were developed for general use among the amateur space observing community and Steyn's software formed part of a simulation environment for the development of the ADCS of SUNSAT.

The selected architecture required the simulation environment to be divided into two components viz. the client component and the server component. The two components will be discussed separately due to the functional differences in the two systems, but it combines into a complete functional unit when implemented. The following discussion will be from the perspective of the HIL simulation.

4.2.1 Client Component

The client component is used on the HIL simulation computer to acquire orbital and sensor data from the server. This component is in essence a GUI for the server in that all the conditions for the simulation such as the start times, stop times, simulation step size and format and type of data required from the simulation is specified by the user via this GUI. The position of the observer and the data-output file is determined by the user by means of this GUI before a simulation can be initiated.

The user specifies the IP address of the server and upon connection between the client and the server, the server transmits the names of the satellites for which TLE's are available, to the client. The user selects a satellite from the list and the name of the satellite along with all the simulation conditions are transmitted to the server when the simulation commences. Upon receiving this message, the server instantiates the simulation. The data generated during every simulation step is transmitted to the client before the next step in the simulation is performed. As it is received, the client saves the data to a file for later use. Upon termination of the simulation, the server terminates the connection to the client. Before commencement of the next simulation, a new connection needs to be established.

The functional layout of the client component software is illustrated in figure 4.3.

4.2.2 Server Component

The server component consists of a small GUI indicating the number of clients connected to it. The GUI is used to start and stop the server and to define the files from which the TLE's should be extracted when the server is started. When a client connects to the server, the list of satellites for which TLE's are available on the server is transmitted to the client. Upon the receival of the simulation data from the client, the simulation is instantiated by the server. This is done by the creation of a propagator thread that is placed in a list consisting of all the propagator threads active on the server. The simulation data received form the client is passed to the propagator thread and the execution of the thread commences. At this stage of the simulation, the propagator thread continues to execute separate from the server and the server is ready to receive another request for data from a different client.

The models for the space environment and the orbit propagator are embedded into the propagator thread. A flow diagram describing the propagator thread is presented in figure 4.4. The data is determined in the format specified by the client and is transmitted to the client via the network as it

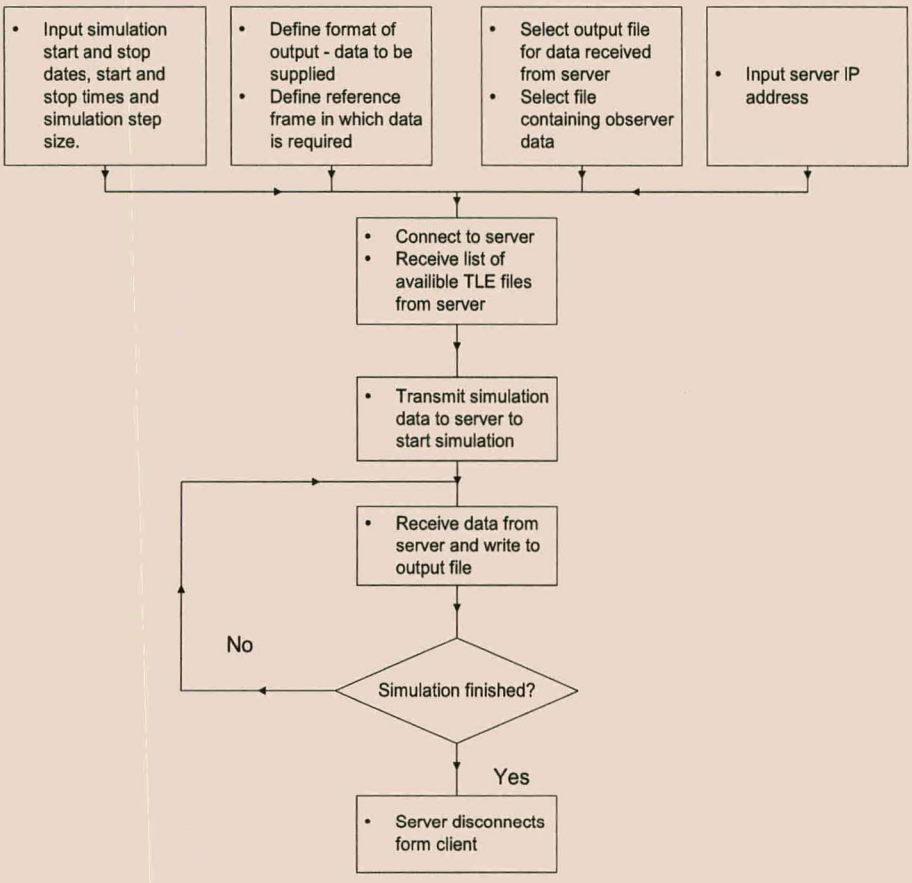

Figure 4.3: The functional layout of the client component software.

is generated. The simulation continues for the client-specified time-interval and upon completion of the simulation, the server closes the connection to the client, removes itself from the thread-list and terminates.

The functional layout of the server component software is illustrated in figure 4.5.

4.3 Evaluation

This section consists of an evaluation of the output data generated by the simulation environment by using the SGP4 propagation algorithm. The evaluation is performed from the perspective of groundstation operations and orbit simulations of SUNSAT. Predictions obtained from the SGP4 algorithm is compared to GPS data measured onboard the Ørsted satellite, predictions made with Satellite Toolkit (STK) and new initial conditions obtained

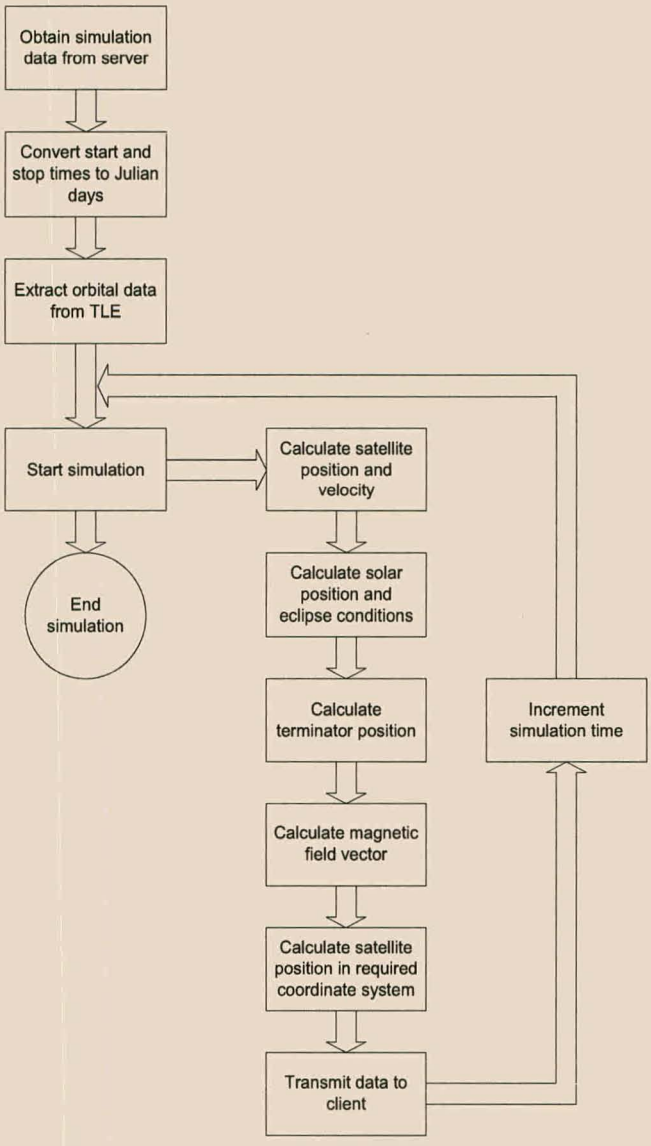

Figure 4.4: The functional layout of the propagator thread.

from two-line element (TLE) files. GPS measurements from the receiver onboard SUNSAT were not available for this study and therefore measurements made onboard Ørsted were used to evaluate the simulation environment. The Ørsted GPS measurements can be considered as representative of measurements made onboard SUNSAT as the two satellites are in identical orbits with the only difference being the positions of the satellites within their respective orbits.

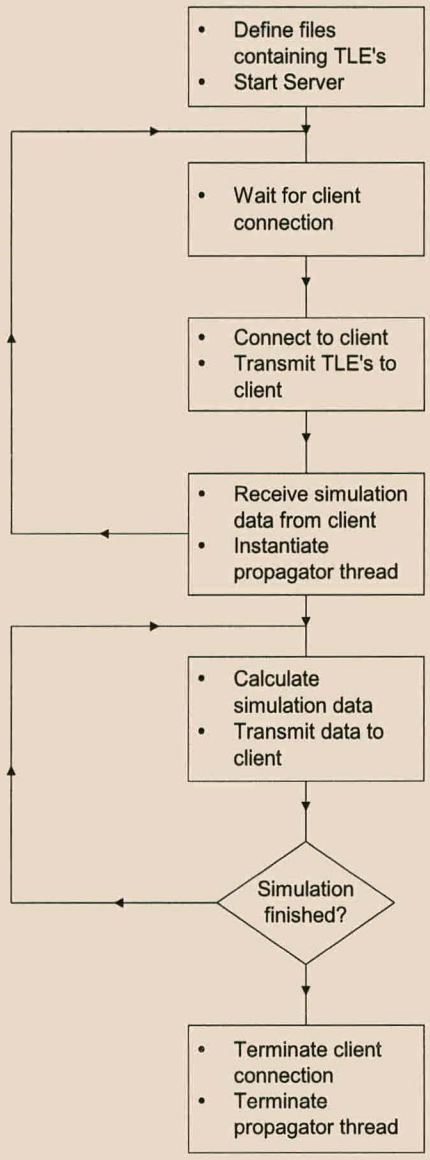

Figure 4.5: The functional layout of the server component software.

4.3.1 Comparison with GPS data

The comparison between GPS data measured onboard the Ørsted satellite and data generated with TLE's in the SGP4 propagator is presented in figure 4.6. The period of evaluation was 25 days. A single TLE set, with epoch at the start of the evaluation period, was used to propagate the position of the satellite for the total period of evaluation. It was compared to GPS measurements which were used as the best available description of the position of the

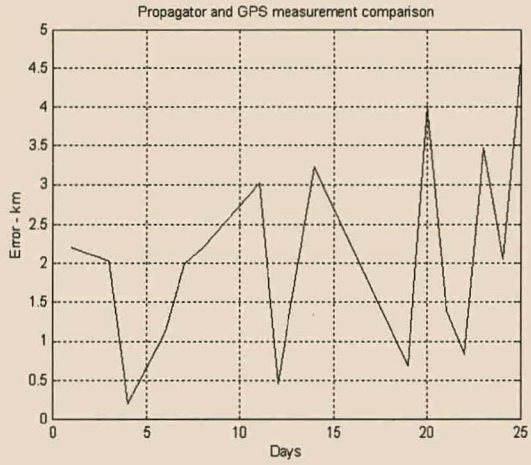

Figure 4.6: A comparison between the predicted position of the satellite with a SGP4 propagator and GPS measurements.

satellite with 50 meter position accuracy. Some of the measurement points seem to indicate erroneous measurements. Most of the measurements used in the comparison were made after a 5 hour period of operation. The GPS receiver should have converged at the time the measurements were made but the data indicate that this was apparently not the case for all the measurements.

It seems like the predicted position of the satellite is approximately 4.5 km accurate at the end of the evaluation period. When compared to the results obtained by Barker et al. [3], it does not seem correct as Barker indicated an error of 4 km after only 7 days. This could be due to the GPS measurements being less accurate than the specified 50 meters, the receiver not having converged at the time that the measurements was made or a misinterpretation of the data obtained from the GPS due to an undocumented telemetry format.

Another possible reason for the difference between the expected and measured predictions, could be that the TLE's generated for SUNSAT could be of extremely high quality. According to Vallado [106] it does sometimes happen that TLE's are generated that contains good approximations of the perturbative effects. These element sets would then provide accurate predictions for a longer period of time than would usually be expected.

4.3.2 Comparison with TLE

The comparison between the initial positions at the epoch of a number of TLE's and data generated with TLE's in the SGP4 propagator is presented in figure 4.7. The position of the satellite was propagated for a period of 28

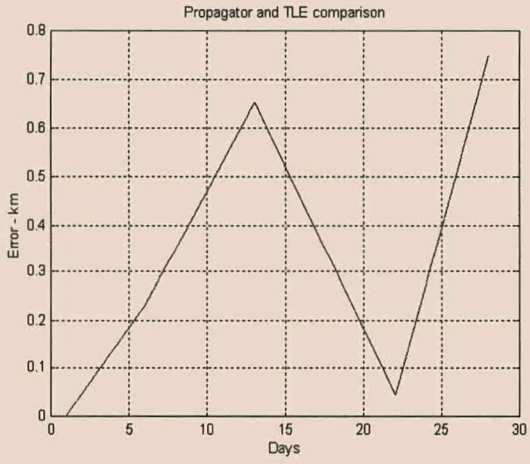

Figure 4.7: A comparison between the SGP4-predicted position of the satellite and the position predicted with new TLE's.

days using a TLE with epoch at the beginning of the evaluation period. It was compared to the positions predicted by TLE's generated during the evaluation period. The TLE's was used as a reasonably accurate—approximately 1 km accurate—indication of the position of the satellite at the epoch of the particular set of elements.

The results indicate a surprisingly small difference between the propagated position and that indicated by the TLE's updated during the evaluation period. These results could be due to the way in which the TLE's are generated with a least squares approximation. The method consists of using the latest available set of TLE's to predict the position of the satellite. These predictions are then combined with position measurements of the satellite in a least squares algorithm to determine an updated set of TLE's at a new epoch which best fits the previous TLE and the measurements.

From the above mentioned results it seems like the TLE-files did not need to be updated during the period of evaluation as the error between the position predicted with the initial TLE and that predicted by the updated TLE's at their respective epochs is very small. It could also indicate that the suggestion made in the previous paragraph concerning the quality of the TLE, was correct.

4.3.3 Comparison with STK

The comparison between the predictions made with Satellite ToolKit (STK) and data generated with TLE's in the SGP4 propagator is presented in figure 4.8.

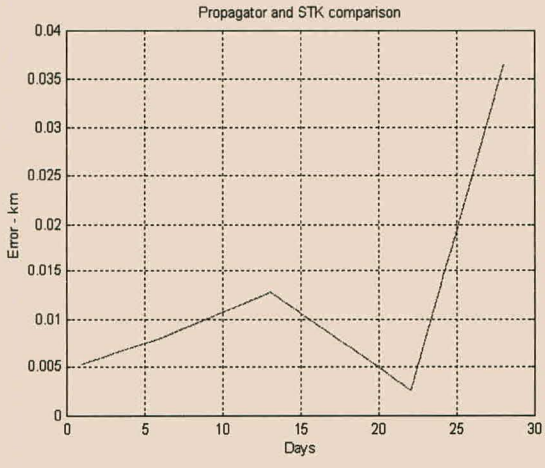

Figure 4.8: A comparison between the SGP4-predicted position of the satellite and STK predictions.

This evaluation was performed over the same period as the comparison with the TLE's. It is seen that the difference between the two predictions is approximately 36 meters after the 28 days of the evaluation. This indicates that the implemented SGP4 algorithm closely resembles the algorithm implemented in the industry standard STK[1].

[1]Refer to Carter [9].

Chapter 5

Conclusions and Recommendations

The objective of this study was to develop a simulation environment to simulate the orbital motion and the space environment experienced by Low Earth Orbit satellites. This simulation environment needed to be able to operate in a multi-computer setup. It required software that could provide the output data via a network (TCP/IP) connection. The nature of the output data had to be representative of the sensor data of the ADCS system of the SUNSAT micro-satellite in order to be used in a hardware-in-the-loop (HIL) simulation and for mission planning purposes. The connection between the orbital propagator and the HIL simulation is presented in figure 1.2. A propagation algorithm was selected which was well defined and easy to use while at the same time it provided the required accuracy of propagation. The main advantage of the selected propagation algorithm, the SGP4 algorithm, is the general availability of orbital elements which is generated specifically for use with this algorithm. The software structure which was selected paved the way for future developments and extensions which can enhance the capability of the developed product.

5.1 Summary of Research

In chapter 2 the criteria is stipulated against which the product of this study should be evaluated. The results which was obtained can be summarised as follows:

1. Research was performed in the field of orbital propagation and the space environment in Low Earth Orbit. This knowledge was essential for a successful mission in more than one way and was used for

    - accurately predicting the position of the satellite for the purposes

of antenna tracking and the calculation of the Doppler shift in radio frequency during a pass of the satellite over the groundstation,

- initial signal acquisition subsequent to launch,
- simulating the change in Sun-time (the position of the Sun with respect to the satellite) throughout the lifetime of the satellite in order to predict periods when high quality imaging sessions would be possible, as presented in Mostert et al. [25],
- trying to predict potentially hazardous events such as the satellite moving through the South Atlantic Magnetic Anomaly—which resulted in data loss onboard the satellite—and loss of communication due to interference from mountains surrounding the groundstation,
- trying to explain the failure of an action on board the satellite, for example, when the coastline should have been photographed, but the final image had only water in sight,
- predicting the position of the satellite for use in upgrading ADCS software,
- the evaluation of different orbit propagators.

2. It was specified that an orbit propagation environment should be developed which was as accurate as possible in its predictions, yet practical and easy to implement. This was achieved satisfactorily by using the SGP4 orbit propagation algorithm along with models of the space environment which have been proven accurate in the past. The term "*accurate*" indicates that results were required which were comparable to actual measurements taken in space. The onboard imaging activities were used as a guideline to determine the level of modelling accuracy that was required from the propagator. The measurement accuracy of the ADCS sensors determined the accuracy by which the modelling was performed. It was seen that the SGP4 algorithm is not a truly high accuracy propagation algorithm and that the initial conditions used in the SGP4 algorithm is of a limited accuracy due to the way it is determined. For this reason, better quality orbital predictions would be obtained by either using a numerical propagation algorithm or, even better, combining onboard sensor measurements with a numerical propagator in an extended Kalman filter.

3. It was required that the developed software had to distribute its data over a TCP/IP network. This objective was achieved and by carefully

selecting the architecture for the network connection, a number of possibilities for future developments to the software were created. The network connections were implemented as a client-server system. The server handles all computations and orbital elements while the clients only need to handle the data transmitted by the server and thus freeing it for other computationally intensive operations. It is possible for multiple users to obtain data from the server at the same time. The user interface for the client is of a general form that is not specific to the HIL setup and can be used by anyone who wants to do orbital propagation. This was illustrated when the software was used in a separate study to obtain orbital information for graphically displaying the position of the satellite.

5.2 The future

Due to the nature of the simulation environment, it can be extended to include a number of new features. The following group of features can be added without too much difficulty or change to the software.

- With the addition of a real-time kernel, the client-server topology can be extended to a real-time system. This will have a few advantages over the current system:
  - For a HIL simulation, the current system has the disadvantage that the client need to obtain the data before the simulation is started. It needs to be stored in a file from which it is read into memory for the duration of the simulation. When a real-time system is implemented, this could all happen real-time. When the server is started, it could synchronise the time via the Internet. Before the simulation is initiated, the client would synchronise its time with that of the server. At the initiation of the simulation, the server would calculate the required data (being either "real" time or simulation time) and at the specified time, transmit it to the client(s). This would add some flexibility to the system in that the client computer, which would be engaged in the HIL simulation, would eliminate disk I/O and would possibly have more computation time available.
  - Another advantage of a real-time kernel would be the simulation of constellations of satellites. Multiple clients could connect to the server with each client requesting data for a different satellite in the constellation. The data from the clients could then be used

to calculate the inter-satellite distances and communication times. The possibility of doing constellation control and simulating the motion of the satellites through this environment can be investigated. It may not in essence be necessary to use the client-server topology for the simulation of constellations, but the fact that the client-server-propagation tools do exist, creates interesting possibilities. An important fact that needs to be kept in mind when the system is extended to include real-time constellation simulations, is the scheduling of processes. Some thought will have to be given concerning the fact that in a multiprogramming environment, it cannot be predicted when a process will terminate. It will be essential that data for all the satellites are generated and that it is available at the "same" time for it to be combined.

- A Sun-Moon-Earth constellation for simulation of the phases of the Moon can be implemented. This will pave the way to answer questions concerning the phase of the Moon and determine whether a satellite would be able to determine the exact time of full Moon. This is of great importance to countries in the Middle East which determine some of their religious days from the phase of the Moon.

- Since the software was written in Delphi, the propagator can be encapsulated in component form. This will make it possible for users without extensive knowledge of orbital propagators to use it as a Delphi component without knowing any detail of its operation.

5.3 Conclusion

Extensive knowledge on orbit modelling was evaluated and documented so that the propagators could be used with confidence in a field of study which constituted a crucial segment of the groundstation operation of the SUNSAT microsatellite. The importance of accurate propagation and verification of the applicable models used in the practical simulations were observed. It was seen that analytical propagators are only of limited accuracy due to the difficulty in describing perturbations by means of analytical methods. This highlighted a problem with the SGP4 algorithm which is an analytical method and for which the orbital elements are only of limited accuracy and quickly degrades with time. When high precision propagation is required, it should be done with a numerical propagation technique which is accurate, but very computationally intensive, or a semianalytical technique which combines

the speed of the analytical techniques with the accuracy of the numerical techniques.

A simulation environment was developed to function in a multi-computer environment. This environment can be used to compute orbital ephemerides for multiple satellites and can distribute the ephemerides via a TCP/IP network to the users. The environment was developed with a generalised architecture that enables it to be used for multiple applications. This generalised architecture can be used to form the foundation for a simulation environment for a constellation of satellites.

A conceptual study was performed on the improvement of the accuracy of orbital predictions by combining onboard sensor measurements with a propagation algorithm in an extended Kalman filter. By comparing the propagation accuracy of propagation algorithms with results obtained from such filters which was found in the literature, it was seen that this method would significantly increase the accuracy of the predictions.

Bibliography

[1] *The Astronomical Almanac for the year 1999*, United States Naval Observatory, Washington DC,USA

[2] Bar-Itzhack, Y. and Shorshi, G. (1995), *Satellite Autonomous Navigation Based on Magnetic Field Measurements*, Journal of Guidance, Control and Dynamics, Vol. 18, No. 4, July-August 1995

[3] Barker, W.N., Casali, S.J. and Wallner, R.N. (1995), *The Accuracy of General Perturbations and Semianalytic Satellite Ephemeris Theories*, Paper AAS-95-432 presented at the AAS/AIAA Astrodynamics Conference, Halifax, Nova Scotia, Canada

[4] Bate, R.R., Mueller, D.M. and White, J.E. (1971), *Fundamentals of Astrodynamics*, Dover Publications, New York, USA

[5] Battin, R.H. (1987), *An introduction to the mathematics and methods of astrodynamics*, AIAA Educational Series, Washington DC, USA

[6] Beuche, F.J. (1986), *Introduction to physics for scientists and engineers — Fourth Edition*, McGraw-Hill, New York

[7] Brown, C.D. (1992), *Spacecraft Mission Design*, AIAA Educational Series, Washington DC, USA

[8] Cardoza, A. (1998), *SUNSAT—Mission Planning and Operations*, Electronic Systems Laboratory, University of Stellenbosch

[9] Carter, S., McLaughlin, C., Sabol, C. and Bir, M. (1995), *Spaceflight Dynamics Support for the Mightysat II.1 Hyperspectral Payload Operations*, Paper AAS-95-345 presented at the AAS/AIAA Astrodynamics Conference, Halifax, Nova Scotia, Canada

[10] Chao, C.C. (1979), *An Analytical Integration of the Averaged Equations of Variation Due to Sun-Moon Perturbations and Its Applications*, The Aerospace Corp., Tech. Rept. SD-TR-80-12

[11] Chobotov, V.A. (1991), *Orbital Mechanics*, AIAA Educational Series, Washington DC, USA

[12] De Villiers, R. (1994), *The blockdiagram simulation of satellite systems*, M.Eng thesis, University of Stellenbosch

[13] Du Plessis, J.A.F. and Engelbrecht, J.A.A. (1999), *An ADCS simulation environment for SUNSAT.*, ESL internal document, Stellenbosch

[14] Du Toit, D.N.J. (1997), *Low Earth Orbit Satellite Constellation Control using Atmospheric Drag*, Ph.D. thesis, University of Stellenbosch

[15] Engelbrecht, J.A.A. (1999), *A Hardware-in-the-loop Simulation Facility for the Attitude Determination and Control System of SUNSAT*, M.Sc.Eng thesis, University of Stellenbosch

[16] Escobal, P.R. (1965), *Methods for Orbit Determination*, Krieger Publishing Company, Malabar, Florida, USA

[17] Franklin, G.F., Powell, J.D. and Workman, M. (1998), *Digital Control of Dynamic Systems - Third Edition*, Addison Wesley, Menlo Park, California, USA

[18] Jacobs, M.J. (1995), *A Low Cost, High Precision Star Sensor*, M.Eng thesis, University of Stellenbosch

[19] Jones, J.P. and Beckerman, M. (1999), *Analysis of Errors in a Special Perturbations Satellite Orbit Propagator*, Oak Ridge National Laboratory, Oak Ridge, Tennessee, USA, Report nr. ORNL/TM-13726

[20] Jordaan, L.J. (1996), *An extended Kalman filter observer for autonomous orbit determination*, M.Eng thesis, University of Stellenbosch

[21] Knowles, S.H. (1995), *a Comparison of Geocentric Propagators*, Paper AAS-95-429 presented at the AAS/AIAA Astrodynamics Conference, Halifax, Nova Scotia, Canada

[22] Meeus, J. (1991), *Astronomical Algorithms*, Willman-Bell Inc., Richmond, Virginia, USA

[23] Meraim, J.L. and Kraige, L.G. (1997), *Engineering Mechanics, Dynamics—Fourth Edition*, John Wiley, New York

[24] Milne, G.W. (1992), *SUNSAT—Technical Specification*, ESL internal document, Stellenbosch

[25] Mostert, S., Cronje, T. and Du Plessis, F. (1998), *The SUNSAT Micro Satellite Program: Technical performance and limits of imaging micro satellites*, Proceedings of the fourth International Symposium for Small Satellites, Systems and Services, Antibes Juan-les-Pins, France

[26] Nagarajan, N., Seetharama Bhat, M. and Kasturirangan, K. (1991), *A Novel Autonomous Orbit Determination System using Earth Sensors (Scanner)*, Acta Astronautica, Vol. 25, No. 2

[27] Pocha, J.J. (1987), *An introduction to mission design for geostationary satellites*, D.Reidel Publishing Company, Dordrecht, The Netherlands

[28] Psiaki, M.L. (1995), *Autonomous Orbit and Magnetic Field Determination Using Magnetometer and Star Sensor Data*, Journal of Guidance, Control and Dynamics, Vol. 18, No. 3, May-June 1995

[29] Psiaki, M.L. (1999), *Autonomous Orbit and Magnetic Field Determination Using Magnetometer and Sun Sensor Data*, Journal of Guidance, Control and Dynamics, Vol. 22, No. 2, March-April 1999

[30] Seidelmann, P.K. (1992), *Explanatory Supplement to the Astronomical Almanac*, University Science Books, Mill Valley, California, USA

[31] Shum, C.K., Ries, J.C., Abusali, P.A.M., Casey, J.M. and Tapley, B.D. (1995), *Application of Precision Orbit Determination Techniques to Space Object Tracking and Radar Calibration*, Paper AAS-95-386 presented at the AAS/AIAA Astrodynamics Conference, Halifax, Nova Scotia, Canada

[32] Steyn, W.H. (1990), *Attitude Control Algorithms and Simulation Programs for Low Earth Orbit Spacecraft*, M.Sc. thesis, University of Surrey, UK

[33] Steyn, W.H. (1995), *A Multi-mode Attitude Determination and Control System for Small Satellites*, Ph.D. thesis, University of Stellenbosch

[34] Tanenbaum, A.S. (1992), *Modern Operating Systems*, Prentice Hall, London

[35] Vallado, D.A. and McClain, W.D. (1997), *Fundamentals of Astrodynamics and Applications*, McGraw-Hill, New York

[36] Wertz, J.R. (1978), *Spacecraft Attitude Determination and Control*, D.Reidel Publishing Company, Dordrecht, The Netherlands

[37] Wertz, J.R. and Larsson, W.J. (editors) (1992), *Space Mission Analysis and Design*, published jointly by Microcosm Inc., California, USA and Kluwer Academic Publishers, Dordrecht, The Netherlands

Electronic references

[100] Bohn, P.M. (1999), Personal correspondence, Ørsted Mission Control, Terma Elektronik AS, Denmark

[101] Dawson, S. (1999), Personal correspondence, Microcosm Inc.

[102] *The European Space Agency's Space Environments and Effects Analysis Section*, http://www.estec.esa.nl/wmwww/wma/ecss.html

[103] Hoots, F.R. and Roehrich, R.L. (1980), *SPACETRACK REPORT NO.3: Models for Propagation of NORAD Element Sets*, http://www.celestrak.com/NORAD/documentation/index.html

[104] Kelso, T.S. , http://www.celestrak.com

[105] Muraoka, H., Cohen, R.H., Ohno, T. and Doi, N. (1998), *Aster Observation Scheduling Algorithm*, SpaceOps 98 Conference, http://yyy.tksc.nasda.go.jp/SpaceOps/paper98/track2/track2.html

[106] Vallado, D.A. (1999), Personal correspondence

Appendix A

Spacecraft Systems Overview

This appendix is an adapted version of the summary done by Cardoza [8] supplemented from Milne [24]. Figure A.1 is a diagram of SUNSAT after second stage separation from the Delta II launch vehicle, but before deployment of the boom. The subsystems are the ADCS, OBC1 (Onboard Computer 1) and OBC2 (Onboard Computer 2), TCMD (Telecommand), TLM, IMS (Image Subsystem) or optics, GPS, Communication and SPS (SUNSAT Power System).

A.1 ADCS

A T800 transputer based computer is responsible for ADCS processing as it has a powerful floating-point instruction set. SGP4 propagation algorithms are used to do satellite position calculations. The ADCS consist of the following subsystems:

A.1.1 Star Sensors

The star sensor enables the ADCS to provide extra fine stability during imaging operations. Two star sensors are included, one mounted on the top plate and the other one fixed on the boom along with the tip mass. Only one of the sensors will normally be used at a time. These star sensors use CCD's (Charge Coupled Device). A complete onboard star catalogue is included and therefor no future updates need to be made. The attitude of the satellite at the time of the stellar sighting need to be available to the star sensor identification software. This is calculated by onboard flight software that extrapolates satellite motion from an initial attitude and set of Keplerian elements.

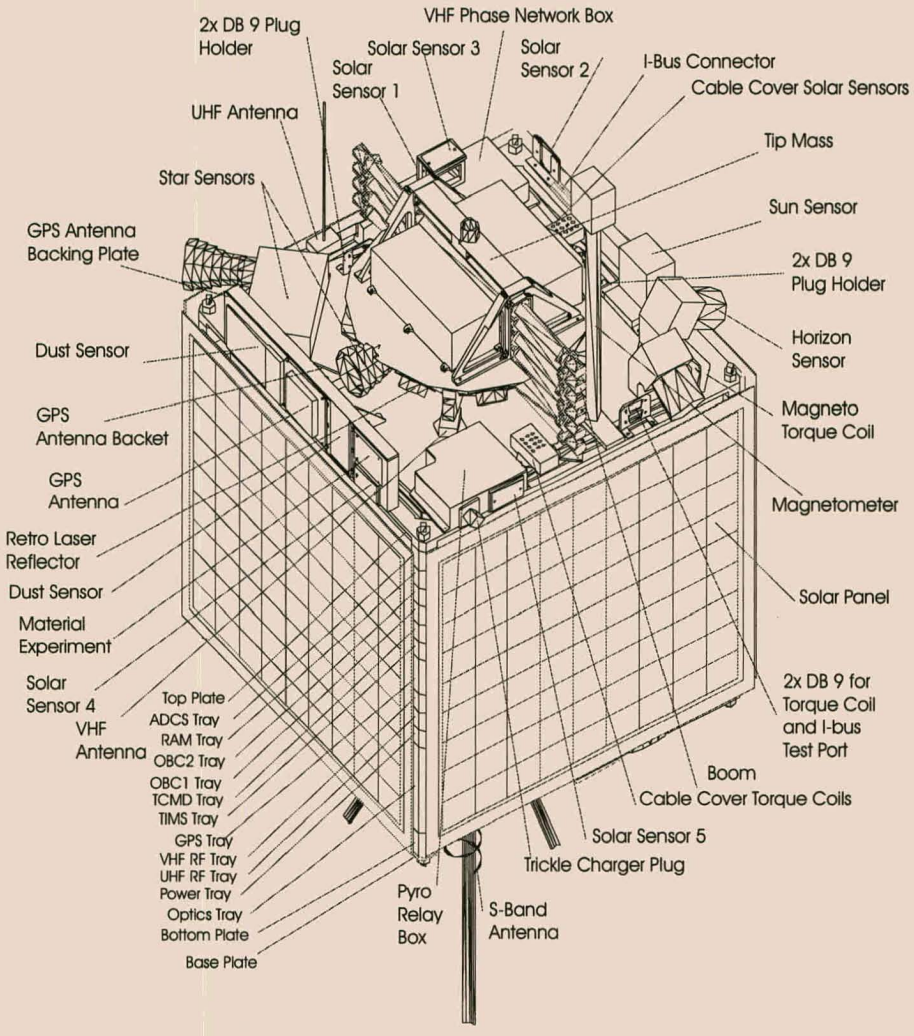

Figure A.1: SUNSAT Satellite - Configuration before boom deployment

A.1.2 Two-Axis Horizon Sensor

Two orthogonal linear CCD and lens assemblies look below the local horizon level, to obtain orthogonal measurements of the sunlit earth horizon.

A.1.3 Sun Sensors

The sun sensor uses a linear CCD sensor that is externally mounted on the top panel of the satellite. Its purpose is to measure the orientation of the sun about the satellite's Z-axis.

The fine sun sensor faces the sun during imaging operation to provide accurate yaw attitude information. When the satellite is spinning, sensor

data will be available on average only 20% of each orbit.

Six cosine-law solar cells mounted on each spacecraft facet are used to obtain full attitude information to within 5° with the aid of the sun and the satellite orbital model. Surface temperature of each cell is also measured to make the necessary sensitivity corrections to all measurements.

A.1.4 Reaction Wheels

The 3-Axis reaction wheels provide accurate and fast attitude corrections that are needed by the pushbroom imager. Precise angled manoeuvres from any known attitude are possible. The z-axis reaction wheel is used to align the satellite before imaging sessions (Steyn [33]).

A.1.5 Magneto Torque Coil

The 3-Axis magnetorquer air coils are initially used for detumbling and attitude capture. These coils wound into channels around the X/Y solar panels and around the Z facets. Magnetic torquing is used as the primary active stabilisation method to do libration damping, Z spin rate control and momentum dumping of reaction wheels. It is highly reliable since no moving parts are used and will be used as backup for possible reaction wheel failure.

A.1.6 Three-Axis Fluxgate Magnetometer

The magnetometer is used to measure the strength and direction of the geomagnetic field vector. This information is used to calculate the magnetic torque and to obtain full attitude data by comparing the measurements to geomagnetic field models. Attitude data from the magnetometer is available throughout the orbit, but is plagued by inaccuracies due to errors in the geomagnetic field models.

A.1.7 Tip Mass and Boom

The 2.3 meter long gravity gradient boom is a passive means to ensure satellite nadir. One of the two star cameras is situated on the boom together with a tip mass of 6.0 kg.

A.2 Communications Subsystem

There are four frequency bands for communicating with SUNSAT. Under normal operations the two uplink bands are on VHF (145 MHz) and L-band

(1.265 GHz), and the two downlinks are on UHF (435 MHz) and S-band (2.250 GHz).

Two different sets of antennae are used for VHF communication. The one antenna is for use on commercial frequencies (COM) and the other is for amateur packet communications (AM). Two different sets of antennae are used for UHF communication. As in the case of the VHF communication system, one antenna is used on commercial frequencies and the other is used for amateur packet communications. The UHF system also contains a QPSK (Phase Shift Key) modem for high-speed data communications. Data can originate from the RAM tray or from the DSP on the OBC1 tray.

L-band frequencies are only used for uplinks to SUNSAT. This uplink can be used for high speed data communications (2M baud), low speed telecommands (1200/9600 baud) or in a transponder configuration.

S-band frequencies are only used for downlinks from SUNSAT. The downlink can be used for high-speed data communication, a colour PAL video link, or as the downlink in a transponder configuration. The S-band system also contains a QPSK modem for high-speed data communications.

All the analogue baseband signals are fed to the modems tray where the signals are multiplexed and routed to other subsystems onboard SUNSAT. These include seven 1200 baud FSK (Frequency Shift Key) modems, two 9600 baud PAM (Pulse Amplitude Modulated) modems and two audio busses.

A.3 Telecommand (TCMD)

Telecommands to be executed onboard SUNSAT will be one of two types:

- ATC (Absolute Time Command) that is issued from the TCMD system terminal on the ground station or onboard subsystems for immediate execution on SUNSAT.
- RTCS (Relative Time Command Sequence), that is issued in the form of a DIARY command file, which includes a sequence of commands, for execution at a specified time.

The TCMD subsystem listens for telecommands on the following channels:

Modem Signal	Baud Rate	Audio Signal	From RX	Default Frequency
RXD1	1200	ARX5	RX1	145.825 MHz
RXD2	1200	ARX3	RX3	436.291 MHz
RXD9	9600	ARX6	Selectable, default RX6	1.265 GHz
RXD10	9600	ARX22	Selectable, default RX2	145.850 MHz

A.4 TLMS

The TLMS (Telemetry System) constructs a frame of data, which may contain up to 255 bytes of data, every 2.56 seconds. OBC1 or OBC2 forward this data for storage to the RAM disk at a rate of 1200 baud or 9600 baud.

A.5 OBC's

At the heart of OBC1 and OBC2 are the INTEL 80C188 and INTEL 80386SX CPU's (Central Processing Units), respectively. General flight management tasks such as scheduling, CCD imager control and communications management are performed by OBC2. Both have access to all peripherals, but OBC2 is the preferred flight controller.

A T800 transputer is dedicated to the ADCS, but its tasks can be taken over by the 386 in case of failure. Seven additional embedded micro controllers provide further support for telemetry, TCMD, power control and ADCS.

A.6 SPS

The SPS (SUNSAT Power System) consists of four body mounted solar arrays and re-chargeable Nickel-Cadmium batteries. Battery lifetime is estimated at 4-5 years. Solar panels are connected to the battery charge regulators and directly to the power bus on the satellite. Distributed regulators ensure that the required voltages are supplied to each of the subsystems. It has a peak power capability of 90 W to handle peak loads during image data transmissions. Depth of discharge of the batteries are limited to 20 % to ensure that the predicted lifetime is reached.

A.7 Payloads

A.7.1 Pushbroom Imager

The high-resolution imager, one of the main payloads, produces stereoscopic, tricolour images. Pixel size was chosen as 15 m square with a swath width of at least 50 km, using the pushbroom scanning method. Output from each of the three linear CCD's, each covering a separate spectral band, are digitised to 8 bits each, resulting in a 24-bit colour picture. The three video channels are implemented independently to reduce the chance of total system failure.

Up to five single colour frame images may be stored onboard, depending on compression.

A.7.2 GPS

NASA's TurboRogue/Turbostar GPS receiver and laser retro-reflector will support experiments in gravity recovery, atmospheric occultation science and ionospheric tomography. Telemetry and command are implemented via a RS422 link from the onboard computers. The GPS receiver provides three-dimensional position and velocity of the satellite together with UTC (Universal Time Coordinate) time all in a digital format to the TCMD. Accuracy of position information is within 60 m, which can subsequently be re-calibrated to provide 1 m accuracy. The GPS receiver has two operational modes, namely a high power mode and a low power mode.

A.7.3 Amateur Packet Radio Services

Onboard software is available to enable amateur packet radio communication. Amateur packet radio communication uses a SCC (Serial Control Card) to do frame synchronisation, bit stuffing and CRC (Cyclic Redundancy Code) checking. The AX.25 (Amateur X.25) communication protocol is run on top of the SSC hardware. FTL0 (File Transfer Level 0), a protocol used for file transfer, is combined with PBP (PACSAT Broadcast Protocol) to form the PACSAT protocol suite. This protocol suite enables store-and-forward applications such as PBBS (Packet Bulletin Board Services) and file transfers via AX.25.

A.7.4 School Experiments

SUNSAT will be flying with two school-projects on board. The first experiment is a CMOS Radiation Experiment developed by the Rhenish Girls High School in Stellenbosch. The experiment monitors radiation damage to CMOS electronic equipment. Its purpose is to investigate the effect of radiation on CMOS logic gates that are used on several of the circuit boards onboard the satellite. The second school experiment, developed by George Campbell Technical High School in Durban, consists of a sensitive microphone, which will pick up vibrations in the structure of the satellite, and a temperature sensor, which will measure the temperature on the inside of the tray.

Although not part of the schools project, two other external experiments were included onboard the satellite. A dust particle impact detection experiment was submitted by the Cape Town Peninsula Technikon. Its purpose

is to detect and measure the frequency of small meteorite impacts on the satellite by using sensors mounted on the satellite's exposed top plate. The Universiti Kebangsaan Malaysia submitted a materials exposure experiment to measure the temperature and conductivity in space of a high temperature superconductor and a glassy carbon sample developed by its Physics department.

Appendix B

Reference systems

In order to describe the position and orientation of an object in space, it is necessary to define a coordinate system towards which the movement of the object can be referenced. This chapter will address all the coordinate systems and the transformations between the coordinate systems used throughout this study. The study of coordinate systems and transformations between these systems requires that a system for the measurement of time should also be defined as time plays an integral part in some of the transformations. As the field of coordinate and time systems are a very wide field of study, this chapter will only address the systems that were used throughout this study. For a complete explanation of coordinate systems used in space flight, refer to Vallado [35], Wertz [36], Escobal [16], Chobotov [11] or any other text on astrodynamics and space flight. Vallado, Wertz and especially Seidelmann [30] handle the topic of time systems and the calculation of time. Seidelmann contains a comprehensive study on this topic, but may be difficult to comprehend for first-time readers. Vallado has made excellent work of explaining the concepts introduced by Seidelmann without too much repetition. It is advised that the work of Vallado should be used along side that of Seidelmann in order to obtain a complete picture of coordinate and time systems.

B.1 Coordinate Systems

The Earth and its orbit around the Sun are used as a reference for most Earth-based coordinate systems. The ***ecliptic*** is described as the mean plane of the Earth's orbit around the Sun. It is defined as the mean plane because the Earth does not move exactly on the ecliptic plane throughout its orbit around the Sun. The ***equatorial plane*** extends the equator from the Earth.

The angle between the Earth's equatorial plane and the ecliptic is called the ***obliquity of the ecliptic,*** ϵ. The value of this angle is approximately 23.5° as it varies slightly over time due to perturbations in the orbit of the Earth. The line of intersection between the equatorial plane and the ecliptic is called the ***line of nodes*** and is used as a principal direction in defining some coordinate systems. The Sun passes through the intersection twice a year with the two passages being called the ***equinoxes***. When the Sun rises from South to North across the equatorial plane in March every year, it is called the ***vernal equinox***. If the Sun was modelled as a satellite of the Earth, the vernal equinox would be the ascending node of the Sun in its orbit around the Earth. The direction of the vernal equinox is designated by Υ and is often referred to as the *first point of Aries.* This direction is used as a basis for an inertial coordinate system, but due to precession and nutation of the Earth, it is not truly inertial in its orientation. A plane that is normal to the fundamental plane of the coordinate system is called a ***meridional plane*** or simply a meridian. The definition of a meridian will differ slightly between coordinate systems.

When a rectangular coordinate system is defined, it is necessary to specify its *origin, fundamental plane, primary axis* and the *positive direction* for each one of the axis. The following sections will describe a number of coordinate systems in terms of these concepts.

B.1.1 Earth Centred Inertial (ECI)

This system originates at the center of the Earth, as its name indicates, and is designated either by the abbreviation ECI, or by the letters IJK. As indicated in figure B.1, the fundamental plane is the Earth's equator. The $\vec{I}$ axis is the primary axis and points towards the vernal equinox, the $\vec{J}$ axis is 90° to the east of the $\vec{I}$ axis in the equatorial plane and the $\vec{K}$ axis extends through the North Pole. This coordinate system does not rotate, but is assumed to be fixed in inertial space. It is one of the most common reference systems used in astrodynamics. Due to the precession and nutation of the Earth, this system is not really fixed in inertial space and it actually moves over time[1]. For this reason, it is necessary to refer this system to a specific time at which the equator's and equinox's orientation is precisely known. Such a time is 12:00 noon on January 1, 2000, or ***J2000***. Therefore this coordinate system is often called J2000-ECI or simply the J2000 system and it is considered *sufficiently inertial* to be used for applications requiring an inertial reference frame. The term *sufficiently inertial* means that New-

[1]See section B.2.1 for a discussion on precession and nutation.

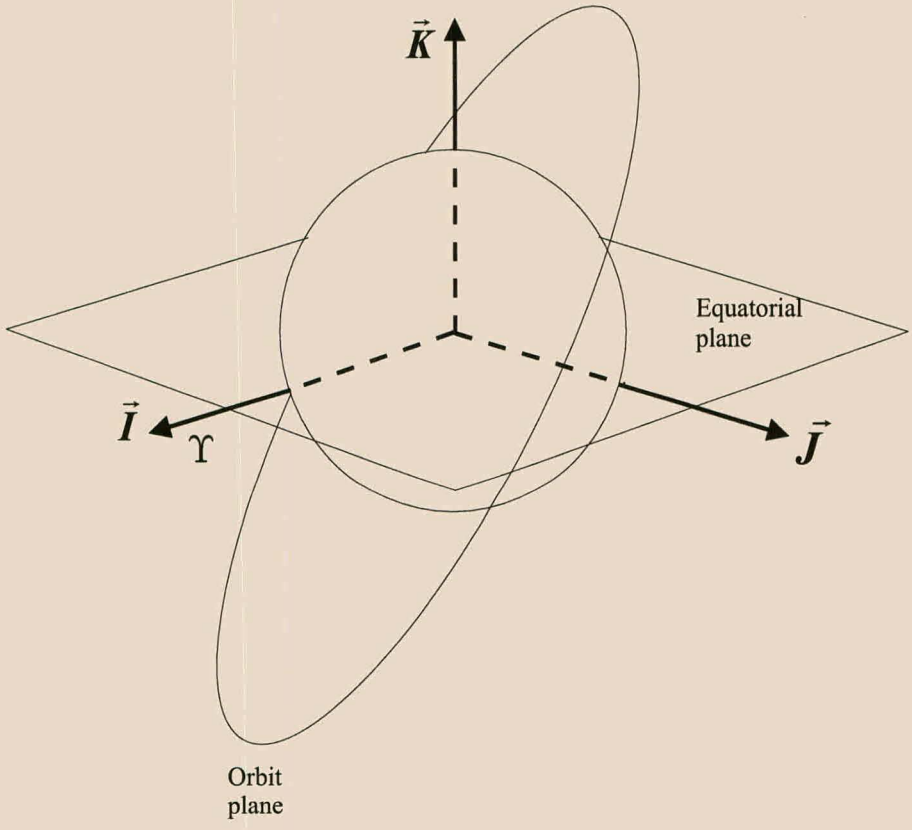

Figure B.1: The Cartesian ECI coordinate system.

ton's laws of motion are valid in this system. By using a set of ***reduction formulas***[2] observations at other times can be referred to this epoch. It should also be noted that simply specifying a coordinate system as ECI is not an accurate enough description since the direction of the vernal equinox depends on time. The ***epoch*** or reference time should always be included in the description of the coordinate system. The Earth Centred Inertial system is often designated by its older ***B1950*** epoch, and care should be taken when transforming between coordinate systems in which the epoch differ. Inertial coordinate systems that are not referred to the J2000 epoch but to a specific time, are called ***true-of-date*** inertial frames since they refer to the true orientation of the equator and equinox on that date. These systems will not be aligned with the J2000-ECI system and measurements—even if it is the same ones—described in a true-of-date system will differ from those described in the J2000-ECI system.

In the ECI reference frame position and velocity are usually expressed

[2]See Vallado [35] and Seidelmann [30] for a thorough discussion on reduction formulas.

in terms of vectors within the IJK Cartesian coordinate system and the first derivatives of these vectors. The state vector obtained in this reference system is designated by

$$\mathbf{x} = [x \quad y \quad z \quad v_x \quad v_y \quad v_z] \tag{B.1}$$

An alternative way of defining the position and velocity of an object in the ECI system is to define it in terms of spherical coordinates. The three variables that are used to define the position of an object is the ***right ascension*** (α), ***declination*** (δ) and ***radial distance*** (r). The orientation of these variables is indicated in figure B.2. The right ascension is the an-

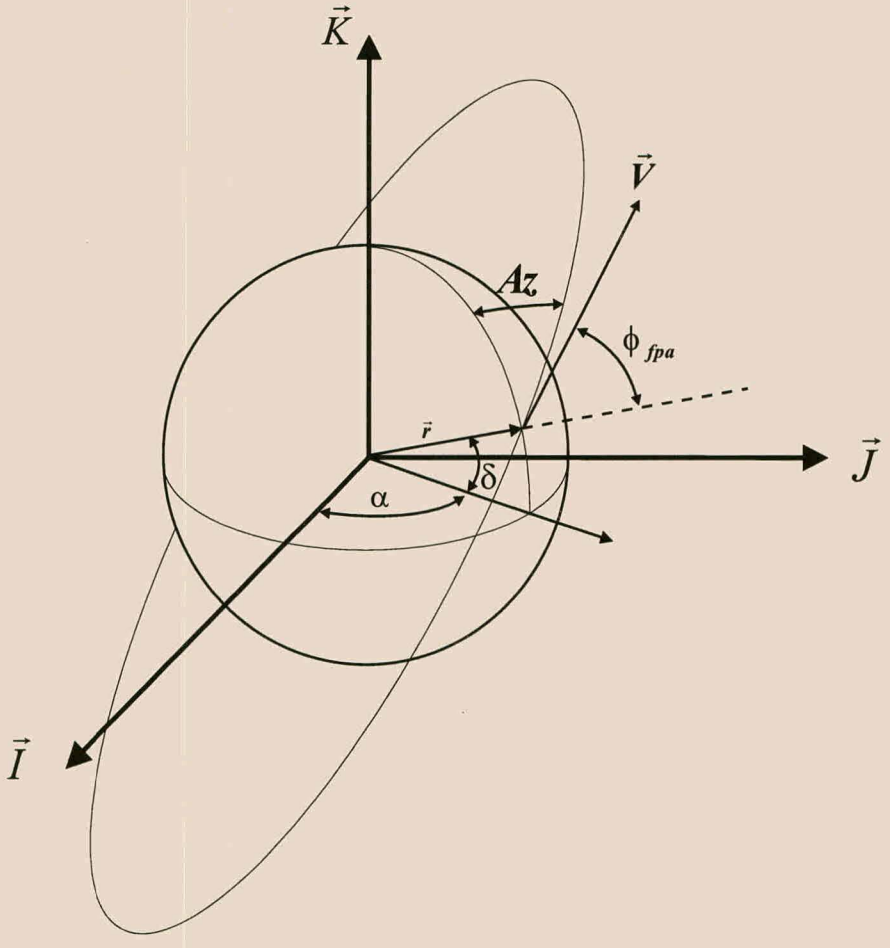

Figure B.2: The spherical ECI coordinate system.

gle measured eastward in the equatorial plane from the vernal equinox to a plane—the meridional plane—which is normal to the equator and contains the object under investigation. The declination is the angle between

the equatorial plane and the object measured in the meridional plane. The radial distance is simply the magnitude of the Cartesian position vector of the object. The velocity of the object in spherical coordinates is defined in terms of the ***inertial speed,*** (V), the ***flight-path angle,*** (ϕ_{fpa}) and the ***azimuth angle***(Az). The inertial speed is the magnitude of the inertial velocity vector as it was measured in the Cartesian system. The flight-path angle is the angle between the position vector of the object, $\vec{r}$, and the velocity vector of the object, $\vec{v}$. The azimuth or heading angle is the angle between the projection of the inertial velocity vector onto the local geocentric horizontal plane and the northerly direction, measured in a clockwise direction.

B.1.2 ECEF Coordinate System

The ***Earth-Centred , Earth-Fixed Coordinate System***, ECEF, is originated at the centre of the Earth, but it rotates with the Earth. The main difference between this system and the ECI system is that the primary axis is always aligned with a meridian that is fixed on the Earth. This meridian is usually the Greenwich meridian resulting in the coordinate system sometimes being called the ***Earth-Fixed Greenwich,*** EFG, coordinate system. Positions in this coordinate system can be specified either in rectangular Cartesian coordinates (x, y, z) where the x-axis is the primary axis, or in spherical coordinates. Spherical coordinates are presented in either the ***geocentric*** coordinate system or the ***geodetic*** coordinate system. The geocentric system is defined with the assumption that the Earth is a perfect sphere and consists of ***latitude,*** ϕ', ***longitude,*** λ', and ***radial distance,*** ρ. The longitude is measured positively to the east from Greenwich and ranges between $\pm 180°$. Latitude is measured from the equator $(0°)$ to $\pm 90°$, positively to the north. The radial distance is the magnitude of the Cartesian position vector. The geodetic coordinate system differs from the geocentric system in that it refers to a model of the Earth that is a spheroid and not a perfect sphere in describing the position of an object. It uses ***geodetic latitude,*** ϕ, ***geodetic longitude,*** λ, and ***geodetic height,*** h, as coordinates. Geodetic longitude is equal to geocentric longitude. Geodetic latitude differs from geocentric latitude in that it refers to the angle between the vector normal to the spheroid and the equatorial plane. The two definitions of latitude is illustrated in figure B.3. The two values may differ by up to 10 minutes of arc (20 km in position) in mid-latitudes. Geodetic height is the distance above the spheroid measured along the normal to the spheroid. The Global Positioning System (GPS) indicates position in the geodetic coordinate system. The position-coordinates on most maps are also indicated

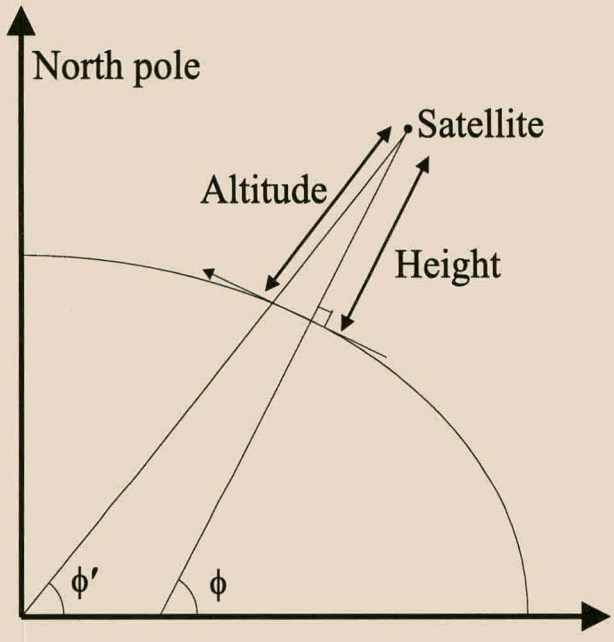

Figure B.3: The difference between the geodetic and geocentric coordinate systems.

in this coordinate system. The transformation between the two coordinate systems is described in section B.3.

B.1.3 Perifocal Coordinate System, PQW

The ***perifocal coordinate system*** is a convenient system for describing satellite observations. The orientation of the coordinate system is indicated in figure B.4. It is a right-handed coordinate system that has the satellite's orbital plane as the fundamental plane. The origin of this system is at the center of the Earth. The $\vec{P}$ axis point towards perigee, the $\vec{Q}$ axis is 90° from the $\vec{P}$ axis in the direction of motion and the $\vec{W}$ axis is normal to the orbit and it completes the right-handed coordinate system. This coordinate system can be described as an inertial system in that it maintains its orientation towards perigee in the orbital plane. Perturbative forces, which act to change the orientation of the orbital plane, will also change the orientation of this coordinate system in inertial space. This system will be used for the transformation from the classical orbital elements to the ECI coordinate system.

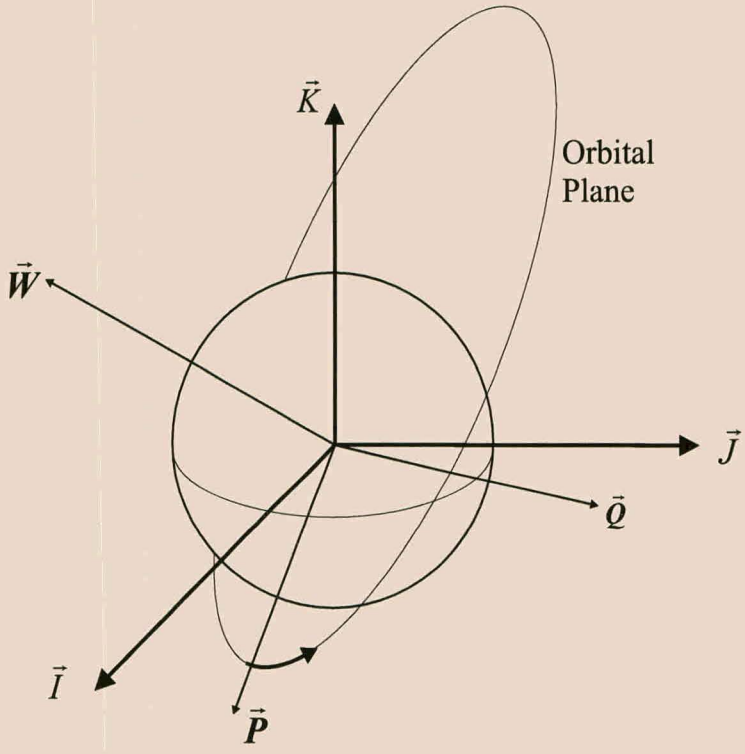

Figure B.4: The perifocal (PQW) coordinate system.

B.1.4 Topocentric Horizon Coordinate System, SEZ

The topocentric horizon coordinate system, SEZ, is very useful for defining observations of satellites and is often used in sensor systems. This system is defined at a particular site on Earth as illustrated in figure B.5. The local horizon is the fundamental plane. The $\vec{S}$ axis always points directly south from the site. The $\vec{E}$ axis points east from the site and is undefined for the North or South Pole. The $\vec{Z}$ (zenith) axis points radially outward along the site's position vector normal to the fundamental plane. This coordinate system is used to define "look angels" which is used to view satellites or celestial bodies from a groundstation. The ***azimuth angle*** is the angle in the fundamental plane measured clockwise from north to the location beneath the satellite. It usually assumes values between 0° and 360°, but other conventions do exist. The ***elevation angle*** is the angle measured perpendicular from the local horizon to the position of the satellite. Elevation angles assume values in the range form −90° to 90°. Objects that are above the horizon have positive values of elevation and objects below the horizon have negative values of elevation.

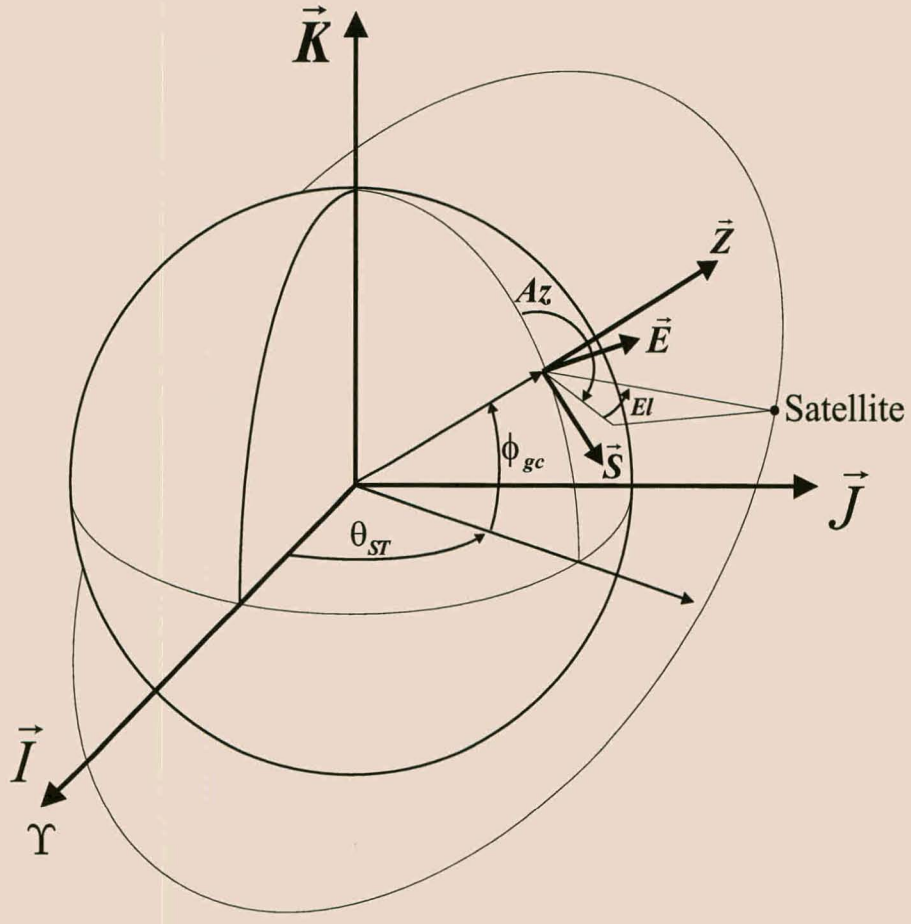

Figure B.5: The topocentric horizon coordinate system.

B.2 Time

In order to accurately describe an event, it is necessary to refer it to the time or ***epoch*** of its occurrence. In order to accurately describe the epoch of an event, it is necessary to be able to accurately measure a time interval and have a fundamental epoch from which the intervals can be counted. From ancient times, the day was the fundamental unit for measuring time. In modern times the motion of the Sun is still used to define time, but the process of measurement of solar time has been refined to satisfy the need for very accurate time measurements. The different needs in terms of accuracy resulted in the four systems of timekeeping that is currently in use. The four systems are ***sidereal time***, ***solar time***, ***dynamical time*** and ***atomical time***.

B.2.1 Precession and Nutation

The equatorial plane of the Earth and the ecliptic plane are used to define an inertial coordinate system, but both planes are not really fixed in inertial space. Perturbative forces acting on the Earth cause the equator to experience a wobbling movement over a period of time and it also results in a secular change in the direction of the vernal equinox. This motion of the Earth introduces errors into the historical method of timekeeping, which was based on observations of the celestial bodies. The result is that if an accurate determination of time is required, the effects of the precession and nutation of the rotational axis of the Earth need to be taken into account.

The gravitational fields of the Sun and the Moon exercise a torque on the equatorial bulge of the Earth. This force combined with the forces applied by the gravitational fields of the other planets in the solar system has the effect that the Earth's axis of rotation experiences a slow drift or ***precession*** as displayed in figure[3] B.6. This motion has a period of 26000 years.

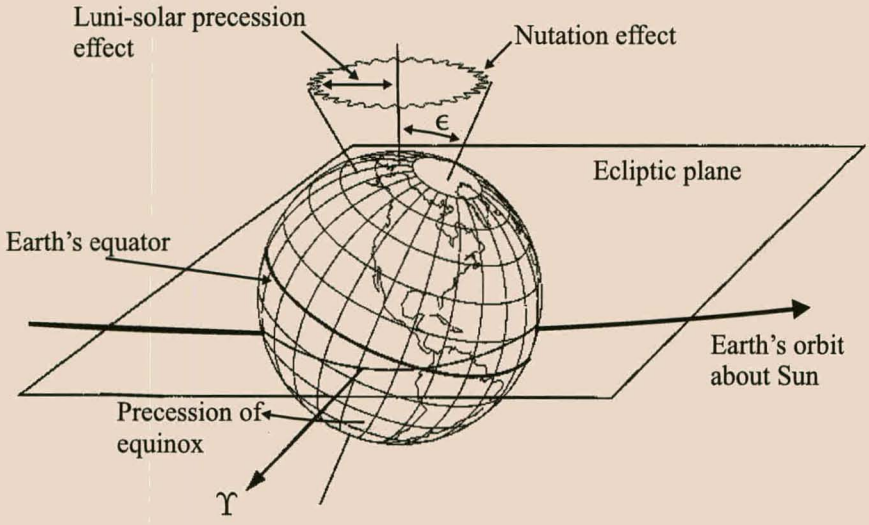

Figure B.6: Precession and nutation of the Earth's rotational axis.

The obliquity of the ecliptic (23.5°) causes the precession of the Earth's axis of rotation to trace out a rough circular shape over each period of rotation. Another effect is that the vernal equinox slowly regresses—move in a westerly direction—along the ecliptic plane. Due to the movement of the vernal equinox, the observed coordinates of celestial bodies continuously change over time. Therefore it is necessary to define the time of observation or the

[3]Image taken from Vallado [35].

epoch of the coordinate system for the observation that was made in order to be able to determine the exact observed position of the celestial body some time after the observation.

The Moon produces an additional torque on the equatorial bulge of the Earth that results in the Earth experiencing ***nutation***. This torque is the result of a very complex superposition of forces caused by the inclination (5°) of the Moon's orbit to the equator and the precession of the Moon's orbit due to solar perturbations. The nutation causes a periodic oscillation of the rotational axis of the Earth around its mean position as indicated in figure B.6. This periodic oscillation advances around the pole of the ecliptic due to the precession of the rotational axis of the Earth.

The motion of the Earth because of nutation can be partitioned into two components, one parallel to the ecliptic and one perpendicular to the ecliptic. The component parallel to the ecliptic is denoted by $\Delta\psi$ and is called ***nutation in longitude***. The component perpendicular to the ecliptic is denoted by $\Delta\epsilon$ and is called the ***nutation in obliquity***. The values of $\Delta\psi$ and $\Delta\epsilon$ are needed to determine the apparent (true) position of a celestial body and for the calculation of apparent sidereal time[4]. Seidelmann [30] supplies approximate procedures for the calculation of the nutations in longitude and obliquity as

$$\begin{aligned} \Delta\psi &= -0.0048^\circ \sin(125.0^\circ - 0.05295^\circ d) \\ &\quad -0.0004^\circ \sin(200.9^\circ + 1.97129^\circ d) \\ \Delta\epsilon &= +0.0026^\circ \sin(125.0^\circ - 0.05295^\circ d) \\ &\quad +0.0002^\circ \cos(200.9^\circ + 1.97129^\circ d) \end{aligned} \tag{B.2}$$

where d is the number of days from Julian day 2451545.0. Equation B.2 is called an approximate calculation of the two nutation terms because it consists of only the dominant terms of a series of terms, but it is still accurate to about 1 second of arc.

From equation B.2 the true obliquity of the ecliptic can be calculated from

$$\epsilon = \epsilon_0 + \Delta\epsilon \tag{B.3}$$

where ϵ_0 is the mean obliquity of the ecliptic that is given by

$$\epsilon_0 = 23^\circ 26' 21.''448 - 46.''8150\ T - 0.''00059\ T^2 + 0.''001813\ T^3 \tag{B.4}$$

T is calculated from equation B.6.

[4]See section B.2.3 for the calculation of apparent sidereal time

B.2.2 Solar Time

Solar time is loosely defined as successive transits of the Sun over a local meridian. ***Apparent solar time*** is the observation of the true motion of the Sun from a particular location. The length of an apparent solar day varies due to the motion of the Earth in an orbit with non-zero inclination and eccentricity. This apparent irregular motion of the Sun—actually the Earth in its orbit around the Sun—makes it difficult to use the Sun as an accurate reference for timekeeping. It necessitated the definition of a *fictitious mean Sun* that represents the position of the Sun as if it were travelling at a constant speed in the equatorial plane throughout the year. This averaged motion of the Earth resulted in the concept of ***mean solar time***. Mean solar time at Greenwich is defined as ***universal time,*** UT. The difference between mean and apparent solar time is called the ***equation of time***.

Universal time must be divided into three values for the purpose of precise timekeeping. These values are ***UT0, UT1*** and ***UT2***. UT0 is the solar time observed at a particular ground station. Because the position of the Sun cannot be measured as accurately as the position of the stars, UT0 is in fact determined from the sidereal time at a specific groundstation. UT1 is determined by correcting UT0 for the irregularities in the motion of the Earth and making it independent of the position of the observer. UT2 is obtained by correcting UT1 for seasonal variations in the orbit of the Earth. UT2 is not commonly used in calculations. ***Coordinated universal time, UTC*** is the time system most commonly used throughout the world for the purpose of civilian timekeeping. It is calculated by combining atomical time and universal time into a value that is accurate to the standards of atomical time and still correct when compared to the motion of the Earth.

Referring to figure B.7, an exaggerated view can be seen of how solar time is measured compared to sidereal time, which will be introduced in section B.2.3. The Greenwich meridian was chosen as a fixed point for determining solar time. It should be clear from this figure that, due to its orbital motion around the Sun, the Earth rotates more than 360° between successive transits of the Sun over Greenwich.

Julian Date

The ***Julian date,*** JD, is an important concept in astrodynamics. It is the continuous amount of time measured in days from the epoch of January 1, 4713 B.C. A Julian day starts at Greenwich mean noon resulting in the Julian date of 00:00 UTC to always end in ".5". The biggest advantage in using the Julian date is that the information of the year, month, day, hour,

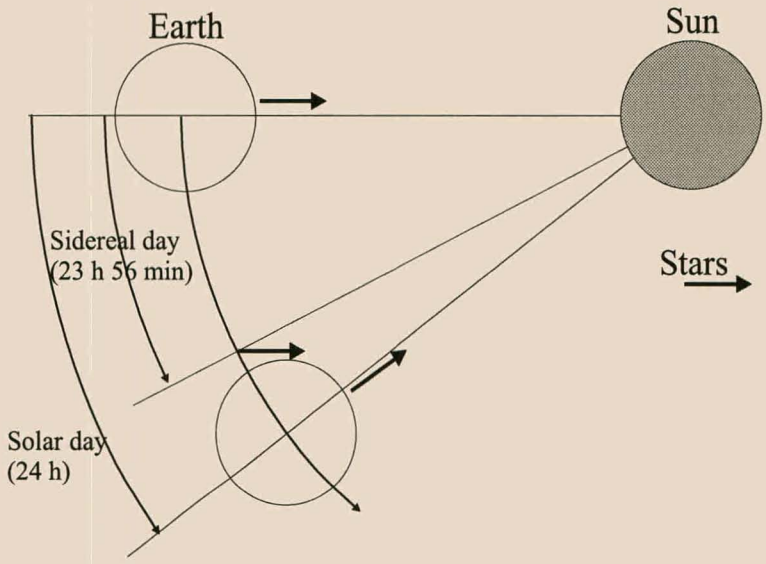

Figure B.7: The measurement of Solar and Sidereal time.

minute and second are all preserved in one variable that is very useful for computer applications. The Julian date for a certain day and time is found by using the following procedure presented by Meeus [22].

For a given calendar date, let Y be the year (four digit value), M the month number and D the day of the month (with decimals if it has any). If $M > 2$ then Y and M should be left unchanged. If $M = 1$ or $M = 2$ then Y should be replaced by $Y - 1$ and M by $M + 12$. The Julian date is then obtained from the formula

$$\begin{aligned} A &= INT\left(\frac{Y}{100}\right) \\ B &= 2 - A + INT\left(\frac{A}{4}\right) \\ \\ JD &= INT(365.25(Y + 4716)) + INT(30.6001(M + 1)) \\ &\quad + D + B - 1524.5 \end{aligned} \tag{B.5}$$

where INT denotes *real* truncation. Other formulations for the calculation of the Julian date do exist, but unlike equation B.5 they are usually only valid for a specific interval of time. Since Julian date is often used as an epoch for observations, the Julian date for 12:00, January 1 2000 (JD 2451545) is commonly assigned the shorthand notation of J2000. For some calculations, it is necessary to use the number of Julian centuries from a certain epoch. The number of Julian centuries from J2000 is often encountered in calculations

and can be calculated from

$$T = \frac{JD - 2451545}{36525} \tag{B.6}$$

B.2.3 Sidereal Time

Sidereal time is defined as the angle, measured in the equatorial plane, between the vernal equinox and a local meridian. Refer to figure B.7 for a comparison between the measurement of solar and sidereal time. It should be clear that sidereal time is a direct measurement of the *diurnal motion*[5] of the Earth. ***Apparent sidereal time*** is the angle between the local meridian and the *true* vernal equinox. The position of the vernal equinox is affected by the precession and nutation of the axis of the Earth. The periodic variations due to nutation introduce periodic variations into the apparent sidereal time. ***Mean sidereal time*** is defined as the time determined from the diurnal motion of the *mean* vernal equinox. Only secular variations in the orientation of the vernal equinox resulting form precession is taken into account when determining the mean sidereal time. The difference between apparent and mean sidereal times is defined as the ***equation of the equinoxes***. For the practical determination of the rotational position of the Earth, it is necessary to obtain the apparent sidereal time. The calculation of mean sidereal time is mathematically well defined. This means that in order to obtain the apparent sidereal time, the mean sidereal time is first calculated from the following formula as presented by Meeus [22]

$$\begin{aligned} \theta_{MST} &= 280.46061837^\circ + 360.98564736629^\circ (JD - 2451545.0) \\ &\quad +0.000387933^\circ\ T^2 - (1/38710000)^\circ\ T^3 \end{aligned} \tag{B.7}$$

where θ_{MST} is the *Mean Sidereal Time* in degrees, T is Julian centuries from J2000 as calculated in equation B.6 and JD is the Julian day-number (and fraction). The formula is presented in this particular format to preserve numeric accuracy when implemented in a computer. The equation of the equinoxes is calculated as

$$\text{equation of equinoxes} = \Delta\psi \cos\epsilon \tag{B.8}$$

where section B.2.1 discusses the computation of $\Delta\psi$ and ϵ. The value obtained from equation B.8 is then added to the value obtained from equation B.7 to obtain the correct value for the apparent sidereal time.

[5] Seidelmann [30] defines diurnal motion as "*the apparent daily motion of celestial bodies across the sky from east to west, caused by the Earth's rotation.*"

B.2.4 Dynamical and Atomical Time

Dynamical time uses observations of the motion of bodies in the solar system to determine time from the mathematical description of the motion of these bodies.

International Atomic Time, *TAI*, is considered the most accurate time system available because it is independent of variations in the Earth's rotation. It is based on the counting of the cycles of oscillation of a high-frequency electrical circuit kept in resonance by a cesium-133 atom in transition. Due to its accuracy, this system of timekeeping is used to correct all other timekeeping systems.

B.3 Coordinate Transformations

Observations of celestial bodies or spacecraft always need to be referred to a coordinate system. It does happen quite frequently that an observation is described in one coordinate system and that it needs to be compared to an observation made in another coordinate system. A transformation between coordinate systems is required to accomplish this. After the transformation of a vector, it is still the same vector, but the numeric value used to describe it has changed according to the definition of the coordinate system in which it is described after the transformation. Since the understanding of coordinate transformations is essential to understanding astrodynamics, this section will describe the coordinate transformations that were used during this study.

B.3.1 Classical Orbital elements to ECI

As it was already indicated, the ECI coordinate system suits the specification for an inertial reference frame as laid down by Newton. Since the ***classical orbital elements*** or Kepler elements, defined in section C.2.3, are defined in an inertial reference frame, the ECI coordinate system will be suitable as a reference frame. The Kepler element set will not be considered as a separate coordinate system, but simply as another coordinate formulation in the ECI system. Instead of using Cartesian coordinates, the position and orientation of the orbital plane and the satellite in the orbit is defined by means of the six Kepler elements. It will still be, however, necessary to define the transformation equations which are necessary to transform the description of an object in classical elements to the ECI coordinate system. This transformation is essential when the propagation of a satellite in its orbit is performed. The transformation will consist of a two-step process.

The first step is to transform the classical elements to the perifocal coordinate system. Referring to figure B.8, it can be seen that the position of the satellite in the perifocal coordinate system can be described in terms of the classical elements as

$$\vec{r}_{PQW} = \begin{bmatrix} r\cos(\nu) \\ r\sin(\nu) \\ 0 \end{bmatrix} \tag{B.9}$$

where r is determined from the trajectory equation (equation C.15). The

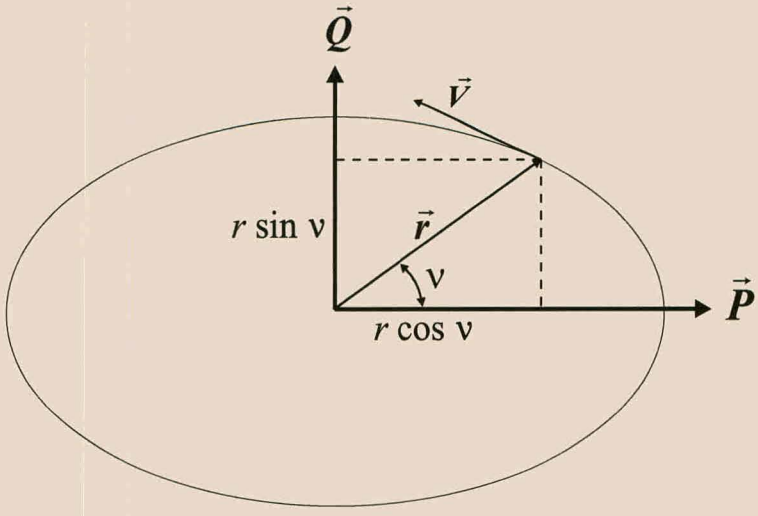

Figure B.8: The position and velocity vectors in the perifocal coordinate system.

$\vec{W}$-component is zero because the $\vec{P}$ and $\vec{Q}$ vectors are situated entirely in the orbital plane. The velocity of the satellite in the perifocal system can be expressed in terms of the classical elements as

$$\vec{v}_{PQW} = \begin{bmatrix} -\sqrt{\frac{\mu}{p}}\sin(\nu) \\ \sqrt{\frac{\mu}{p}}\left(e + \cos(\nu)\right) \\ 0 \end{bmatrix} \tag{B.10}$$

where p is the semi-parameter as defined in equation C.14.

The second step in the transformation from classical elements to the ECI system is to transform the position and velocity vectors obtained in perifocal coordinates to the ECI coordinate system. From figure B.9 is should be clear that the PQW axis of the perifocal coordinate system can become the IJK axis of the ECI coordinate system by three successive rotations. These rotations consist of

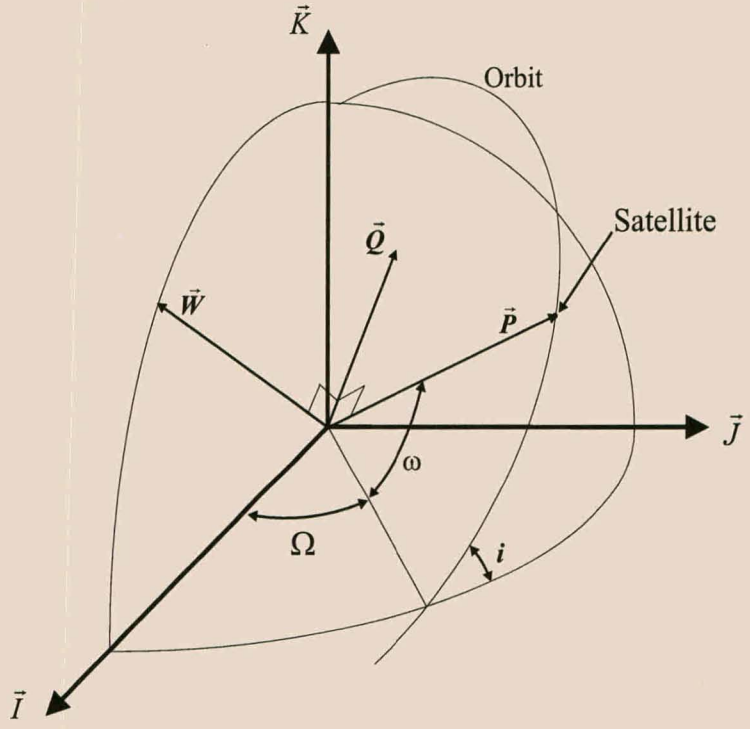

Figure B.9: The relationship between the ECI and the PQW coordinate systems.

1. a rotation about the $\vec{W}$ axis by $-\omega$,
2. a rotation about the $\vec{P}'$ axis by $-i$ and
3. a rotation about the $\vec{W}''$ axis by $-\Omega$.

In the rotations the first rotation changes the PQW axis to the $P'Q'W'$ axis, the second rotation changes the $P'Q'W'$ axis to the $P''Q''W''$ axis and the third rotation changes the $P''Q''W''$ axis to the IJK axis. In matrix notation the three transformations can be presented as follows:

$$\begin{bmatrix} P' \\ Q' \\ W' \end{bmatrix} = \begin{bmatrix} \cos\omega & -\sin\omega & 0 \\ \sin\omega & \cos\omega & 0 \\ 0 & 0 & 1 \end{bmatrix} \begin{bmatrix} P \\ Q \\ W \end{bmatrix} \tag{B.11}$$

$$\begin{bmatrix} P'' \\ Q'' \\ W'' \end{bmatrix} = \begin{bmatrix} 1 & 0 & 0 \\ 0 & \cos i & -\sin i \\ 0 & \sin i & \cos i \end{bmatrix} \begin{bmatrix} P' \\ Q' \\ W' \end{bmatrix} \tag{B.12}$$

$$\begin{bmatrix} I \\ J \\ K \end{bmatrix} = \begin{bmatrix} \cos\Omega & -\sin\Omega & 0 \\ \sin\Omega & \cos\Omega & 0 \\ 0 & 0 & 1 \end{bmatrix} \begin{bmatrix} P'' \\ Q'' \\ W'' \end{bmatrix} \tag{B.13}$$

The complete transformation is then

$$\begin{bmatrix} I \\ J \\ K \end{bmatrix} = [T_1][T_2][T_3] \begin{bmatrix} P \\ Q \\ W \end{bmatrix} \tag{B.14}$$

where T_1 is the rotation matrix in equation B.11, T_2 the rotation matrix in equation B.12 and T_3 the rotation matrix in equation B.13. The three successive rotations are sometimes combined into a single matrix expression $[R] = [T_1][T_2][T_3]$ to ease the implementation in a computer. The combined expression is

$$[R] = \begin{bmatrix} C_\Omega C_\omega - S_\Omega S_\omega C_i & -C_\Omega S_\omega - S_\Omega C_\omega C_i & S_\Omega S_i \\ S_\Omega C_\omega + C_\Omega S_\omega C_i & -S_\Omega S_\omega + C_\Omega C_\omega C_i & -C_\Omega S_i \\ S_\omega S_i & C_\omega S_i & C_i \end{bmatrix} \tag{B.15}$$

where C_{angle} and S_{angle} are used to denote the sine and cosine values of the angles. Equation B.14 can be used for transforming both the position and the velocity vectors from the perifocal coordinate system to the ECI coordinate system. For an inverse transformation from the ECI system to the perifocal system, the inverse of the R-matrix must be used. For a complete transformation from the ECI coordinate system to the classical elements, a different technique is necessary. This technique will be introduced in the following section.

B.3.2 ECI to Classical Orbital Elements

Although observations are commonly made in terms of the SEZ or spherical ECI coordinate systems, the observations of a satellite are usually reduced to position and velocity vectors. These vectors are convenient for numerical processing and locating the satellite in general, but they are not very descriptive to a mission analyst. The analysis of an orbit is much easier if the classical elements are known. Most commercial propagation software uses the classical elements as input and therefore it will frequently be necessary to transform the position and velocity vectors to classical elements. The equations that are necessary to perform the transformation are presented as the definitive equations for the classical elements in section C.2.3. They will be presented here again in order to present the complete set of equations which is used for the transformation.

The first two values that are needed are the magnitude of the position and velocity vectors, which are

$$r = \sqrt{x^2 + y^2 + z^2} \tag{B.16}$$

and

$$v = \sqrt{v_x^2 + v_y^2 + v_z^2} \tag{B.17}$$

The angular momentum vector will be needed and is defined as

$$\vec{h} = \vec{r} \times \vec{v} \qquad h = |\vec{h}| \tag{B.18}$$

The node-vector pointing to the ascending node is defined as

$$\vec{n} = \vec{K} \times \vec{h} \tag{B.19}$$

With the orbit in the equatorial plane, the node-vector will be zero which will cause the right ascension of the ascending node to be undefined.

The eccentricity is calculated as

$$\vec{e} = \frac{\left(v^2 - \frac{\mu}{r}\right)\vec{r} - (\vec{r} \cdot \vec{v})\vec{v}}{\mu} \qquad e = |\vec{e}| \tag{B.20}$$

with the eccentricity vector always pointing towards perigee.

The semimajor axis is calculated from the *vis viva* equation that states that

$$v^2 = \mu\left(\frac{2}{r} - \frac{1}{a}\right) \tag{B.21}$$

The inclination is determined from

$$i = \cos^{-1}\frac{\vec{K} \cdot \vec{h}}{h} \tag{B.22}$$

The right ascension of the ascending node is determined from

$$\Omega = \cos^{-1}\frac{\vec{I} \cdot \vec{n}}{|\vec{n}|} \tag{B.23}$$

The quadrant in which Ω is situated should be verified. If $\vec{J} \cdot \vec{n} < 0$ then $\Omega = 360° - \Omega$.

The argument of perigee is calculated from

$$\omega = \cos^{-1}\frac{\vec{n} \cdot \vec{e}}{|\vec{n}||\vec{e}|} \tag{B.24}$$

if $\vec{K} \cdot \vec{e} < 0$ then $\omega = 360° - \omega$.

The final value that needs to be calculated is the true anomaly that is determined from

$$\nu = \cos^{-1} \frac{\vec{e} \cdot \vec{r}}{|\vec{e}||\vec{r}|} \tag{B.25}$$

if $\vec{r} \cdot \vec{v} < 0$ then $\nu = 360° - \nu$.

This set of calculations will only be valid for elliptical inclined orbits. For orbit configurations which have either zero inclination (equatorial orbit) or which are circular, the sequence of transformations will not be valid since some of the equations will become singular. Vallado [35] defines variations in the classical orbital elements which should be used for these alternative orbit configurations.

B.3.3 ECI and ECEF

Both the ECI and the ECEF reference frames depend on the Earth's equator as the fundamental plane. The only difference between the ECI and the ECEF reference frames is that the ECI system can be considered as fixed in its orientation in inertial space while the ECEF system rotates with the Earth. This has the effect that the transformation between the two systems is simply a rotation about one of the axis with the rotation angle of the Earth. This rotation angle is determined from the calculation of the apparent sidereal time of the Earth as presented in section B.2.3. If θ_{AST} is the apparent sidereal time at Greenwich at the moment of performing the transformation, then the transformation from the ECI to the ECEF systems is performed as follows:

$$\vec{r}_{ECEF} = \begin{bmatrix} \cos\theta_{AST} & \sin\theta_{AST} & 0 \\ -\sin\theta_{AST} & \cos\theta_{AST} & 0 \\ 0 & 0 & 1 \end{bmatrix} \vec{r}_{ECI} \tag{B.26}$$

The transformation from the ECEF system to the ECI system is performed by using the same transformation matrix which was used in equation B.26 with the angle substituted with $-\theta_{AST}$. The measurement of the Earth's rotation angle is illustrated in figure B.10.

B.3.4 ECEF, Geocentric and Geodetic Coordinates

As it was indicated earlier in section B.1.2, the ECEF reference system is a Cartesian coordinate system that rotates with the Earth. The position of

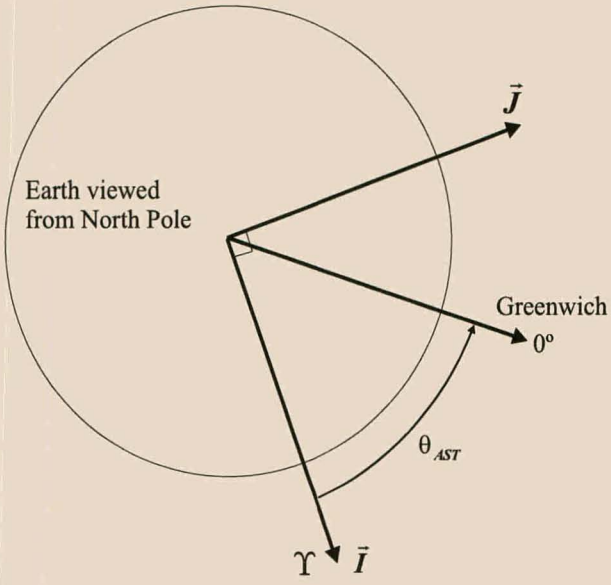

Figure B.10: The relationship between the ECI and the ECEF coordinate systems.

an object in this reference system can be described either in terms of the Cartesian coordinates or in terms of spherical coordinates.

The logical first choice for a spherical description of position is the geocentric coordinate system since it is simply the spherical equivalent of the Cartesian coordinates. The transformation from the Cartesian ECEF coordinates, $[x \quad y \quad z]$, to geocentric coordinates, $[\phi' \quad \lambda \quad r]$ is

$$\begin{bmatrix} \phi' \\ \lambda \\ r \end{bmatrix} = \begin{bmatrix} \tan^{-1} \dfrac{z}{\sqrt{x^2+y^2}} \\ \tan^{-1} \dfrac{y}{x} \\ \sqrt{x^2+y^2+z_2} \end{bmatrix} \tag{B.27}$$

This value of λ is determined following the transformation from ECEF to ECI coordinates. It is often found that the longitude needs to be calculated directly from the ECI coordinates. This can be calculated from

$$\lambda = \alpha - \theta_{GST} \tag{B.28}$$

where $\alpha = \tan^{-1}\left(\frac{y}{x}\right)$ is the right ascension of the object in the ECI system and θ_{GST} is the apparent sidereal time at the Greenwich meridian. The

inverse transformation, from geocentric to ECEF coordinates, is given by

$$\begin{bmatrix} x \\ y \\ z \end{bmatrix} = r \begin{bmatrix} \cos\phi' \cos\lambda \\ \cos\phi' \sin\lambda \\ \sin\phi' \end{bmatrix} \tag{B.29}$$

The transformation that is most often needed in practice is the conversion from the Cartesian coordinate system (either the ECI or the ECEF systems) to the geodetic coordinate system. This process usually involves iteration as it will be shown shortly, but Chobotov [11] supplies a high accuracy closed-form solution for converting from the ECI system which eliminates the iteration. This closed-form solution for calculating the geodetic coordinates from ECI coordinates will be presented first, followed by the iterative procedure. In the closed-form solution the height is calculated from

$$h = r - a_e \left[1 - f \sin^2\delta - \frac{f^2}{2} \sin^2 2\delta \left(\frac{a_e}{r} - \frac{1}{4} \right) \right] \tag{B.30}$$

where r is the magnitude of the position vector, δ is the declination of the object in the ECI system, a_e is the equatorial radius of the Earth and $f = 1/298.257$ is the flattening of the Earth. The geodetic latitude of the object is calculated from

$$\phi = \delta + \sin^{-1}[\sin(\phi - \delta)] \tag{B.31}$$

where

$$\sin(\phi - \delta) = \frac{a_e}{r} \left[f \sin 2\delta + f^2 \sin 4\delta \left(\frac{a_e}{r} - \frac{1}{4} \right) \right] \tag{B.32}$$

Since the value for the longitude is the same for both geodetic and geocentric coordinates, it can still be calculated from equation B.28.

The iterative procedure for the calculation of geodetic coordinates from ECEF coordinates is explained in the Astronomical Almanac [1]. It will be presented here for obtaining insight in the coordinate system. The first values to be calculated are

$$\lambda = \tan^{-1}\left(\frac{y}{x}\right) \qquad r' = \sqrt{x^2 + y^2} \qquad e^2 = 2f - f^2 \tag{B.33}$$

where x, y and z refer to the components of the position vector in the ECEF coordinate system.

The first approximation of ϕ is calculated from $\phi = \tan^{-1}(z/r')$. The following iteration is then performed until ϕ is unchanged to the required precision:

$$\begin{aligned} \phi_1 &= \phi \\ C &= (1 - e^2 \sin^2 \phi_1)^{-1/2} \\ \phi &= \tan^{-1} \frac{z + a_e C e^2 \sin \phi_1}{r'} \end{aligned} \tag{B.34}$$

then the geodetic height, h, is calculated from

$$h = r' \cos \phi - a_e C \tag{B.35}$$

The final conversion is the conversion from geodetic to ECEF Cartesian coordinates. This is obtained from

$$\begin{bmatrix} x \\ y \\ z \end{bmatrix} = r \begin{bmatrix} (N_\phi + h) \cos \phi \cos \lambda \\ (N_\phi + h) \cos \phi \sin \lambda \\ ((1 - e^2) N_\phi + h) \sin \phi \end{bmatrix} \tag{B.36}$$

where

$$e = \sqrt{2f - f^2} \qquad N_\phi = \frac{a}{\sqrt{1 - e^2 \sin^2 \phi}} \tag{B.37}$$

B.3.5 ECI and SEZ

The transformation from ECI coordinates to the Topocentric Horizon coordinate system is often needed for accurate antenna pointing during a pass of a satellite over a particular groundstation. The first value that should be determined is the vector from the observer to the satellite in the ECI coordinate system, $\vec{\rho}_{IJK}$. This is obtained by subtracting the ECI position vector of the groundstation for a particular moment, $\vec{r}_{siteIJK}$, from the ECI position vector of the satellite, $\vec{r}_{satIJK}$, at the same moment.

$$\vec{\rho}_{IJK} = \vec{r}_{satIJK} - \vec{r}_{siteIJK} \tag{B.38}$$

The transformation of the vector in the ECI system to the SEZ system is performed via the rotation

$$\vec{\rho}_{SEZ} = \begin{bmatrix} S_\phi C_{\theta_{LST}} & S_\phi S_{\theta_{LST}} & -C_\phi \\ -S_{\theta_{LST}} & C_{\theta_{LST}} & 0 \\ C_\phi C_{\theta_{LST}} & C_\phi S_{\theta_{LST}} & S_\phi \end{bmatrix} \vec{\rho}_{IJK} \tag{B.39}$$

where C_{angle} and S_{angle} are used to denote the sine and cosine values of the angles, ϕ is the geodetic latitude of the observer and θ_{LST} is the local apparent sidereal time which is the sum of the Greenwich apparent sidereal time and the longitude of the observer. The range to the satellite is calculated from

$$\rho = \sqrt{\rho_S^2 + \rho_E^2 + \rho_Z^2} \tag{B.40}$$

the elevation is calculated from

$$El = \sin^{-1} \frac{\rho_Z}{\rho} \tag{B.41}$$

and the azimuth is calculated from

$$Az = \tan^{-1} \frac{-\rho_E}{\rho_S} \tag{B.42}$$

The minus sign is necessary in the calculation of the azimuth angle because azimuth is measured clockwise from north instead of being measured counter-clockwise from south as it should normally be done for a right-handed orthogonal coordinate system. The quadrant for the azimuth must always be checked to ensure that the correct value for the azimuth is used.

B.3.6 ECI Rectangular and ECI Spherical

The position vector in the rectangular ECI reference frame can be obtained from the right ascension, α, and declination, δ, through the relationship

$$\vec{r}_{IJK} = \begin{bmatrix} r\cos(\delta)\cos(\alpha) \\ r\cos(\delta)\sin(\alpha) \\ r\sin(\delta) \end{bmatrix} \tag{B.43}$$

The rectangular velocity vector can be obtained from the spherical coordinates as

$$\vec{v}_{IJK} = \begin{bmatrix} v_I \\ v_J \\ v_K \end{bmatrix} \tag{B.44}$$

where

$$\begin{aligned} v_I &= V\left(\cos\alpha(-\cos Az \sin\phi_{fpa}\sin\delta + \cos\phi_{fpa}\cos\delta) - \sin Az \sin\phi_{fpa}\sin\alpha\right) \\ v_J &= V\left(\sin\alpha(-\cos Az \sin\phi_{fpa}\sin\delta + \cos\phi_{fpa}\cos\delta) + \sin Az \sin\phi_{fpa}\cos\alpha\right) \\ v_K &= V\left(\cos Az \cos\delta \sin\phi_{fpa} + \cos\phi_{fpa}\sin\delta\right) \end{aligned} \tag{B.45}$$

where the variables are defined in section B.1.1.

The transformation from the rectangular ECI coordinates to the spherical ECI coordinates is defined as

$$\begin{aligned}
\sin\alpha &= \frac{y}{\sqrt{x^2+y^2}} \\
\cos\alpha &= \frac{x}{\sqrt{x^2+y^2}} \\
\alpha &= \tan^{-1}\left(\frac{\sin\alpha}{\cos\alpha}\right) \\
\delta &= \sin^{-1}\left(\frac{z}{r}\right) \\
\phi_{fpa} &= \cos^{-1}\left(\frac{\vec{r}\cdot\vec{V}}{r\cdot V}\right) \\
\vec{W} &= \frac{\vec{r}\times\vec{V}}{|\vec{r}\times\vec{V}|} \\
\vec{A} &= \frac{\vec{W}\times\vec{r}}{|\vec{W}\times\vec{r}|} \\
\vec{P} &= \frac{(\vec{r}\times\vec{k})\times\vec{r}}{|(\vec{r}\times\vec{k})\times\vec{r}|} \\
\cos Az &= \vec{A}\cdot\vec{P} \\
\sin Az &= \vec{A}\times\vec{P}\cdot\frac{\vec{r}}{r} \\
Az &= \tan^{-1}\left(\frac{\sin Az}{\cos Az}\right)
\end{aligned} \tag{B.46}$$

Appendix C

Orbital mechanics

This chapter discusses concepts that form the foundation for the description of the orbital motion of a satellite. A brief historical background will be presented followed by a derivation of the equations of two-body motion. Finally, the different representations of the orbital state of a satellite will be provided.

C.1 Historical background

A large number of astrologers worked for many centuries trying to understand the principles behind the orbital motion of the planets. These governing principles that they were looking for could only be grasped as a result of the work done by a new era of astronomers which started emerging in the fifteenth century. The work done by Nicholas Copernicus (1473-1543), Galileo Galilei(1564-1642), Johannes Kepler(1571-1630) and Isaac Newton (1642-1727) was integrated into a unified theory describing the orbital motion of the planets. They brought together the historic theories and observations made earlier and combined it with their own theories to form a basic set of equations describing the orbital motion of the planets. These formulae are not only applicable to the motion of the planets, but, when simplified, also describe the motion of a satellite in orbit around a planet.

Copernicus was the first in the emerging era of astronomers and was, like his predecessors, still thinking mainly in terms of circular orbits. He was the first astronomer to suggest that the Sun is at the center of our solar system, but he could not prove it. By making his own observations, he started a divergence in thinking from the theories of Ptolemy which, up to that time, have been dominating the thoughts of the astronomical community for almost 1500 years.

Kepler continued the process that was initiated by Copernicus. His close study of the orbit of Mars led him to formulate his three laws of orbital motion with which he attempted to correct the flaws in the theories formulated by Copernicus and those before him. The three laws are:

1. orbits of planets are ellipses, which are orientated in a fixed inertial plane around the Sun, and it has the Sun at its one focus,

2. the line joining the planets to the Sun sweeps out equal areas in equal times and

3. the square of the period of a planet is inversely proportional to the cube of its mean distance to the Sun.

Kepler's laws were quite remarkable considering the equipment he had, but it did not completely solve all the questions surrounding planetary motion.

Galileo picked up where Copernicus ended his work. He proved the theory of Copernicus by studying the moons of Jupiter with his telescope. His observations and initial calculation of the value of gravity, was a significant contribution to the work of Newton.

Newton brought it all together. He mathematically formulated the laws of nature that control the motion of the planets. His mathematics proved the observations of Copernicus, Kepler and Galileo and with the formulation of his *Universal law of gravitation*, it was possible to describe the forces between celestial bodies and also the positions of the planets in relation to one another. It was the tools supplied by the great astronomers that enabled scientists in the twentieth century to achieve the wonders of space flight. To put it in the words of Newton: *"We stand on the shoulders of giants."*

C.2 Orbital motion

C.2.1 Basic parameters

The first formulation of the *Laws of Orbital Motion* formulated by Kepler can be extended to include all types of satellite and planetary motion.

Kepler's first law states that orbits of celestial bodies (including those of satellites around a planet) are conic sections. Celestial bodies which are permanently connected follow elliptical orbits which means that satellites follow elliptical orbits when in a permanent orbit around a planet. The following properties of conic sections are important when defining an orbit and is illustrated in figure C.1.

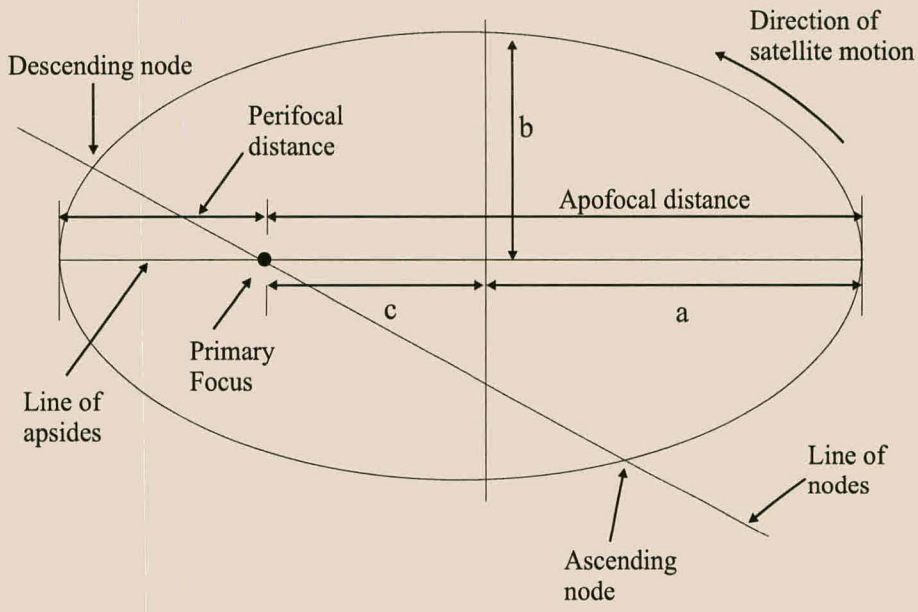

Figure C.1: The most important properties of elliptical orbits.

- Every conic section has two foci. In astrodynamics the foci are important because when the mass of one of the bodies in a two-body system is negligible, the planetary center of the major body coincides with one focus, this focus being called the ***primary focus***. Circular and elliptical orbits are called ***closed orbits*** since the satellites more or less retrace their positions over time. These two types of orbits have foci at finite positions. Hyperbolic and parabolic orbits are called ***open orbits*** since the satellites in general do not retrace their positions. Parabolas have one focus at infinity and hyperbolas have a different open branch of orbital motion associated with each focus.

- The scale (size) of a conic section is determined by the value of the major axis. The parameters that is used to describe the scale is the ***semimajor axis, a***, the ***semiminor axis, b*** and ***half the distance between the foci, c*** with a and b being half the value of the major and minor axis respectively. For circular and elliptical orbits, the value of a is positive, it is undefined for parabolic orbits and it is negative for hyperbolic orbits.

- The ***eccentricity*** (e) is a parameter which is used to specify the shape of the conic section. It is defined as the ratio of the distance from either focus to the orbit and the distance to a stationary line called the ***directrix***. For an elliptical orbit the eccentricity is always between 0

and 1 with it being 0 in the case of an exact circular orbit and 1 when the orbit is parabolic (the satellite is on the verge of escaping from the gravitational field of the planet). For hyperbolic (or interplanetary) orbits the value of e is greater than 1. Circular and parabolic orbits do not exist in practice. Perturbative forces acting on the satellites have the effect that all closed orbits are always either elliptical (even if only very slightly so) or hyperbolic.

The extreme points of an elliptical orbit are called the ***apoapsis*** and ***periapsis*** with the apoapsis being the farthest and the periapsis being the nearest points of the orbit to the central body. For satellites orbiting the Earth, these extreme positions are called the ***apogee*** and the ***perigee***, respectively. The line connecting the apogee and perigee is defined as the line of apsides.

C.2.2 Two-body motion

The two-body problem is a simplified version of the motion of a satellite in orbit, but it is crucial to understanding astrodynamics. The discussion of the two-body problem will serve as an introduction to orbital mechanics and it will be used as a foundation for the more advanced topics such as perturbations and different types op orbital propagators.

Equation of motion

Newton's second law and his universal law of gravitation is the starting point for virtually any study of orbital motion, especially when combined with Kepler's Laws. Newton's law of gravitation states that any two particles of mass M and m, distance r apart, are attracted toward each other with a force which is equal, but opposite in direction. For the case where the larger body is the Earth and the smaller one is a satellite orbiting the Earth, the force of gravity that the Earth exercises on the satellite is

$$\vec{F} = -\frac{GMm}{r^2}\frac{\vec{r}}{r} \tag{C.1}$$

where G is a universal constant called the gravitational constant. The value of G and the value of M, where M is the mass of the Earth, is known to a limited accuracy, but the value of $\mu = GM$ is known to a much higher accuracy and this value is therefore used for astrodynamic calculations.

Newton's second law states that the time rate of change of linear momentum is proportional to the force applied. For a fixed mass system, this means

that

$$\sum \vec{F} = \frac{d(m\vec{v})}{dt} = m\ddot{\vec{x}} \tag{C.2}$$

The result is that for a system with constant mass, the sum of all the forces, $\vec{F}$, acting on a body is equal to the mass, m, times the acceleration, $\ddot{\vec{x}}$, of that body.

To determine the equation of motion, equations C.1 and C.2 are combined. There are two ways to determine the equation of motion for a two-body system. The two methods are the general two-body problem and the restricted two-body problem which can be defined as the process of determining the relative motion between a small mass, m, and a larger mass, M, which are moving in an inertial reference frame. The position vectors for the large mass and the small mass in the inertial reference frame are $\vec{R}$ and $\vec{\rho}$, respectively. The vector between the two bodies (from the Earth to the satellite) will be defined as $\vec{r} = \vec{\rho} - \vec{R}$. The general two-body problem results when $\vec{R} \neq 0$. The restricted two-body problem results when the larger mass is situated at the origin of the inertial reference frame. Combining the two laws stated above, it is found that for the general two-body problem

$$M\ddot{\vec{R}} = \frac{GMm\vec{r}}{r^3} \tag{C.3}$$

and for the smaller mass, m,

$$m\ddot{\vec{\rho}} = \frac{GMm\vec{r}}{r^3} \tag{C.4}$$

Isolating the acceleration on the left sides of both equations and then subtracting equation C.4 from equation C.3 yields

$$\ddot{\vec{r}} = -\frac{G(M+m)\vec{r}}{r^3}$$

or

$$\ddot{\vec{r}} + \frac{G(M+m)\vec{r}}{r^3} = 0 \tag{C.5}$$

In a restricted two-body problem, the principal mass,M, is assumed to be fixed in inertial space. This implies that $M \gg m$, so that m does not affect the motion of M. By letting M be at the origin of the inertial reference frame, the force on the mass m is

$$\vec{F} = -\frac{G(M+m)\vec{r}}{r^3} = m\ddot{\vec{r}}$$

where $\vec{\rho} = \vec{r}$. It can therefore be seen that

$$\ddot{\vec{r}} + \frac{GM\vec{r}}{r^3} = 0 \tag{C.6}$$

or in simplified form

$$\frac{d^2\vec{r}}{dt^2} = -\mu\frac{\vec{r}}{r^3} \tag{C.7}$$

where $\frac{d^2\vec{r}}{dt^2} = \ddot{\vec{r}} =$ acceleration of mass m relative to the inertial frame.

The general and the restricted two-body problems differ only in the gravitational constant term. Since, for satellites orbiting the Earth, $M \gg m$, the difference between the two problems is negligible and the simpler solution to the restricted two-body problem can be used to describe two-body orbital motion. Equation C.7 is the basic two-body equation of motion that will be used as a basis to explain more complex orbital motion.

Conservation of Angular Momentum

An expression can be obtained for the angular momentum of a satellite with this expression being independent of the mass of the satellite and constant for the specific orbit. This *specific angular momentum, h*, for a satellite can be derived by starting with the vector-multiplication of the two-body equation and the position vector, $\vec{r}$:

$$\vec{r} \times \ddot{\vec{r}} + \vec{r} \times \frac{\mu\vec{r}}{r^3} = 0 \tag{C.8}$$

Because $\vec{r} \times \vec{r} = 0$, the second term in equation C.8 disappears. Now consider the following differential:

$$\frac{d}{dt}\left(\vec{r} \times \dot{\vec{r}}\right) = \dot{\vec{r}} \times \dot{\vec{r}} + \vec{r} \times \ddot{\vec{r}} = \vec{r} \times \ddot{\vec{r}} \tag{C.9}$$

This can be substituted into equation C.8, but since the derivative is equal to zero, the internal quantity, $\vec{r} \times \dot{\vec{r}}$, must be of a constant value $\vec{h}$. When the position derivative is substituted with the velocity, v, it is found that

$$\vec{h} = \vec{r} \times \vec{v} = \text{constant} \tag{C.10}$$

Equation C.10 defines the angular momentum[1] of the satellite. Due to the absence of mass in this equation, it is called the *specific* angular momentum. Since the vector $\vec{h}$ is the cross product between the two vector quantities, $\vec{r}$

[1]Refer to Meriam and Kraige [23] for a discussion on angular momentum.

and $\vec{v}$, it is in a direction perpendicular to the plane (the orbital plane) which contains $\vec{r}$ and $\vec{v}$. This and the fact that $\vec{h}$ is constant is a verification of the first law of Kepler which states that "*the orbits of planets are ellipses which are orientated in a fixed inertial plane around the Sun*". For the ideal case where there are no perturbative forces to change the orientation, the plane defined by $\vec{r}$ and $\vec{v}$ will stay fixed in inertial space and the satellite's motion will be confined to this plane.

From figure B.2 it is seen that, using the flight-path angle, ϕ_{fpa}, the angular momentum can be described as

$$h = rv\sin(\phi_{fpa}) \tag{C.11}$$

At apoapsis and at periapsis the position and velocity vectors are perpendicular resulting in the flight-path angle being zero. The respective angular momenta are then given by

$$\begin{aligned} h &= r_a v_a \\ h &= r_p v_p \end{aligned} \tag{C.12}$$

From analytical geometry the angular momentum of a body undergoing curvilinear motion can be written as

$$h = \sqrt{\mu p} \tag{C.13}$$

with p being the ***semi-parameter*** or ***semilatus rectum*** which is defined as

$$p = a(1 - e^2) \tag{C.14}$$

a and e is the semimajor axis and the eccentricity of the orbit, respectively.

Another equation that is important in describing the motion of a satellite in orbit is the ***trajectory equation*** that is defined as

$$r = \frac{p}{1 + e\cos\nu} \tag{C.15}$$

This equation can be derived in a way that is equivalent to the derivation of the angular momentum equation, but will not be derived[2] here since the derivation of this equation is not considered of importance to this discussion. Equation C.15 is of importance for some transformations between coordinate systems, as it defines the relationship between the classical orbital elements a, e and ν and the magnitude of the position vector of the satellite.

[2]See Chobotov [11], Bate et al. [4] or Vallado [35] for the derivation of equation C.15.

Conservation of Mechanical Energy

The energy constant of motion that is independent of mass—the ***specific mechanical energy***—will now be derived for a satellite undergoing two-body motion. Consider equation C.6 in the form

$$\ddot{\vec{r}} + \frac{\mu \vec{r}}{r^3} = 0 \tag{C.16}$$

Scalar multiplication of equation C.16 by $\dot{\vec{r}}$ with the substitution of $\dot{\vec{v}} = \ddot{\vec{r}}$, results in

$$\vec{v} \cdot \dot{\vec{v}} + \vec{v} \cdot \frac{\mu}{r^3} \vec{r} = 0 \tag{C.17}$$

Generally the form of the dot product is $\vec{r} \cdot \vec{v} = rv\cos(\theta)$ which is a scalar quantity with the angle $\theta = \phi_{fpa}$ being the angle between $\vec{v}$ and $\vec{r}$. Also, $v\cos(\theta) = \dot{r}$, with $\dot{r}$ being the radial component of change in the position vector of the satellite (not the magnitude of the velocity vector, $\vec{v}$). When substituting all these equations, it yields $\vec{r} \cdot \vec{v} = r\dot{r}$ and $\vec{v} \cdot \dot{\vec{v}} = v\dot{v}$. Equation C.17 can now be written as

$$v\dot{v} + \dot{r}\frac{\mu}{r^3} r = 0 \tag{C.18}$$

and noticing that

$$\frac{d}{dt}\left(\frac{v^2}{2}\right) = v\dot{v} \qquad \frac{d}{dt}\left(-\frac{\mu}{r}\right) = \frac{\mu}{r^2}\dot{r} \tag{C.19}$$

equation C.18 becomes

$$\frac{d}{dt}\left(\frac{v^2}{2}\right) + \frac{d}{dt}\left(-\frac{\mu}{r}\right) = 0 \tag{C.20}$$

If the time rate of change in equation C.20 is zero, the quantity which is differentiated must be a constant. If both sides of this equation are integrated with respect to time, the differentials disappear and the right hand side becomes a constant. This constant is called the *specific mechanical energy,* ξ, and can be expressed as

$$\xi = \frac{v^2}{2} - \frac{\mu}{r} \tag{C.21}$$

Equation C.21 is known as the *energy integral* or the *vis-viva equation.*

When equations C.12, C.13 and C.14 are substituted into equation C.21, the value for ξ is found to be

$$\xi = -\frac{\mu}{2a} \tag{C.22}$$

Equations C.21 and C.22 can then be combined into a formula which can be used to determine the speed of the satellite at different positions in the orbit:

$$v^2 = \mu\left(\frac{2}{r} - \frac{1}{a}\right) \tag{C.23}$$

Period of orbital motion

The third law of Kepler states that "*the square of the period of a planet is inversely proportional to the cube of its mean distance to the Sun*". This law can be expressed as

$$P = 2\pi\sqrt{\frac{a^3}{\mu}} \tag{C.24}$$

where P is the period of the orbit. It can also be expressed as

$$n = \frac{2\pi}{P} = \sqrt{\frac{\mu}{a^3}} \tag{C.25}$$

where n represent the ***mean motion*** of the satellite in units of radians per unit of time. Equation C.25 is important in designing and analysing orbits since it relates the period of rotation of the satellite to the size of its orbit.

C.2.3 Satellite orbital state representation

Six quantities are used to define what is called the ***orbital state*** of a satellite in space. These six quantities may take on many equivalent forms. The orbital state is called either a ***state vector*** (Vallado [35]) which is associated with position and velocity vectors, or it is called an ***element set*** (elset) consisting of scalar magnitude and angular representations of the orbit. These elements in the elset are commonly known as ***orbital elements***. Either of the above mentioned quantities completely specifies the orbit of the satellite and provides a complete set of initial conditions for solving an initial value class of differential equations such as can be obtained from the basic two-body equation of motion. Time is an inherent quantity in both the above-mentioned sets of data and it is often considered a seventh component. In fact, without the time at which the state vector or elset was formed, the information is useless. The orbital elements are used to generate a list containing the position of a satellite at specific times. This list of orbital data is commonly known as an ***ephemeris*** with the plural form being ***ephemerides***.

State vectors and element sets are referenced to a particular coordinate frame. Appendix B describes different coordinate reference frames. The element sets have different formats due to the variety of representations of

orbital elements used to form this vector. The most commonly used representation of the orbital state of the satellite is the set of ***classical orbital elements*** that is also known as ***Keplerian elements***. Alternative methods which is used to represent the orbital elements are the ***2-line elements*** (TLE's or NORAD elements), equinoctial elements, Delauney elements and Poincaré elements. The last four types of orbital representations were developed to avoid the difficulties experienced with the classical orbital elements for certain orbital geometries. Appendix G describes different formats in which orbital elements are presented.

Keplerian Elements

The Keplerian or classical orbital elements consist of six parameters with a few augmentation parameters. All these parameters can be divided into 3 groups viz.

1. parameters which define the shape and size of the orbit,
2. parameters which define the orientation of the orbital plane in inertial space and
3. parameters which define the position of the satellite in the orbit.

As stated previously, time is an inherent quantity in the orbital parameters and for this reason, the parameters are specified at a specific time or ***epoch***. The definitions of the orbital elements are illustrated in figure C.1 and in figure C.2.

Since the orbits under consideration are Low Earth Orbit which are either elliptical or circular, the parameters which define the ***shape and size*** of the orbit are similar to the parameters defined in section C.2.1. It can be summarised as:

- The ***semimajor axis,*** a, is usually used to define the size of the orbit, but the ***mean motion,*** n as defined in equation C.25 can be used interchangeably with a. Either the semiparameter or the radii of apoapsis and periapsis can also be used to determine the size of the orbit. When the velocity and position vector of the satellite is available at a specific time, it is possible to determine the value of a with the *vis-viva* equation.
- The ***eccentricity,*** e, specifies the shape of the orbit. Although it is not generally used in that way, the eccentricity is in fact the magnitude of

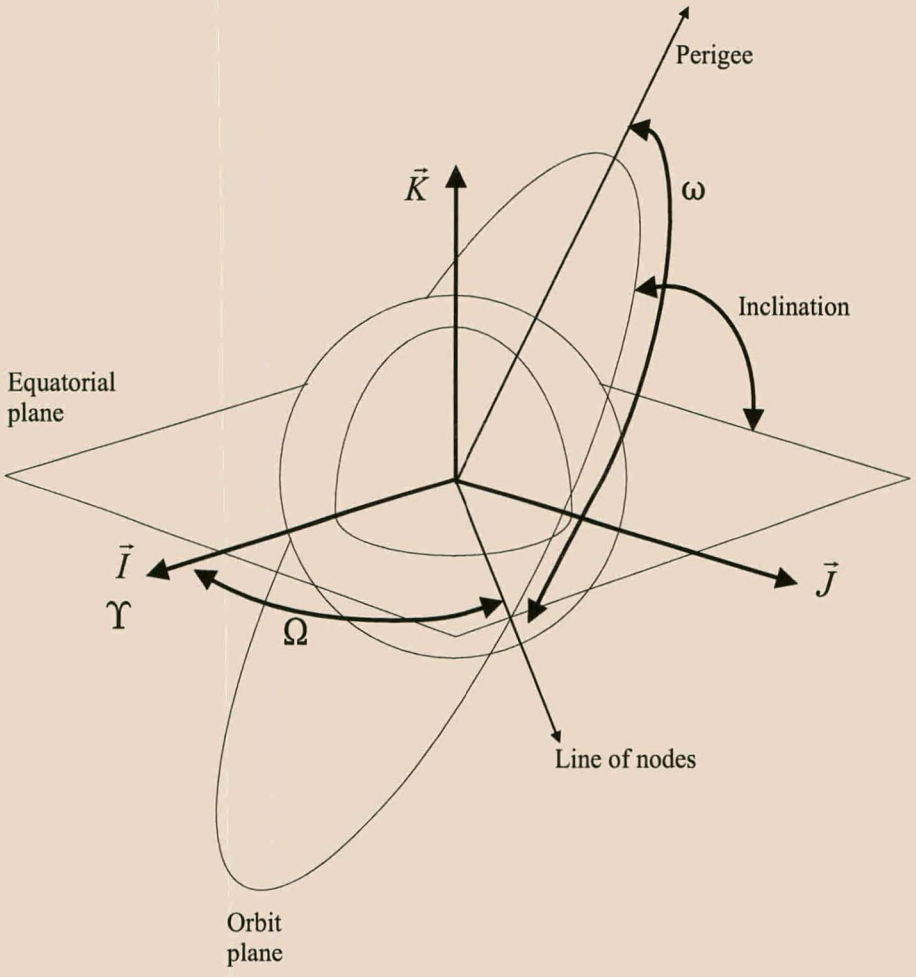

Figure C.2: The classical orbital elements.

a vector quantity. It can be determined from the velocity and position vectors as

$$\vec{e} = \frac{\left(v^2 - \frac{\mu}{r}\right)\vec{r} - (\vec{r}\cdot\vec{v})\vec{v}}{\mu} \tag{C.26}$$

This vector points towards the perigee. The value of e can also be determined by using the semimajor axis, a, and the semiminor axis, c, through the equation $e = c/a$.

The following parameters define the ***orientation*** of the orbital plane in inertial space.

- The ***inclination,*** i refers to the tilt of the orbit plane and is measured with respect to the Earth's equatorial plane. The value of the inclination can be determined via the relationship

$$i = \cos^{-1} \frac{\vec{K} \cdot \vec{h}}{|\vec{K}||\vec{h}|} \tag{C.27}$$

with $\vec{K}$ the vector from the center of the Earth through the North pole and $\vec{h}$ the angular momentum vector. Orbits with values of inclination between 0° and 90° is known as *direct* or *prograde* orbits. When the value of the inclination is between 90° and 180°, the orbit is called a retrograde orbit.

- The ***right ascension of the ascending node,*** Ω, or longitude of the ascending node is measured counterclockwise in the inertial plane (when viewed from the North pole) from the direction of the ***vernal equinox*** (the $\vec{I}$ vector) to the location of the ***ascending node***. The ascending node is the point in the equatorial plane where the satellite crosses the equator from south to north. The ***descending node*** is the position where the satellite crosses the equatorial plane from north to south. For orbits with zero inclination, the nodes are undefined. The line connecting the two nodes is known as the ***line of nodes***. The value for Ω can be determined as follows

$$\Omega = \cos^{-1} \frac{\vec{I} \cdot \vec{n}}{|\vec{I}||\vec{n}|} \tag{C.28}$$

where $\vec{n} = \vec{K} \times \vec{h}$ is the node-vector.

- The ***argument of perigee,*** ω, is measured counterclockwise (when viewed from the North pole) in the orbit plane from the ascending node to the perigee. This parameter is used to locate the position of the perigee in the orbit. It can be defined as

$$\omega = \cos^{-1} \frac{\vec{n} \cdot \vec{e}}{|\vec{n}||\vec{e}|} \tag{C.29}$$

The angle is undefined for circular orbits.

The third group of parameters defines the ***position*** of the satellite within the orbit.

- The ***true anomaly,*** ν is used to locate the satellite in the orbital plane and is the angular displacement measured from the perigee to the position vector along the direction of motion. This parameter can be mathematically defined as

$$\nu = \cos^{-1} \frac{\vec{e} \cdot \vec{r}}{|\vec{e}||\vec{r}|} \tag{C.30}$$

  The true anomaly will vary from 0° to 360° as the satellite travels through one revolution of motion. This angle is not defined for circular orbits because they have no perigee. Usually computer software routines account for this special case by selecting a point in the orbit to replace the perigee as the location for initial measurement.

- The ***mean anomaly,*** M and the ***eccentric anomaly,*** E are auxiliary parameters originally defined by Kepler. The eccentric anomaly is defined in figure C.3. It is used in conjunction with an auxiliary circle

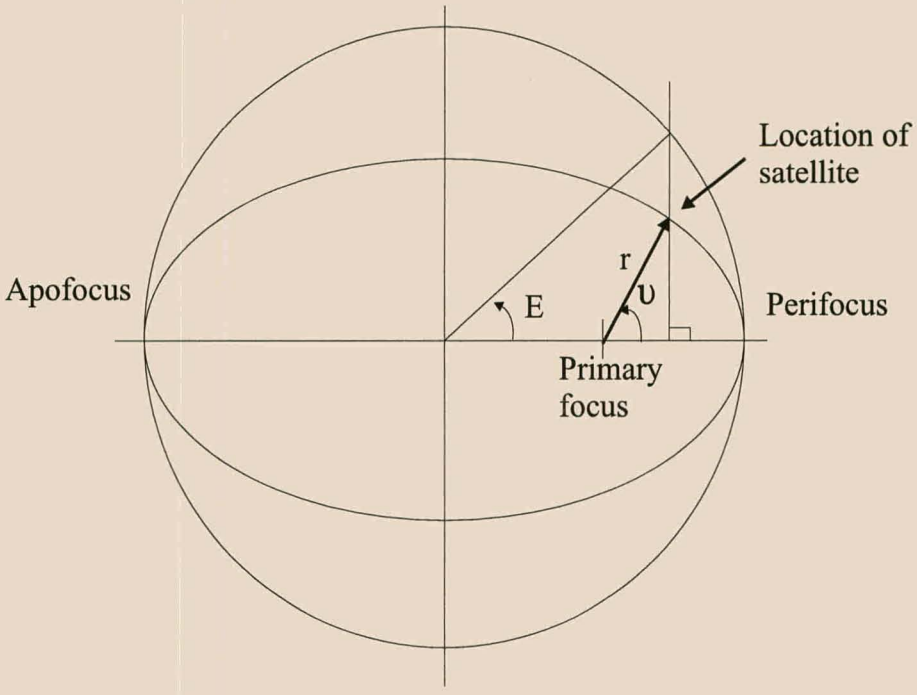

Figure C.3: The relationship between the true anomaly and the eccentric anomaly.

  to describe the true anomaly. The original intention of the eccentric anomaly parameter was to express the relationship between Kepler's

second law and the true position (ν) of the satellite in the orbit. The problem when describing the motion of a satellite in its orbit is that the true anomaly varies non-linearly with an increase in time and the eccentric anomaly do not use the center of the Earth as reference. This necessitated the formulation of a parameter which varies linearly with increase in time and which could be combined with the mean motion to determine the position of the satellite with time. This parameter, the ***mean anomaly,*** M, describes the position of the satellite as if the orbit was circular. In fact, when the orbit is circular, the mean anomaly, eccentric anomaly and true anomaly all assume the same value. The relationship between the mean anomaly and the eccentric anomaly is defined as:

$$M = E - e\sin(E) = n\Delta t \tag{C.31}$$

where n is the mean motion as defined in equation C.25 and Δt is the time that has passed since the epoch-time of the Kepler elements. The relationship $M = E - e\sin(E)$ is known as ***Kepler's equation***. A more thorough discussion concerning the use of equation C.31 is given in section 3.1.1 that describes the propagation of orbital parameters using the two-body equation of motion. The relationship between the true anomaly and the eccentric anomaly is defined as

$$\nu = \cos^{-1}\left(\frac{\cos(E) - e}{1 - e\cos(E)}\right) \tag{C.32}$$

From the parameters discussed above the set of classical orbital elements can be extracted. This set consists of the parameters

$$\mathbf{x}_{Kep} = [a \quad e \quad i \quad \Omega \quad \omega \quad v(t)] \tag{C.33}$$

Various alternate definitions and combinations for the classical elements exist which are used to describe the motion of satellites in special orbits. These definitions are described by Vallado [35] and are used for describing circular orbits for which the perigee is undefined and uninclined orbits for which the inclination is zero and the node-parameters are undefined.

Two-line elements

The classical orbital elements are widely known, understood and used to define the position of a satellite in orbit, but they are not always the most

suitable orbital data to use. The North American Aerospace Defence Command (NORAD) uses a set of elements called the ***two-line element set***[3], the two-line elements are probably the most widely used type of orbital data used to generate orbital ephemerides for satellites orbiting the Earth.

The data is presented in a text file (commonly known as a TLE-file) consisting of two lines of data. A number of parameters are presented in the file with the most important ones being

$$\begin{array}{lllllll} \bar{n} = \sqrt{\frac{\mu}{\bar{a}^3}} & e & i & \Omega & \omega & M & \\ \frac{\dot{n}}{2} & \frac{\ddot{n}}{6} & B^* = \frac{1}{2}\frac{c_D A}{m}\rho_o & UTC & & & \end{array} \tag{C.34}$$

where ρ_o is the atmospheric density at perigee (assumed to be $2.461 \times 10^{-5} kg/m^2/ER$), c_D is the drag coefficient and A is the effective cross-sectional area of the satellite. ER refer to one Earth radius. n is in units of revolutions per day.

The first six values are the independent quantities required for calculations and represent roughly the same variables as the classical elements. The other four parameters listed in equation C.34 are the mean motion rate, mean motion acceleration, a drag-like parameter (B^*) and the epoch time for the elements which is presented in a packaged format containing the number of the day in the year and UTC time. The classical elements were used to present the precise location of the satellite at a certain time, but the two-line elements represent the mean values of the orbital elements. The barred parameters are the *Kozai* mean values for the mean motion and the semimajor axis. The significance of the Kozai mean values is discussed in section 3.1.1. Another parameter that differs from the classical elements is the presentation of the satellite's position in the orbit in terms of the mean anomaly in stead of the true anomaly. As the name indicates, this parameter do not represent the true position of the satellite in the orbit, but an "average" position as a linear function of time. The B^* term is used to calculate the true ballistic coefficient, BC, of the satellite. The ballistic coefficient is used when perturbations due to atmospheric drag is taken into account in the calculation of orbital ephemerides.

Equinoctial Orbital Elements

Equinoctial orbital elements are useful for overcoming difficulties experienced with the special geometry orbits and are useful in the study of

[3]Refer to appendix G.2 which is similar but not identical to the classical orbital elements. Due to its availability on the Internet for an explanations of the format of the elements and a key to the composition of the TLE-file.

perturbations. New parameters are introduced to define the parameters that become undefined due to the geometry of the orbit. This set of elements is described in Vallado [35] and it is used in virtually all high-accuracy computer programs to eliminate problems with specific orbit geometries.

Canonical Variables

For some applications such as the construction of some of the perturbation solutions, the equations of motion need to be presented in a form where it can be written as a 6×6 matrix multiplied by a 6×1 state vector. When the classical elements are written in this format, the 6×6 matrix contains non-zero elements off the diagonal. In order to avoid any non-zero terms off the diagonal of the 6×6 matrix, it is written in canonical form. When the classical elements are written in its canonical form, it is known as the ***Delauney variables***. There is no real difference between this form and the classical form in that it still possesses singular points for uninclined or circular orbits. In order to overcome the singular points in the Delauney variables, the equinoctial elements can also be written in canonical form. This representation of the elements is known as the ***Poincaré variables***. The definitions of these variables can be found in Vallado [35].

Appendix D

Orbital perturbations

"In problems of celestial mechanics, the simple solutions are not good and the good solutions are not simple."

Unknown astronomer

The derivation of the two-body equations of motion was made by Newton with the assumption that the only forces present were the mutual gravitational attraction between the two bodies under consideration. With the advent of the space age, the gaps in the initial assumption started to show. The first satellites were launched into orbits of around 100 km altitude and the motion of satellites in these orbits could no longer be accurately predicted using the general two-body equation. It became apparent that atmospheric drag still played an important part in low-Earth orbit and that other forces caused the predicted position of the satellite to differ considerably from the observed position. The need for accurate predictions of the motion of a satellite in Earth-orbit became crucial since huge amounts of money were involved and the lives of astronauts depended on predicting when a satellite would be in view of a groundstation and when it would re-enter the atmosphere. All these factors initiated a complete new field of study of space which is still in progress today: the study of disturbing forces, known as ***perturbative forces***, which cause the true orbit of a satellite to deviate from the orbit predicted by the two-body equation of motion. The perturbing forces experienced by the satellite include forces due to the non-spherical shape of the Earth and its non-symmetrical mass distribution, atmospheric drag, solar radiation pressure, the tides of the Earth's oceans and gravitational attractions from the Sun and the Moon.

A complete knowledge of perturbative forces and the formulation of these forces are not easy to obtain and not needed by everyone involved with space-operations, but the fundamentals involved are very important. Knowing

why and how a satellite is influenced by the perturbative forces will lead to a better understanding of the motion and operation of a satellite. First order approximations of the dominating forces are used everyday for mission planning and these approximations play an important part in the design of orbits for specific mission requirements.

This chapter will consist of two parts. The first part will be a general discussion of the major perturbations to the orbits of artificial satellites in Earth-orbit. It will be attempted to equip the reader with a basic knowledge and an intuitive feeling of the different perturbations. The second part will address the mathematical foundations of orbital perturbations and the general methods used to describe the influence that the perturbative forces have on the motion of the satellite. For a more thorough discussion of perturbations and the mathematical foundations involved, the reader should refer to Vallado [35], Chobotov [11], Bate et al. [4] or Escobal [16]. Wertz [36] presents a discussion of perturbative forces from the viewpoint of attitude determination and control. The work of Battin [5] consists of an almost exhaustive collection of the descriptive mathematics of orbital motion.

D.1 Introduction to Perturbations

Perturbations in the orbit of a satellite are mirrored in the description of the satellite's motion. Describing the satellite's motion in terms of position and velocity vectors conceals the obvious effect of perturbative forces, but when the motion is described by means of the classical elements, the perturbations become apparent and their effect can be analysed quite easily. The variations in the satellite's motion which are reflected in the classical elements consist of *secular* and *periodic* variations.

Secular variations grow with time. This growth is usually a linear function of time, but can be proportional to some power of time. This type of variation provides the primary contribution to deviations from general two-body motion. Secular variations are often called mean variations in the orbit as this is the change in the orbit that is experienced over a long time when the periodic variations are ignored.

Periodic variations can be divided into ***short-periodic*** and ***long-periodic*** variations. Short-periodic variations typically have a period of repetition on the order of the orbital period of the satellite. Long-periodic variations usually have a period of repetition much longer than the orbital period of the satellite and the duration of the variations vary significantly depending on the source of the perturbation. Escobal [16] presents a way of describing the perturbative effects on the classical elements in a Fourier

series. This description was extended by Vallado [35] into the form

$$c = c_0 + \dot{c}_1(t - t_0) + K_1 \cos(2\omega) + K_2 \sin(2\nu + \omega) + K_3 \cos(2\nu) \quad \text{(D.1)}$$

where K_1, K_2 and K_3 are constants which can be expressed as sums and products of polynomials of the orbital elements. c_0 is the initial value of an element in the classical set, $\dot{c}_1$ represents the secular change in the element, 2ω represents the long-periodic change, 2ν represents the short-periodic change and $(2\nu + \omega)$ represents the mixed-periodic change in the element. These variations are illustrated in figure[1] D.1. When analytical solutions are for-

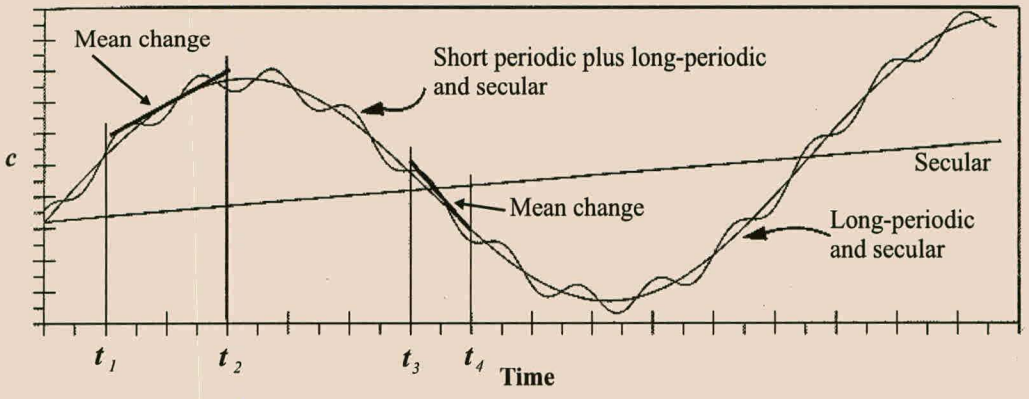

Figure D.1: The effect of perturbative forces on the orbital elements of a satellite.

mulated, the inclusion of all the variations presented in equation D.1 is not always possible as this will lead to a very complex model which is difficult to develop. Numerical solutions do not pose this problem since the formulation of the numerical solution encapsulates all the variations into the solution.

Not all the classical elements experience the full combination of perturbative effects described by equation D.1. Each perturbative force influences the set of classical elements in a different way and may result in one of the elements experiencing a secular variation for the one perturbative force and a short-periodic variation for another force. The perturbative forces themselves can be divided into two groups viz. *conservative* and *non-conservative* forces. ***Conservative forces*** do not change the total energy of the satellite—it stays constant. ***Non-conservative forces*** result in a change in the energy of the satellite, mainly due to friction or external sources. Central-body and third-body effects are examples of conservative forces while atmospheric

[1]Image was obtained from Vallado [35].

drag, solar-radiation pressure and the tidal friction are examples of non-conservative forces.

D.1.1 Earth's Oblateness

The Earth is not perfectly spherical. The polar radius is approximately 22 km less than the equatorial radius and for this reason the Earth is often modelled as an ellipse rotated about its minor axis. This shape, called an ellipsoid, does not exactly represent the shape and mass distribution of the Earth, but is a good first order approximation. The non-spherical shape of the Earth results in the vector of gravitational attraction of the Earth on an orbiting satellite to not be directed exactly to the center of the Earth. All Earth-orbiting satellites experience the perturbative effects of an oblate Earth and for satellites above the densest part of the atmosphere—above approximately 300 km—and below 8000 km, it is the major perturbative force. When this perturbation is described in terms of the classical elements, it is found that all six elements experience periodic variations. The variations in a, e and i average to zero over an orbit, but M, Ω and ω experience secular variations beside the periodic variations. These secular variations are of primary interest and can in general be considered the largest perturbative effect for low-Earth orbit satellites.

In order to understand the primary effect that the oblate Earth has on the orbit, the Earth can be modelled as a point mass with a ring of uniform density in the equatorial plane which represents the equatorial bulge. The added attraction of the equatorial bulge introduces a force component towards the equator which accelerates the satellite and cause it to reach the equator short of the crossing point for a spherical Earth as illustrated in figure[2] D.2. This force combines with the angular momentum vector of the satellite to cause the orbital plane to experience precession in a westerly direction. This effect results in a secular variation in Ω and is called the ***regression of the nodes***. For an orbit with $i < 90°$ (direct orbit) the value of Ω decreases (regresses), but for $i > 90°$ (retrograde orbit) the value of Ω increases (advances). The regression of the nodes come in very handy when orbits for remote sensing satellites are developed. It is possible to place the satellite in such an orbit—typically $i = 98.7°$ and a mean altitude of 833 km—that Ω advances with 0.9856° per day. This is the exact same value of the daily movement of the mean position of the Sun as observed from Earth and results in the satellite experiencing the same lighting conditions every time it passes over a particular site on the surface of the Earth.

[2]Image taken from Vallado [35].

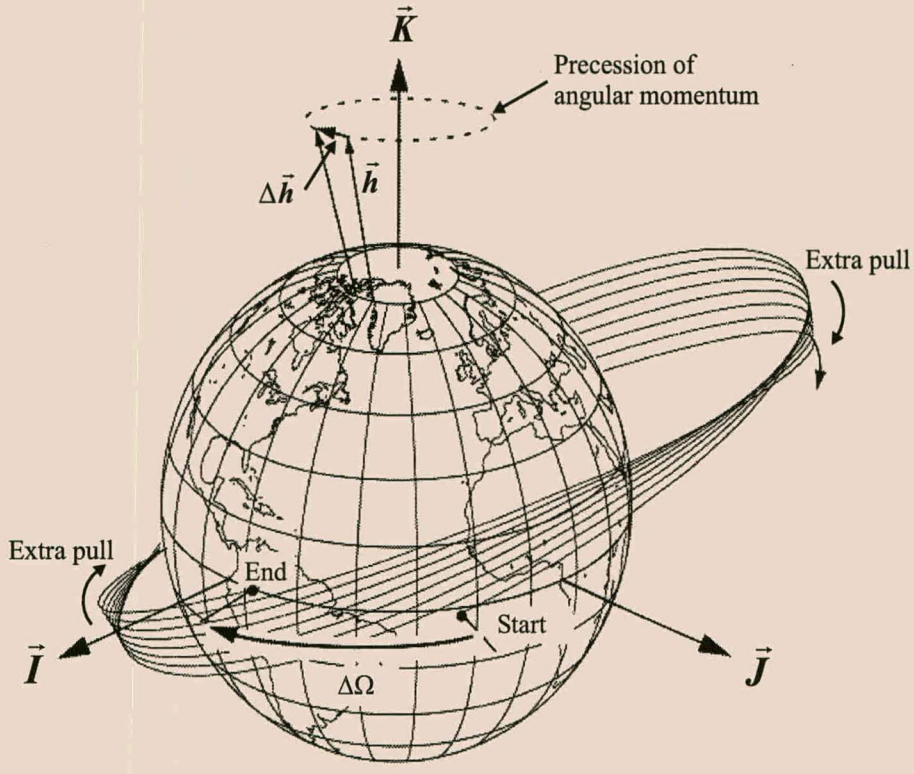

Figure D.2: Nodal regression.

Another important effect that is caused by the nonspherical shape of the Earth is the ***rotation of the apsides***. This effect is illustrated in figure[3] D.3. The added gravitational attraction of the equatorial bulge on the satellite increases the satellite's angular velocity. This cause the satellite to curve more strongly in its motion around the Earth and has the effect that the position of the apogee and perigee—connected by the line of apsides—will be shifted in the direction of motion with every orbital rotation of the satellite. For direct orbits this will result in an increase in ω and for retrograde orbits ω will decrease.

Table D.1 shows two TLE files for SUNSAT. The format of the data is explained in appendix G. The first set of data was generated on 22 August 1999 at 19:56:59 UTC and the second set was generated on 18 September 1999 at 16:54:48 UTC.

The value for the right ascension of the ascending node—the fourth value in the bottom row of each set—is 146.4131 for the first set and 166.8279

[3]Image taken from Vallado [35].

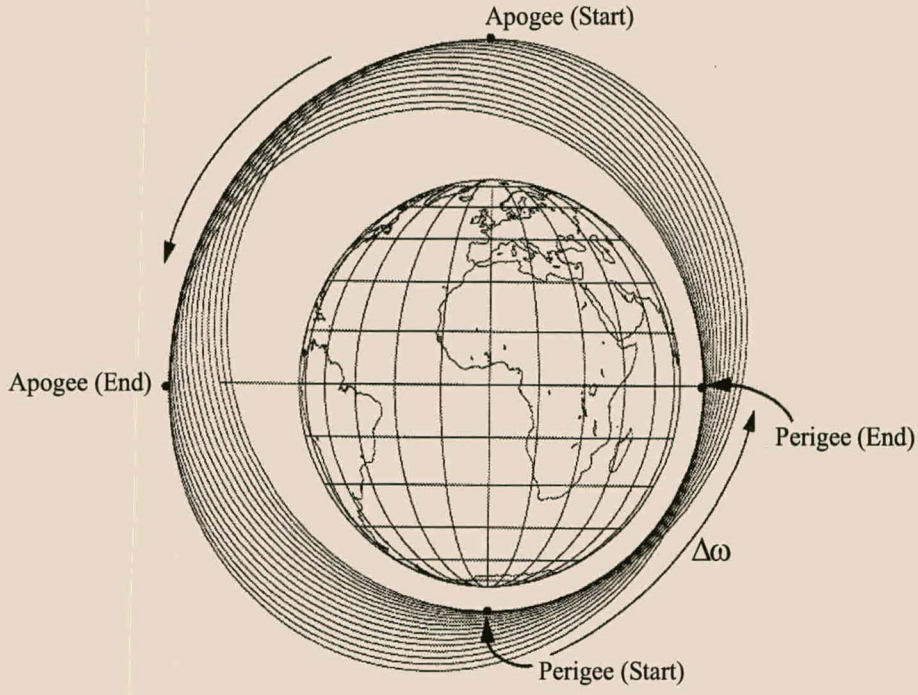

Figure D.3: Apsidal rotation.

```
SUNSAT
1 25636U 99008C   99234.83124324  .00000350  00000-0  10255-3 0   919
2 25636  96.4835 146.4131 0155017  45.1154 316.2490 14.40913668 25978

SUNSAT
1 25636U 99008C   99261.70472423  .00000371  00000-0  10947-3 0  1025
2 25636  96.4775 166.8279 0152478 320.7002  38.3229 14.40946227 29841
```

Table D.1: Two examples of real orbital data for SUNSAT.

for the second set of data. The interval between the two measurements was approximately 27 days which indicate a value for the regression of the nodes of 0.76° per day. The value is positive which indicate that the node is in fact advancing. This was to be expected as SUNSAT is in a retrograde orbit.

The value for the argument of perigee—the fourth value in the bottom row of each set—is 45.1154 for the first set and 320.7002 for the second set of data. As the interval between the two measurements was approximately 27 days, the value for the rotation of the apsides is −3.126° per day. The value is negative as SUNSAT is in a retrograde orbit. The period of a complete

rotation of the position of the perigee through the orbit plane is 115 days.

D.1.2 Aerodynamic Drag

Aerodynamic or ***atmospheric drag*** is a retarding force applied to the motion of the satellite due to friction against the Earth's upper atmospheric. For elliptical orbits, the atmosphere is the densest at perigee resulting in the largest force being applied at this position in the orbit. This force is non-conservative and it acts in a similar way as an in-plane velocity reduction manoeuvre to decrease the total energy of the satellite. For all satellites below 1000 km altitude this effect becomes important and for very low-orbit satellites—such as manned missions with orbits below 300 km—it is the dominating perturbative effect which can even dominate the basic laws of two-body motion in some cases. The atmospheric drag slows the satellite at each perigee passage resulting in a secular decrease in the apogee height, semimajor axis and eccentricity as indicated in figure[4] D.4. The apogee

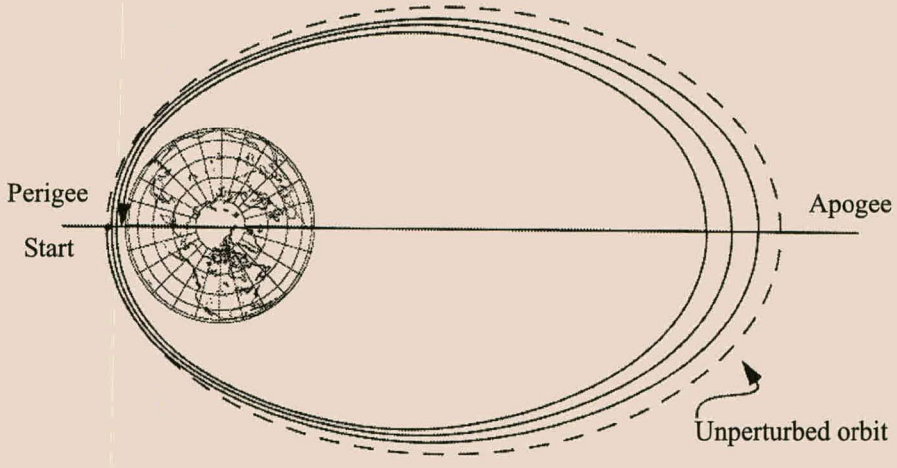

Figure D.4: The decay of an orbit under the influence of drag.

height will decrease until it is equal to the perigee height and the shape of the orbit becomes circular. The process of reduction in the energy of the satellite and the decrease in the apogee height is known as ***orbital decay***. When the orbit has decayed from elliptical to circular, it will continue to decay until it enters the densest part of the atmosphere where it will either burn up or fall to the surface of the Earth. The decrease in the size of the orbit increases the velocity of the satellite. This is known as the ***drag***

[4]Image taken from Vallado [35].

paradox because the satellite is sped up by atmospheric friction as it spirals inward toward its final decay. The explanation for the drag paradox can be found in Kepler's third law, which states that

$$\mu = n^2 a^3 = \text{constant} \tag{D.2}$$

and it can be seen that a decrease in the semimajor axis, a, will lead to an increase in the mean motion, n.

The time from launch until the final orbital decay of the satellite is known as its *orbital lifetime*. Wertz [36] provides a graph which can be used as an indication of the lifetime of a satellite, but this is only an approximate value. To truly predict the lifetime of a satellite, a complete model of the upper atmosphere is required. This is a very complex task since accurate models include the day-night variation in the atmospheric density over different parts of the Earth, the exponential variation in atmospheric density with height, the influence of the variations in the intensity of the Sun, the position and orientation of the satellite over the Earth and the influence of the magnetic field. The shape, attitude and weight of the satellite have a dominant effect on its motion under the influence of aerodynamic drag and it needs to be taken into consideration when the satellite's motion is determined to a high accuracy. In recent years, the influence of drag has been used as a means to save propellant during orbit-transfer manoeuvres. In order to lower the apogee, the drag force at perigee is increased. This is done by using the attitude control system to increase the cross-sectional area of the satellite with the solar panels which increases the drag force and gradually lowers the apogee. By orienting the satellite in such a way that the solar panels create a lifting force, energy can be added to the satellite and the perigee and apogee heights can be increased. The use of atmospheric drag as a control-force is illustrated by Du Toit [14].

To indicate the problems that can be experienced with atmospheric drag, Vallado [35] refers to a problem of highly eccentric orbits in which atmospheric drag couples with third-body effects. Long-periodic variations in the position and height of perigee due to third-body effects can shift the perigee to new positions where the atmospheric conditions differ completely from the conditions at its initial position. The result is that the initial position of the Sun, Moon and the position of the satellite's orbit can either lower the perigee height to such a degree that the satellite can re-enter much earlier than expected or it can increase the perigee height which cause an increase in the lifetime of the satellite. Such unexpected events can be avoided with the use of a simulation package that incorporates a high-accuracy atmospheric model in combination with precise planetary ephemerides.

D.1.3 Third-Body Attractions

The perturbative effects caused by the oblate Earth decrease with increasing distance from the Earth. As the distance increases, perturbations from the gravitational forces of the Sun and the Moon—called ***luni-solar*** perturbations—become more important. Above 700 km altitude, these third-body attractions need to be taken into consideration for accurate orbit predictions. At a distance of 8000 km the influence of the oblate Earth has decreased and the forces of the Sun and Moon increased to such a measure, that the contributions of the two types of perturbations to the orbit are the same. For interplanetary flights third-body attractions are dominating and the spacecraft would altogether miss their target-planets were it not for the influence of the other planets in the solar system. Wertz [36] presents a method—originally introduced by Laplace (Battin [5])—called the *spheres of influence* to determine when simple two-body motion is valid and when the attraction of a third body needs to be taken into consideration for simulating an orbit.

To understand the long-term influence of a third body on the orbit of a satellite, first consider the influence of the Sun. For this explanation the orbit of the satellite will be represented by an elliptic ring located in its orbital plane and the orbit of the Sun by such a ring located in the ecliptic. The mutual gravitational attractions will create a torque about the line of nodes that will tend to turn the satellite's orbital plane into the ecliptic. The gyroscopic effect of the torque on the spinning satellite ring will induce a gyroscopic precession of the orbit plane about the pole of the ecliptic. This precession will result in a regression of the nodes and apsidal rotation similar to that caused by the oblate Earth. The Moon will cause a similar effect about the axis normal to the Moon's orbit plane—the Moon's orbit plane has a 5° inclination to the ecliptic. The combined effect of the Moon and the Sun is that the orbit plane will experience the regression about some mean pole lying between the Earth's pole and the ecliptic pole. The amplitude of the precession depends on the inclination and size of the orbit and is quite often so small that the effect is obscured by more pronounced effects from other perturbations. Analysing the effect of a third body on the orbit is difficult because the period of the variations in the orbital elements are usually very long and it requires the use of very accurate ephemerides to locate the third body.

The luni-solar perturbations effect the orbit and the description of the orbit by means of the classical elements, in the same way as the oblateness of the Earth. Since the perturbative force is conservative, the value of the semi-major axis stays constant. Secular variations appear in the right ascension of the ascending node, Ω, and the argument of perigee, ω, with long-periodic

variations experienced by the eccentricity, the inclination, Ω and ω.

An important operation resulting from third-body perturbations involves the station-keeping of geostationary satellites at an altitude of approximately 36000 km. At this altitude, the influence of the Sun and the Moon result in the most dominant perturbations to the orbit. For a satellite with an initial inclination of 0°, third-body effects will increase the inclination with 1° per year for the first 10 years and 17 years after launch it would have increased to 15°. After this the inclination decreases to 0° in another 27 years. This drifting in the inclination is not desired and would usually require huge amounts of fuel for the purpose of stationkeeping. The option that is exercised whenever it is possible, is to choose the orbit such that the inclination first reduces to zero and then starts to increase. The initial inclination is sometimes selected as 3.5° with a negative drift in its value. After 3.5 years the inclination reaches a value of 0° at which time it starts to increase and again reaches a value of 3.5° at 7.7 years after launch. This means that the fuel load needed for stationkeeping due to third-body interaction is reduced by a significant amount since, for a position accuracy of 3.5°, stationkeeping is required for the first time 7.7 years after launch.

D.1.4 Solar Radiation Pressure

The impact of light-energy (photons) from the Sun induces a significant perturbing force on the motion of a satellite. For altitudes above 900 km, it may exceed the effect of atmospheric drag. The magnitude of the perturbing force is proportional to the effective surface area of the satellite and the optical reflectivity of the satellite's surface. When the satellite moves toward the Sun, the impact of the photons will reduce its total energy and decrease the value of the semimajor axis. When the satellite moves away form the Sun the energy of the satellite and the value of the semimajor axis will be increased. It should be clear that for a satellite that is in the sunlight for the whole duration of its orbit, the net effect of solar radiation pressure would reduce to zero. However, when the satellite passes through the shadow of the Earth during its orbit, the solar radiation pressure has the effect of a non-conservative force. This is the case for the majority of low-Earth orbits. The effect that the force has on the orbit can, however, be controlled with attitude manoeuvres that involves the orientation of the solar panels to reduce or increase the effect of the pressure.

Long-term periodic variations appear in all classical elements with the most pronounced variations being those to the semimajor axis and the eccentricity. The periodic variations can have a period of up to a year due to the motion of the Earth around the Sun. Accurate analyses of the effect of

solar radiation pressure on the orbit are difficult as it requires accurate modelling and prediction of the solar cycles and variations. Periods of intense solar activity can greatly affect the orbit. The variations in the intensity of the solar radiation force can couple with aerodynamic drag and the influence of third bodies to create a very complex motion. This combined effect of the perturbative forces can, as in the case of aerodynamic drag, significantly change the orbital lifetime of a satellite if it is not taken into consideration during the mission planning phase.

D.2 Mathematical Foundations of Perturbations

The basic two-body equation of motion as derived in appendix C.2.2 states that

$$\frac{d^2\vec{r}}{dt^2} = -\mu\frac{\vec{r}}{r^3} \tag{D.3}$$

where $\vec{r}$ is the position vector of the satellite in the Earth Centred Inertial coordinate system and μ is the product of the universal gravitational constant and the mass of the central body. Equation D.3 was derived with the assumption that the only force experienced by the satellite is the gravitational force of a perfectly spherical Earth with symmetrical mass distribution. Because of the presence of perturbing forces, the assumption that was made with the derivation of equation D.3 is not valid for an accurate description of the orbit. The presence of perturbing forces require equation D.3 to be written in the following, more general, form

$$\frac{d^2\vec{r}}{dt^2} = -\mu\frac{\vec{r}}{r^3} + \vec{a}_p \tag{D.4}$$

where $\vec{a}_p$ is the sum of all the perturbing accelerations which cause the orbit to deviate from a true Keplerian orbit as described by equation D.3.

It is customary to distinguish between two classes of solutions to equation D.4—general perturbations and special perturbations. ***General perturbations*** consists of methods of describing the effect of perturbations on the two-body motion in terms of closed-form analytic solutions. It is not always possible to obtain a closed-form solution and for this reason the perturbations are usually described by infinite trigonometric series expansions which are integrated term by term. ***Special perturbations*** consist of all the numerical methods used to describe the motion of the satellite by direct numerical integration of equation D.4.

D.2.1 General Perturbations

Variation of Parameters

When no perturbations are considered in the description of the motion of a satellite, the classical elements stay constant and the state of the satellite at any time can be computed from a single set of classical elements. When the perturbations are taken into consideration, the classical elements are no longer constants. The ***variation of parameters***, VOP, is a method used to describe the influence of perturbative forces as variations in the classical elements. It is done in such a way that the position and velocity at any time can be computed from a single set of elements as if there were no perturbative forces involved.

Louis LaGrange (1736-1813) used the VOP method to develop his solutions to the perturbed motion problem from his interest in the disturbances in the orbits of the planets. Since the disturbances are caused by the gravitational fields of the Sun and other planets, his solutions are only valid for conservative perturbative forces. All the conservative forces can be described as the gradient to a potential function and this lead LaGrange to the particular formulation of his solution. LaGrange's method of VOP is sometimes called the ***perturbing function approach*** and it is the solution to

$$\frac{d^2\vec{r}}{dt^2} = -\mu\frac{\vec{r}}{r^3} + \frac{\partial R}{\partial \vec{r}} \tag{D.5}$$

where R is called the ***perturbing*** or ***disturbing function*** which is a function of the position of the satellite. R represents the force causing the deviation from Keplerian motion. LaGrange found a solution for equation D.5 in terms of the classical elements and the disturbing function that is described by

$$\begin{aligned}
\frac{da}{dt} &= \frac{2}{na}\frac{\partial R}{\partial M} \\
\frac{de}{dt} &= \frac{x^2}{na^2e}\frac{\partial R}{\partial M} - \frac{x}{na^2e}\frac{\partial R}{\partial \omega} \\
\frac{dM}{dt} &= n - \frac{x^2}{na^2e}\frac{\partial R}{\partial e} - \frac{2}{na}\frac{\partial R}{\partial a} \\
\frac{d\Omega}{dt} &= \frac{1}{na^2x\sin i}\frac{\partial R}{\partial i} \\
\frac{d\omega}{dt} &= \frac{x^2}{na^2e}\frac{\partial R}{\partial e} - \frac{\cos i}{na^2x\sin i}\frac{\partial R}{\partial i}
\end{aligned}$$

$$\frac{di}{dt} = \frac{\cos i}{na^2 x \sin i}\frac{\partial R}{\partial \omega} - \frac{1}{na^2 x \sin i}\frac{\partial R}{\partial \Omega} \tag{D.6}$$

where $x = \sqrt{1-e^2}$. These equations are known as ***LaGrange's planetary equations***. To use these equations for the description of the variations in the classical elements, the particular force need to be described in terms of a perturbing function, R, and substituted into equation D.6. The derivation of equation D.6 does not fall in the scope of this study, but is presented in full by Battin [5] and Vallado [35].

Friedrich Gauss (1777-1855)was also investigating the influence of perturbations on the orbits of the planets. He used exactly the same formulation as presented in equation D.4 to define the problem. This approach is especially useful for some applications as the rate of change in the elements are expressed in terms of the disturbing forces. For this reason Gauss' approach is often called the ***force component approach***. Another advantage of his approach is that it can be used to describe both conservative and non-conservative perturbation forces. Gauss divided the force which cause the perturbing accelerations into three components. The three components of the force are F_r, F_s and F_w. F_r defines the components of the force along the position vector, $\vec{r}$, F_s is the component along the vector 90° from $\vec{r}$ in the velocity increasing direction and F_w is the component normal to the orbit plane. His solution to the problem in terms of the six classical elements is defined as

$$\begin{aligned}
\frac{da}{dt} &= \frac{2e\sin\nu}{nx}F_r + \frac{2ax}{nr}F_s \\
\frac{de}{dt} &= \frac{x\sin\nu}{na}F_r + \frac{x}{na^2 e}\left(\frac{a^2x^2}{r} - r\right)F_s \\
\frac{di}{dt} &= \frac{r\cos u}{na^2 x}F_w \\
\frac{d\Omega}{dt} &= \frac{r\sin u}{na^2 x\sin i}F_w \\
\frac{d\omega}{dt} &= -\frac{x\cos\nu}{nae}F_r + \frac{p}{eh}\left[\sin\nu\left(1+\frac{1}{1+e\cos\nu}\right)\right]F_s \\
&\quad -\frac{r\cos i\sin u}{na^2 x\sin i}F_w \\
\frac{dM}{dt} &= n - \frac{1}{na}\left(\frac{2r}{a} - \frac{x^2}{e}\cos\nu\right)F_r - \frac{x^2}{nae}\left(1+\frac{r}{ax^2}\right)\sin\nu F_s
\end{aligned} \tag{D.7}$$

where

ν = true anomaly
r = magnitude of $\vec{r}$
x = $\sqrt{1-e^2}$
u = $\nu + \omega$, argument of latitude
p = $a(1-e^2)$
h = $\sqrt{\mu p}$

Equation D.7 can be used to determine the influence of perturbations of the orbital elements by expressing the perturbing force in its three components, F_r, F_s and F_w, and substituting it into the equation. The derivations of these equations are supplied in the works of Battin [5] and Vallado [35].

Perturbative Forces Descriptions

The VOP techniques developed by Gauss and LaGrange can be used to describe the influence of perturbations on the orbital elements. LaGrange's solution to the problem requires the perturbing force to be expressed in terms of the disturbing function, which is the gradient of the potential function describing the force. Gauss' formulation requires the force to be expressed in terms of its three orthogonal components. Both these solutions require the perturbation to be described by means of an analytical expression. Accurate analytical expressions for describing the perturbative forces are very complex. The effect of the non-spherical Earth and atmospheric drag can be described with a series expansion and approximate values, respectively, but high-accuracy analytical expressions for solar radiation pressure and third-body effects are not very common. Analytical theories describing all the relevant perturbations to a high degree of accuracy do exist, but since they are not easy to use, it is often easier to revert to numerical techniques when high precision propagation is required. The accuracy of the analytical techniques are also reduced as only a limited amount of terms from the infinite series expansions of the forces can be included into the solutions. The following discussion will attempt to provide some of the more common descriptions of the perturbative forces for use in the VOP solutions of LaGrange and Gauss.

Central-Body analysis The gravitational force of the Earth is a conservative force that can be described very accurately with a potential function. LaGrange's planetary equations were developed for the description of a conservative disturbing force in terms of its potential function. The R-function used by him represents the deviation in the potential function from that of

a spherical Earth

$$R = U - U_{2-body} \tag{D.8}$$

where U is the potential function for the non-spherical Earth and $U_{2-body} = \mu/r$ is the potential function for a spherical Earth. The potential function, U, is a series expansion of the form

$$\begin{aligned} U &= \frac{\mu}{r}\left[1 - \sum_{n=2}^{\infty}\left(\frac{a_e}{r}\right)^n J_n P_n(\cos\phi)\right. \\ &\quad \left. + \sum_{n=2}^{\infty}\sum_{m=1}^{n} J_{nm}\left(\frac{a_e}{r}\right)^n P_{nm}(\cos\phi)\cos m(\lambda - \lambda_{nm})\right] \end{aligned} \tag{D.9}$$

where

J_{nm} = harmonic coefficients
= $\sqrt{C_{nm}^2 + S_{nm}^2}$
C_{nm}, S_{nm} = coefficients to be determined from observations
J_n = J_{n0} = the coefficient of the nth zonal gravitational harmonic
$P_n(\cos\phi)$ = the Legendre functions
ϕ = the geocentric co-latitude
λ = geodetic longitude
λ_{nm} = equilibrium longitude for J_{nm}
= $\tan^{-1}\left(\frac{S_{nm}^2/C_{nm}^2}{m}\right)$
a_e = mean equatorial radius of the Earth

Equation D.9 describes the mass distribution of the Earth in terms of zonal, sectorial and tesseral harmonics. The ***zonal harmonics*** are presented by the first line of equation D.9 and describes the mass distribution of the Earth as symmetrical about the polar axis. These harmonics represents the major deviation from a spherical Earth and is quite often considered as an adequate description of the Earth's gravitational field. It is denoted by the values $J_2 = 0.0010826269$, $J_3 = -0.0000025323$, $J_4 = -0.0000016204$, etc. It can be seen that J_2 is approximately 400 times larger than J_3 and for this reason it is often the only gravity harmonic taken into consideration in calculating the oblateness effect of the Earth. Since the contributions of the sectorial and tesseral harmonics are omissible compared to the zonal harmonics, they are generally not used in simple calculations. The ***sectorial*** and ***tesseral harmonics*** are described by the second line in equation D.9. The sectorial harmonics describe the mass distribution in terms of alternating "orange sliced" sectors of positive and negative mass contributions which align with the meridians of longitude of the Earth. The tesseral harmonics

divide the Earth into a checkerboard of squares in which each square has different mass properties.

The procedure that is usually followed when analytical theories are derived is to divide the expressions into secular, short periodic and long periodic variations. This is done by deriving separate expressions for the different effects which is then combined into a complete theory. Following the method of Kozai which is presented by Escobal [16], the secular variations in the elements from an oblate Earth will now be calculated.

From equations D.8 and D.9 the disturbing function is determined to the order of J_2 as

$$R = -\frac{3}{2}\frac{\mu}{r}J_2\left(\frac{a_e}{r}\right)^2\left(\sin^2(i)\sin^2(\omega+\nu)-\frac{1}{3}\right) \tag{D.10}$$

When the secular effects are required, all the periodic effects are ignored. The impact of this step on the disturbance function is that all terms which are coefficients of ν and ω are considered as periodic terms and may be ignored and the radial distance, r, of the satellite vary over each orbital revolution and need to be averaged. The average value of the radial distance is determined by integrating the expression for these values over one revolution of the mean anomaly. The result of this whole process is that an averaged disturbing function of the following form is found

$$R_{avg} = -\frac{3}{2}n^2a_e^2J_2\left(\frac{1}{(1-e^2)^{3/2}}\right)\left(\frac{\sin^2 i}{2}-\frac{1}{3}\right) \tag{D.11}$$

When this expression is substituted into the equation D.6, the following expressions are found

$$\bar{n} = \frac{dM}{dt} = \sqrt{\frac{\mu}{a_0^3}}\left[1+\frac{3}{2}\frac{J_2a_e^2}{p^2}\left(1-\frac{3}{2}\sin^2 i\right)(1-e^2)^{\frac{1}{2}}\right] \tag{D.12}$$

$$\frac{d\Omega}{dt} = -\frac{3}{2}\frac{J_2a_e^2}{p^2}\,\bar{n}\cos i \tag{D.13}$$

$$\frac{d\omega}{dt} = \frac{3}{2}\frac{J_2a_e^2}{p^2}\,\bar{n}\left(2-\frac{5}{2}\sin^2 i\right) \tag{D.14}$$

These equations represent the secular variations due to first order gravitational harmonics.

When the secular perturbations are required to a higher order of accuracy, the disturbing function, equation D.10, needs to be derived from equation D.9 with more of the J-terms included in the expression for R. This would

then lead to the higher order harmonics appearing in the expression for R_{avg} and consequently also in the expressions for the secular variations in the elements.

When the periodic terms is required in the expressions for the perturbations, the terms which are coefficients of ω and ν in equation D.10 should not be ignored. Referring to equation D.1 again, the terms in ω represent the long-periodics, the terms in ν represent the short-periodics and combination-terms of ν and ω represent mixed periodics.

Drag Analysis The accurate analytical description of the effects that atmospheric drag has on the orbit of a satellite is an almost impossible task. The following description will attempt to provide some insight into the process of deriving analytical expressions for drag-effects, but since it is an approximate process, high accuracy results can only be obtained via a numerical technique. The secular influence of drag on the classical elements will be considered.

The acceleration experienced by the satellite under conditions of atmospheric drag can be presented by the equation

$$\vec{a}_{drag} = -\frac{1}{2}\frac{c_D A}{m}\rho v_{rel}^2 \frac{\vec{v}_{rel}}{v_{rel}} \tag{D.15}$$

where

c_D	=	the dimensionless ***coefficient of drag*** which depends on the shape of the satellite—often designated a value of 2
A	=	the effective area of the satellite normal to the velocity vector
m	=	the mass of the satellite
ρ	=	atmospheric density
$\vec{v}_{rel}$	=	velocity vector of the satellite relative to the moving atmosphere
v_{rel}	=	magnitude of the velocity vector

For the analytical process, the atmospheric density can be approximated as an exponential decrease in density with an increase in height. The density can be calculated from

$$\rho = \rho_0 \exp\left(-\frac{h - h_0}{H}\right) \tag{D.16}$$

where ρ_0 is the atmospheric density at the perigee height, h_0, h is the altitude of the satellite and H is the density scale height of the atmosphere at perigee[5].

[5]Refer to Wertz [36] p.820 for a table of values for H and ρ_0. Jordaan [20] p.19 presents an example of the calculation.

The force that creates the acceleration in equation D.15 is a non-conservative force and for that reason Gauss' form of the VOP equations are used. The result obtained from the VOP equations present the variation of the classical elements as functions of time. The solution for a is presented by Vallado [35] as

$$\frac{da}{dt} = -\rho\frac{c_D A}{m}v^2\left(\frac{\sqrt{1+e^2+2e\cos(\nu)}}{n\sqrt{1-e^2}}\right) \tag{D.17}$$

and the solution for e is presented by Battin [5] as

$$\frac{de}{dt} = -2\rho\frac{c_D A}{m}\frac{pna}{r}\cos E\frac{\sqrt{1+e\cos E}}{\sqrt{1-e\cos E}} \tag{D.18}$$

As the secular variations of the elements are under consideration here, the expressions for the variations in the elements need to be written as a function of the eccentric or mean anomalies. Escobal [16] presents the secular variations in a, e and i as a function of the eccentric anomaly. These expressions are then integrated over one revolution of the eccentric anomaly that provides the variation in the orbital elements over one orbital revolution. Vallado [35] presents the variations in the elements due to atmospheric drag by using modified Bessel functions of the first kind. He also uses a more complex representation of the atmosphere where the influence of the rotation of the Earth on the atmosphere is taken into consideration. His representations consist of the following equations

$$\begin{aligned}\Delta a_{rev} &= -2\pi\delta a^2\rho_0\left[B_0 + 2eB_1 + \frac{3e^2}{4}(B_0+B_2)+\right.\\ &\qquad \left.\frac{e^3}{4}(3B_1+B_3)\right]\exp^{-c}\end{aligned} \tag{D.19}$$

$$\begin{aligned}\Delta e_{rev} &= -2\pi\delta a^2\rho_0\left[B_1 + \frac{e}{2}(B_0+B_2) - \frac{e^2}{8}(5B_1+B_3)-\right.\\ &\qquad \left.\frac{e^3}{16}(5B_0+4B_2-B_4)\right]\exp^{-c}\end{aligned} \tag{D.20}$$

$$\begin{aligned}\Delta i_{rev} &= -\frac{\pi a\omega_e\delta\rho_0}{2n\sqrt{Q}}\sin(i)\left[B_0 - 2eB_1 +\right.\\ &\qquad \left.(B_2-2eB_1)\cos(2\omega)\right]\exp^{-c}\end{aligned} \tag{D.21}$$

$$\Delta\Omega_{rev} = -\frac{\pi a \omega_e \delta \rho_0}{2n\sqrt{Q}}\left[B_2 - 2eB_1\right]\sin(2\omega)\exp^{-c} \tag{D.22}$$

$$\Delta\omega_{rev} = -\Delta\Omega_{rev}\cos(i) \tag{D.23}$$

where

$c = \frac{ae}{H}$

$\delta = \frac{QA\,c_D}{m}$

$Q = 1 - \frac{2\omega_e(1-e)^{3/2}}{n\sqrt{1+e}}\cos(i)$

$=$ factor which includes the rotation of the atmosphere $(0.9 \leq Q \geq 1.1)$

$\omega_e = 0.0000729211586$ rad/sec = angular rate of Earth

$B_s =$ modified Bessel functions of the first kind of order s, in all cases having the argument c and denoted with a B instead of the usual J to avoid confusion with the gravitational harmonics.

Escobal [16] presents a semianalytic approach to the derivation of the equivalent of equations D.19 to D.23. The significance of his approach is that it provides some insight into the use of these equations. Escobal interprets the change in the elements over one orbital revolution as the mean change in the classical elements for the orbit defined by a particular set of classical elements. Dividing this mean change by 2π provide a mean angular change in the elements. This mean angular change can be used to update the initial set of elements during an orbital revolution or at a particular instance in every revolution to get an updated classical element set with corrections for atmospheric drag. Although this method is not of very high accuracy, it gives an indication of the change in the orbit due to drag.

Third-Body Analysis The analytical description of the perturbations due to the gravitational forces of the Sun and the Moon are complex, due to the continual change in the orientation of the third bodies. Analytical expressions for these perturbations usually consist of lengthy series expressions which are difficult to analyse and implement. Vallado [35] provides a few analytical expressions for the perturbations due to the attraction of the Sun and the Moon, but he does not present the derivations. Chao [10] does present the

derivations of his formulations of the perturbations and it will be presented here to provide some insight into the problem.

Chao developed his theory for use in the design of a station-keeping strategy of the Global Positioning System satellites. These satellites with their 12 hour orbital periods experience considerable disturbances from the influence of the Sun and the Moon. Chao considered the orbits of the Sun and the Moon as circular orbits. His approach is based on the use of a single averaged disturbing function to determine the variations in the classical orbital elements.

He starts with the disturbing function due to third-body perturbations in the ECI coordinate system in the form

$$R_3 = \frac{\mu}{r_3}\left[\left(1+\left(\frac{r}{r_3}\right)^2 - \frac{2r}{r_3}\cos S\right)^{-\frac{1}{2}} - \frac{r\cos S}{r_3}\right] \tag{D.24}$$

where

r_3 = distance from the center of the Earth to the third body
r = distance from the center of the Earth to the satellite
S = angle between $\vec{r}$ and $\vec{r_3}$

For Sun-Moon perturbations it is found that $r/r_3 \ll 1$. Chao then presents equation D.24 in the simplified form

$$\begin{aligned} R_3 = {} & \frac{a^2 n_3^2}{2}\left(\frac{a_3}{r_3}\right)^2 \left\{\left[\frac{3}{2}\left(A^2+B^2\right)-1\right]\left(1+\frac{3e^2}{2}\right)\right. \\ & \left. +\frac{3}{2}\left(A^2-B^2\right)\frac{5e^2}{2}\right\} \end{aligned} \tag{D.25}$$

where

A = $\vec{P}\cdot\vec{u_3}$
B = $\vec{Q}\cdot\vec{u_3}$
$\vec{P}$,$\vec{Q}$ = two of the axis in the PQW coordinate system
$\vec{u_3}$ = unit position vector of the third body

Equation D.25 is substituted into the LaGrange planetary equations to obtain analytical expressions for the variations in the classical elements. The terms (A^2+B^2) and (A^2-B^2) are expanded into series-expressions. It is found that the major secular variations occurs in Ω and in ω. The simplified expressions for the secular variations are

$$\dot{\Omega}_{sec} = -\frac{3}{8}\frac{n_3^2}{n}\frac{(1+(3/2)e^2)}{\sqrt{1-e^2}}\cos i(3\cos^2 i_3 - 1) \tag{D.26}$$

$$\dot{\omega}_{sec} = \frac{3}{4}\frac{n_3^2}{n}\frac{(1-(3/2)\sin^2 i_3)}{\sqrt{1-e^2}}\left(2-\frac{5}{2}\sin^2 i+\frac{e^2}{2}\right) \tag{D.27}$$

where n and i are the mean motion and inclination, respectively, of the satellite, and n_3 and i_3 are the mean motion and inclination, respectively, of the third body. Equations D.26 and D.27 can be used exactly as presented for the perturbative effect due to the Sun, but for the Moon both equations need to be divided by the Earth-Moon mass ratio of 81.3.

Chao combined the secular and periodic effects of the third body attractions with the J_2 to J_4 terms for the oblate Earth to create an analytical general perturbation theory. He compared the results with the results of numerical integration and found it accurate for a period of approximately 800 days for low-eccentricity orbits.

Solar Radiation Pressure Analysis Vallado [35] and Chobotov [11] present an analytical technique, developed by G.E. Cook in 1962, to describe the variations in the orbital elements due to solar radiation pressure. The force on the satellite due to solar radiation pressure is described by the expression

$$F_{SR} = p_{SR} c_R A_\odot \tag{D.28}$$

where

p_{SR}	=	the solar pressure force per unit area
	=	$4.51 \times 10^{-6}\text{N.m}^{-2}$
c_R	=	the reflectivity of the satellite
A	=	area of the satellite exposed to the Sun

The ***reflectivity*** of the satellite varies between a value of 0.0 and 2.0 where a value of 0.0 indicates that the satellite is transparent to solar radiation, 1.0 indicates the absorption of all solar radiation and 2.0 indicates that the satellite acts like a mirror as it reflects all the solar radiation. The reflectivity is a parameter similar to the drag coefficient that is difficult to determine. It is usually only accurately determined through a process of differential correction[6].

The force in equation D.28 can be expressed in terms of its different components for substitution into equation D.7. The components F_r and F_s can be presented by

$$\begin{aligned} F_r &= F_{SR}\left\{\left[\cos^2\left(\frac{\epsilon}{2}\right)\cos(\omega+\Omega-\lambda_\odot)\right.\right. \\ &\quad \left.\left.+\sin^2\left(\frac{\epsilon}{2}\right)\cos(\omega+\Omega+\lambda_\odot)\right]\cos^2\left(\frac{i}{2}\right)\right. \\ &\quad \left.\left[\cos^2\left(\frac{\epsilon}{2}\right)\cos(\omega-\Omega+\lambda_\odot)\right.\right. \end{aligned}$$

[6]Refer to Vallado [35] or Escobal [16] for a discussion of differential correction.

$$+\sin^2\left(\frac{\epsilon}{2}\right)\cos(\omega-\Omega-\lambda_\odot)\Big]\sin^2\left(\frac{i}{2}\right)$$
$$+\frac{1}{2}[\cos(\omega-\lambda_\odot)-\cos(\omega+\lambda_\odot)]\sin(i)\sin(\epsilon)\Big\} \quad \text{(D.29)}$$

$$\begin{aligned} F_s &= -F_{SR}\Big\{\Big[\cos^2\left(\frac{\epsilon}{2}\right)\sin(\omega+\Omega-\lambda_\odot) \\ &\quad +\sin^2\left(\frac{\epsilon}{2}\right)\sin(\omega+\Omega+\lambda_\odot)\Big]\cos^2\left(\frac{i}{2}\right) \\ &\quad \Big[\cos^2\left(\frac{\epsilon}{2}\right)\sin(\omega-\Omega+\lambda_\odot) \\ &\quad +\sin^2\left(\frac{\epsilon}{2}\right)\sin(\omega-\Omega-\lambda_\odot)\Big]\sin^2\left(\frac{i}{2}\right) \\ &\quad -\frac{1}{2}[\sin(\omega-\lambda_\odot)-\sin(\omega+\lambda_\odot)]\sin(i)\sin(\epsilon)\Big\} \end{aligned} \quad \text{(D.30)}$$

In these two equations ϵ refer to the obliquity of the ecliptic and $\lambda_\odot$ is the ecliptic longitude of the Sun.

When equations D.29 and D.30 are substituted into equation D.7, it is found that the most significant effect is on the eccentricity and the perigee height, r_p. These variations are described by

$$\dot{a} = \frac{1}{\pi n a}\left[r_{ee\nu}F_s + a\{\cos(E_{ent})-\cos(E_{exit})\}F_r\right] \quad \text{(D.31)}$$

$$\begin{aligned} \dot{e} &= \frac{nF_r}{2\pi\mu}\left[3a^2\sqrt{1-e^2}\tau_{ee} - \frac{1}{2e}r_{ee\nu 2} + \frac{a}{2e}(1-4e^2)r_{ee\nu}\right] \\ &\quad -\frac{nF_r}{4\pi\mu}\Big[r_{ee2} + \frac{a(1-e^2)}{e^2}r_{ee} + \frac{1}{e}\Big\{r_{ent}^2\cos(\nu_{ent}) \\ &\quad -r_{exit}^2\cos(\nu_{exit})\Big\}\Big] \end{aligned} \quad \text{(D.32)}$$

$$\dot{r}_p = \frac{n}{2\pi}[(1-e)\dot{a} - a\dot{e}] \quad \text{(D.33)}$$

where

$$\tau_{ee} = \tan^{-1}\left(\frac{\sqrt{1-e^2}\tan\left(\frac{\nu_{ent}}{2}\right)}{1+e}\right) - \tan^{-1}\left(\frac{\sqrt{1-e^2}\tan\left(\frac{\nu_{exit}}{2}\right)}{1+e}\right)$$

$$r_{ee} = r_{ent} - r_{exit} \qquad r_{ee2} = r_{ent}^2 - r_{exit}^2$$

$$r_{ee\nu} = r_{ent}\sin(\nu_{ent}) - r_{exit}\sin(\nu_{exit})$$

$$r_{ee\nu 2} = r_{ent}^2\sin(\nu_{ent}) - r_{exit}^2\sin(\nu_{exit})$$

and ν_{ent} is the true anomaly when the satellite enters the shadow of the Earth and ν_{exit} is the true anomaly when the satellite exits the shadow of the Earth. When the satellite is in the sunlight for the duration of an entire orbit, $\nu_{ent} = \nu_{exit} + 360°$ and $r_{ent} = r_{exit}$ which lead to simplified expressions for the perturbations. Vallado [35] presents the equations for the variations in all the other classical elements.

D.2.2 Special Perturbations

In special perturbations, there are two basic methods used to solve the problem of the perturbed motion of the satellite. The two methods are Cowell's method and Encke's method. The two methods differ in their approach to the numerical integration of the perturbed equation of motion.

Cowell's Method

The approach of Phillip Herbert Cowell (1870-1949) was to formulate the perturbed equation of motion in the form presented in equation D.4. For this reason, this equation is known as Cowell's formulation. He reduced equation D.4 to a first order differential equation of the form

$$\begin{cases} \dot{\vec{r}} &= \vec{v} \\ \dot{\vec{v}} &= -\frac{\mu}{r^3}\vec{r} + \vec{a}_p \end{cases} \tag{D.34}$$

where $\vec{a}_p$ is the vector sum of all the perturbing accelerations to be included in the integration. Cowell's formulation of the problem does not require that the magnitude of $\vec{a}_p$ should be small, which makes it a very useful and general formulation of the problem.

Numerically calculated orbit predictions are found from the direct integration of equation D.34. The step size of the integration process should be chosen small enough to ensure that the truncation and round-off errors are smaller than the desired prediction accuracy. This is one of the disadvantages of Cowell's method in that, for high accuracy predictions, a small integration step size is required that increases the computer time required to make the predictions. The increased computational power of modern computers tends to nullify this disadvantage.

Encke's Method

The formulation to the perturbed motion problem presented by Johann Franz Encke (1791-1865) starts with an osculating or reference orbit. This orbit is

defined as the orbit at a particular instant in time when the influence of all the perturbative forces on the orbit is ignored. This reference orbit is defined as

$$\ddot{\vec{\rho}} = -\frac{\mu}{\rho^3}\vec{\rho} \tag{D.35}$$

where ρ denote the position vector in the reference orbit. The difference vector between the true orbit and the reference orbit is defined as

$$\delta\vec{\rho} = \vec{r} - \vec{\rho} \tag{D.36}$$

where $\vec{r}$ is the true position vector of the satellite in the perturbed orbit. The difference in motion between the two orbits are then defined as

$$\delta\ddot{\vec{r}} = \mu\left(\frac{\vec{\rho}}{\rho^3} - \frac{\vec{r}}{r^3}\right) - \vec{a}_p \tag{D.37}$$

The advantage of this formulation is that only the difference between the two orbits needs to be integrated. The value of $\delta\vec{r}$ is much smaller than that of $\vec{r}$ and it has a slow rate of change. Encke's method of orbit prediction is computationally more efficient compared to Cowell's method since the required numerical precision in calculations is reduced and larger integration step sizes can be used. The disadvantage of this method is that the magnitude of $\delta\vec{r}$ increases with time and the accuracy of the predictions will degrade with time. A new reference orbit then needs to be initialised through a process known as rectification. This adds some complexity to this method of prediction.

Disturbing Forces

In order to numerically integrate either Cowell's or Encke's formulation of the perturbed orbit, representations for each one of the perturbative accelerations are required. These representations can be analytical expressions such as those discussed in the section under general perturbations, or it may be tables of values. This section will provide an overview of the expressions for the perturbative accelerations required for numerical integration.

Central-Body Effect The perturbative acceleration created by the non-spherical Earth can be determined by taking the gradient of the potential defined in equation D.9 in spherical coordinates from

$$\vec{a} = \frac{\partial U}{\partial r}\left(\frac{\partial r}{\partial \vec{r}}\right)^T + \frac{\partial U}{\partial \phi}\left(\frac{\partial \phi}{\partial \vec{r}}\right)^T + \frac{\partial U}{\partial \lambda}\left(\frac{\partial \lambda}{\partial \vec{r}}\right)^T \tag{D.38}$$

It can be expressed in the ECI coordinate system as

$$a_I = \left\{ \frac{1}{r}\frac{\partial U}{\partial r} - \frac{r_K}{r^2\sqrt{r_I^2 + r_J^2}}\frac{\partial U}{\partial \phi} \right\} r_I - \left\{ \frac{1}{r_I^2 + r_J^2}\frac{\partial U}{\partial \lambda} \right\} r_J \tag{D.39}$$

$$a_J = \left\{ \frac{1}{r}\frac{\partial U}{\partial r} - \frac{r_K}{r^2\sqrt{r_I^2 + r_J^2}}\frac{\partial U}{\partial \phi} \right\} r_J + \left\{ \frac{1}{r_I^2 + r_J^2}\frac{\partial U}{\partial \lambda} \right\} r_I \tag{D.40}$$

$$a_K = \frac{1}{r}\frac{\partial U}{\partial r} r_K + \frac{\sqrt{r_I^2 + r_J^2}}{r^2}\frac{\partial U}{\partial \phi} \tag{D.41}$$

The accuracy of the modelled acceleration will depend on the number of gravitational harmonics modelled in equation D.9. For maximum accuracy all the available C_{nm} and S_{nm} coefficients should be used in the calculation of the gravitational potential. These coefficients are obtained from terrestrial based and satellite based observations and is defined in a gravitational model. Some of the models in use are the *Joint Gravitational Model* (JGM-2) which is of size 70×70, the *World Geodetic Survey* (WGS-84), a 41×41 model which is periodically updated and the 50×50 *Goddard Earth Model* (GEM).

Atmospheric Drag The acceleration of the satellite due to atmospheric drag is described by equation D.15. The important parameter that needs to be determined in this equation is the value of the atmospheric density. This parameter can be determined from a variety of available models of varying complexity. Vallado [35] discusses some of the atmospheric density models currently in use. One of the most commonly used models is the Jacchia-Roberts model, which is described in detail by Vallado. This model is very accurate, but very complex. The rule, which can be followed, is that, whenever the atmospheric density needs to be modelled, the lowest complexity model that provides a satisfactory accuracy should be used. The reason being that the complexity of the model and consequently the complexity of the calculations increase with increased accuracy. Du Toit [14] indicates the validity of this statement. He needed a limited complexity atmospheric model that included the major variations in atmospheric density. These included variations with change in altitude, the day-night variations and the influence of the solar flares. He used the exponential model provided by equation D.16 with some adjustments made to the calculation of the atmospheric density at perigee.

Third-Body Attractions Battin [5] provides an expression for the acceleration resulting from the gravitational attraction of a third body as

$$a_p = -\frac{\mu_3}{d^3}\left[\vec{r} + f(q)\vec{r}_3\right] \tag{D.42}$$

where d is the distance between the satellite and the third body, μ_3 is the gravitational parameter of the third body and $\vec{r}_3$ is the position vector of the third body in the ECI coordinate system. The value $f(q)$ is introduced into the expression to avoid numerical instability which may introduce errors into the calculations. It is defined as

$$f(q) = q\frac{3 + 3q + q^2}{1 + (1+q)^{3/2}} \tag{D.43}$$

with q defined as

$$q = \frac{\vec{r} \cdot (\vec{r} - 2\vec{r}_3)}{\vec{r}_3 \cdot \vec{r}_3} \tag{D.44}$$

The orbit of the third body needs to be modelled with a separate algorithm. The position of the third body is included in equation D.42 as the position vector $\vec{r}_3$. Methods for accurate modelling of the position of the Sun and the Moon are provided in Meeus [22].

Solar Radiation Pressure The perturbing force experienced by the satellite due to solar radiation pressure is presented by the expression in equation D.28. The assumption is sometimes made that the area of the satellite exposed to the Sun stays constant and that the reflectivity of the satellite does not change. Under these assumptions the perturbing acceleration can be expressed with the use of Newton's second law as

$$\vec{a}_{radiation} = -\frac{p_{SR} c_R A_\odot}{m}\frac{\vec{r}_{\odot sat}}{r_{\odot sat}} \tag{D.45}$$

where $\vec{r}_{\odot sat}$ is the vector from the satellite to the Sun.

Equation D.45 provides the expression for the acceleration experienced by the satellite due to solar radiation pressure, but almost all satellites experience periodic eclipses behind the Earth during which the expression for the acceleration is not valid. For this reason, a strategy is required to determine when the perturbing acceleration from solar radiation should be included in the propagation and when it should be ignored. Escobal [16] presents a solution to this problem with an expression which relates the angular separation angle of the satellite to the Sun as a function of the orbital elements. This solution indicates when the satellite is eclipsed and whether it enters or exits the shadow of the Earth.

Appendix E

IGRF Magnetic Field Modelling

The algorithm for the determination of the magnetic field vector at a particular location is provided by Wertz [36]. A summary of the most important expressions in the IGRF algorithm will be presented in this chapter.

The dominant characteristics of the magnetic field of the Earth, $\vec{B}$, can be modelled as the gradient of a scalar potential function, V, with

$$\vec{B} = -\nabla V \tag{E.1}$$

V can be represented by a series of spherical harmonics as

$$V(r, \theta, \phi) = a_e \sum_{n=1}^{k} \left(\frac{a_e}{r}\right)^{n+1} \sum_{m=0}^{n} (g_n^m \cos m\phi + h_n^m \sin m\phi) P_n^m(\theta) \tag{E.2}$$

where g_n^m and h_n^m are the Gaussian IGRF coefficients[1], $a_e = 6378.135$ km is the mean equatorial radius of the Earth, $P_n^m(\theta)$ are the Schmidt normalised Legendre functions and r, θ and ϕ are the geocentric distance, coelevation and longitude, respectively.

The computational time for the algorithm can be significantly reduced when the Legendre functions are calculated recursively. To do this, the Schmidt normalised Legendre functions, P_n^m, are converted to Gauss normalised functions, $P^{n,m}$, through the relationship

$$P_n^m = S_{n,m} P^{n,m} \tag{E.3}$$

where

$$S_{n,m} = \left[\frac{(2 - \delta_m^0)(n-m)!}{(n+m)!}\right]^{1/2} \frac{(2n-1)!!}{(n-m)!} \tag{E.4}$$

[1]These coefficients can be obtained via the Internet from *ftp://nssdc.gsfc.nasa.gov/models/geomagnetic/igrf/*.

with $\delta_j^i = 1$ if $i = j$ and 0 otherwise.

Using the $S_{n,m}$ functions with the Gaussian coefficients is computationally more efficient and in order to take advantage of this property, the Gaussian coefficients should be defined as

$$\begin{aligned} g^{n,m} &= S_{n,m} g_n^m \\ h^{n,m} &= S_{n,m} h_n^m \end{aligned} \tag{E.5}$$

The advantage of the $S_{n,m}$ functions is that it must only be determined once during a simulation. The functions can be computed recursively from

$$\begin{aligned} S_{0,0} &= 1 \\ S_{n,0} &= S_{n-1,0}\left[\frac{2n-1}{n}\right] \qquad n \geq 1 \\ S_{n,m} &= S_{n,m-1}\sqrt{\frac{(n-m+1)(\delta_m^1+1)}{n+m}} \qquad m \geq 1 \end{aligned} \tag{E.6}$$

In a similar way the $P^{n,m}$ coefficients can be determined from

$$\begin{aligned} P^{0,0} &= 1 \\ P^{n,n} &= \sin\theta P^{n-1,n-1} \\ P^{n,m} &= \cos\theta P^{n-1,m} - K^{n,m} P^{n-2,m} \end{aligned} \tag{E.7}$$

where

$$\begin{aligned} K^{n,m} &= 0 \qquad n = 1 \\ K^{n,m} &= \frac{(n-1)^2 - m^2}{(2n-1)(2n-3)} \qquad n > 1 \end{aligned} \tag{E.8}$$

From equation E.1 it is seen that the gradient must be determined which requires the partial derivatives of $P^{n,m}$. The recursive expressions for the partial derivatives are

$$\begin{aligned} \frac{\partial P^{0,0}}{\partial\theta} &= 0 \\ \frac{\partial P^{n,n}}{\partial\theta} &= (\sin\theta)\frac{\partial P^{n-1,n-1}}{\partial\theta} + (\cos\theta)P^{n-1,n-1} \qquad n \geq 1 \\ \frac{\partial P^{n,m}}{\partial\theta} &= (\cos\theta)\frac{\partial P^{n-1,m}}{\partial\theta} - (\sin\theta)P^{n-1,m} - K^{n,m}\frac{\partial P^{n-2,m}}{\partial\theta} \end{aligned} \tag{E.9}$$

The value of $\sin m\phi$ and $\cos m\phi$ can be determined from a recursion relation as

$$\begin{aligned} \cos m\phi &= \cos((m-1)\phi)\cos\phi - \sin((m-1)\phi)\sin\phi \\ \sin m\phi &= \sin((m-1)\phi)\cos\phi + \cos((m-1)\phi)\sin\phi \end{aligned} \tag{E.10}$$

From these expressions the field, $\vec{B}$, can be calculated as

$$\begin{aligned}
B_r &= -\frac{\partial V}{\partial r} \\
&= \sum_{n=1}^{k} \left(\frac{a_e}{r}\right)^{n+2} (n+1) \sum_{m=0}^{n} (g^{n,m} \cos m\phi + h^{n,m} \sin m\phi) P^{n,m}(\theta) \\
B_\theta &= \frac{-1}{r} \frac{\partial V}{\partial \theta} \\
&= -\sum_{n=1}^{k} \left(\frac{a_e}{r}\right)^{n+2} \sum_{m=0}^{n} (g^{n,m} \cos m\phi + h^{n,m} \sin m\phi) \frac{\partial P^{n,m}(\theta)}{\partial \theta} \\
B_\phi &= \frac{-1}{r \sin\theta} \frac{\partial V}{\partial \phi} \\
&= \frac{-1}{\sin\theta} \sum_{n=1}^{k} \left(\frac{a_e}{r}\right)^{n+2} \sum_{m=0}^{n} m(-g^{n,m} \sin m\phi + h^{n,m} \cos m\phi) P^{n,m}(\theta)
\end{aligned} \tag{E.11}$$

where B_r is the radial component (outward positive), B_θ is the coelevation component (south positive) and B_ϕ is the azimuth component (east positive). These components can be converted to the ECEF coordinate system through the transformation

$$\begin{aligned}
B_x &= (B_r \cos\delta + B_\theta \sin\delta) \cos\alpha - B_\phi \sin\alpha \\
B_y &= (B_r \cos\delta + B_\theta \sin\delta) \sin\alpha + B_\phi \cos\alpha \\
B_x &= (B_r \sin\delta - B_\theta \cos\delta)
\end{aligned} \tag{E.12}$$

where $\delta = 90° - \theta$ is the geocentric latitude.

Appendix F

The SGP4 model

This chapter is a shortened version of the "Spacetrack Report no.3" [103]. Only the SGP4 propagation model is included without the FORTRAN code.

The NORAD mean element sets can be used for prediction with SGP4. All symbols not defined below are defined in the list of symbols at the end of this chapter.

F.1 The SGP4 model

The original mean motion (n_o'') and semimajor axis (a_o'') are first determined from the input elements by the equations

$$a_1 = \left(\frac{k_e}{n_o}\right)^{\frac{2}{3}}$$

$$\delta_1 = \frac{3}{2}\frac{k_2}{{a_1}^2}\frac{(3\cos^2 i_o - 1)}{(1-{e_o}^2)^{\frac{3}{2}}}$$

$$a_o = a_1\left(1 - \frac{1}{3}\delta_1 - {\delta_1}^2 - \frac{134}{81}{\delta_1}^3\right)$$

$$\delta_o = \frac{3}{2}\frac{k_2}{{a_o}^2}\frac{(3\cos^2 i_o - 1)}{(1-{e_o}^2)^{\frac{3}{2}}}$$

$$n_o'' = \frac{n_o}{1+\delta_o}$$

$$a_o'' = \frac{a_o}{1-\delta_o}.$$

For perigee between 98 kilometers and 156 kilometers, the value of the constant s used in SGP4 is changed to

$$s^* = a_o''(1 - e_o) - s + a_E$$

For perigee below 98 kilometers, the value of s is changed to

$$s^* = 20/\text{XKMPER} + a_E.$$

If the value of s is changed, then the value of $(q_o - s)^4$ must be replaced by

$$(q_o - s^*)^4 = \left[[(q_o - s)^4]^{\frac{1}{4}} + s - s^*\right]^4.$$

Then calculate the constants (using the appropriate values of s and $(q_o - s)^4$)

$$\theta = \cos i_o$$

$$\xi = \frac{1}{a_o'' - s}$$

$$\beta_o = (1 - {e_o}^2)^{\frac{1}{2}}$$

$$\eta = a_o'' e_o \xi$$

$$C_2 = (q_o - s)^4 \xi^4 n_o''(1 - \eta^2)^{-\frac{7}{2}} \left[a_o'' \left(1 + \frac{3}{2}\eta^2 + 4e_o\eta + e_o\eta^3\right) + \frac{3}{2}\frac{k_2\xi}{(1 - \eta^2)}\left(-\frac{1}{2} + \frac{3}{2}\theta^2\right)(8 + 24\eta^2 + 3\eta^4)\right]$$

$$C_1 = B^* C_2$$

$$C_3 = \frac{(q_o - s)^4 \xi^5 A_{3,0} n_o'' a_E \sin i_o}{k_2 e_o}$$

$$C_4 = 2n_o''(q_o - s)^4 \xi^4 a_o'' {\beta_o}^2 (1 - \eta^2)^{-\frac{7}{2}} \left(\left[2\eta(1 + e_o\eta) + \frac{1}{2}e_o + \frac{1}{2}\eta^3\right] - \frac{2k_2\xi}{a_o''(1 - \eta^2)} \times \left[3(1 - 3\theta^2)\left(1 + \frac{3}{2}\eta^2 - 2e_o\eta - \frac{1}{2}e_o\eta^3\right) + \frac{3}{4}(1 - \theta^2)(2\eta^2 - e_o\eta - e_o\eta^3)\cos 2\omega_o\right]\right)$$

$$C_5 = 2(q_o - s)^4 \xi^4 a_o'' {\beta_o}^2 (1 - \eta^2)^{-\frac{7}{2}} \left[1 + \frac{11}{4}\eta(\eta + e_o) + e_o\eta^3\right]$$

$$D_2 = 4a_o''\xi {C_1}^2$$

$$D_3 = \frac{4}{3}a_o''\xi^2(17a_o'' + s){C_1}^3$$

$$D_4 = \frac{2}{3}a_o''\xi^3(221a_o'' + 31s){C_1}^4.$$

The secular effects of atmospheric drag and gravitation are included through the equations

$$M_{DF} = M_o + \left[1 + \frac{3k_2(-1+3\theta^2)}{2a_o''^2\beta_o{}^3} + \frac{3{k_2}^2(13-78\theta^2+137\theta^4)}{16a_o''^4\beta_o{}^7}\right] n_o''(t-t_o)$$

$$\omega_{DF} = \omega_o + \left[-\frac{3k_2(1-5\theta^2)}{2a_o''^2\beta_o{}^4} + \frac{3{k_2}^2(7-114\theta^2+395\theta^4)}{16a_o''^4\beta_o{}^8} + \frac{5k_4(3-36\theta^2+49\theta^4)}{4a_o''^4\beta_o{}^8}\right] n_o''(t-t_o)$$

$$\Omega_{DF} = \Omega_o + \left[-\frac{3k_2\theta}{a_o''^2\beta_o{}^4} + \frac{3{k_2}^2(4\theta-19\theta^3)}{2a_o''^4\beta_o{}^8} + \frac{5k_4\theta(3-7\theta^2)}{2a_o''^4\beta_o{}^8}\right] n_o''(t-t_o)$$

$$\delta\omega = B^*C_3(\cos\omega_o)(t-t_o)$$

$$\delta M = -\frac{2}{3}(q_o-s)^4B^*\xi^4\frac{a_E}{e_o\eta}[(1+\eta\cos M_{DF})^3 - (1+\eta\cos M_o)^3]$$

$$M_p = M_{DF} + \delta\omega + \delta M$$

$$\omega = \omega_{DF} - \delta\omega - \delta M$$

$$\Omega = \Omega_{DF} - \frac{21}{2}\frac{n_o''k_2\theta}{a_o''^2\beta_o{}^2}C_1(t-t_o)^2$$

$$e = e_o - B^*C_4(t-t_o) - B^*C_5(\sin M_p - \sin M_o)$$

$$a = a_o''[1 - C_1(t-t_o) - D_2(t-t_o)^2 - D_3(t-t_o)^3 - D_4(t-t_o)^4]^2$$

$$\mathbb{L} = M_p + \omega + \Omega + n_o''\left[\frac{3}{2}C_1(t-t_o)^2 + (D_2+2{C_1}^2)(t-t_o)^3 + \frac{1}{4}(3D_3+12C_1D_2+10{C_1}^3)(t-t_o)^4 + \frac{1}{5}(3D_4+12C_1D_3+6{D_2}^2+30{C_1}^2D_2+15{C_1}^4)(t-t_o)^5\right]$$

$$\beta = \sqrt{(1-e^2)}$$

$$n = k_e \Big/ a^{\frac{3}{2}}$$

where $(t - t_o)$ is time since epoch. It should be noted that when epoch perigee height is less than 220 kilometers, the equations for a and $\mathbb{L}$ are truncated after the C_1 term, and the terms involving C_5, $\delta\omega$, and δM are dropped.

Add the long-period periodic terms

$$a_{xN} = e\cos\omega$$

$$\mathbb{L}_L = \frac{A_{3,0}\sin i_o}{8k_2 a\beta^2}(e\cos\omega)\left(\frac{3+5\theta}{1+\theta}\right)$$

$$a_{yNL} = \frac{A_{3,0}\sin i_o}{4k_2 a\beta^2}$$

$$\mathbb{L}_T = \mathbb{L} + \mathbb{L}_L$$

$$a_{yN} = e\sin\omega + a_{yNL}.$$

Solve Kepler's equation for $(E+\omega)$ by defining

$$U = \mathbb{L}_T - \Omega$$

and using the iteration equation

$$(E+\omega)_{i+1} = (E+\omega)_i + \Delta(E+\omega)_i$$

with

$$\Delta(E+\omega)_i = \frac{U - a_{yN}\cos(E+\omega)_i + a_{xN}\sin(E+\omega)_i - (E+\omega)_i}{-a_{yN}\sin(E+\omega)_i - a_{xN}\cos(E+\omega)_i + 1}$$

and

$$(E+\omega)_1 = U.$$

The following equations are used to calculate preliminary quantities needed for short-period periodics.

$$e\cos E = a_{xN}\cos(E+\omega) + a_{yN}\sin(E+\omega)$$

$$e\sin E = a_{xN}\sin(E+\omega) - a_{yN}\cos(E+\omega)$$

$$e_L = ({a_{xN}}^2 + {a_{yN}}^2)^{\frac{1}{2}}$$

$$p_L = a(1 - {e_L}^2)$$

$$r = a(1 - e\cos E)$$

$$\dot{r} = k_e \frac{\sqrt{a}}{r} e \sin E$$

$$r\dot{f} = k_e \frac{\sqrt{p_L}}{r}$$

$$\cos u = \frac{a}{r}\left[\cos(E+\omega) - a_{xN} + \frac{a_{yN}(e\sin E)}{1+\sqrt{1-{e_L}^2}}\right]$$

$$\sin u = \frac{a}{r}\left[\sin(E+\omega) - a_{yN} - \frac{a_{xN}(e\sin E)}{1+\sqrt{1-{e_L}^2}}\right]$$

$$u = \tan^{-1}\left(\frac{\sin u}{\cos u}\right)$$

$$\Delta r = \frac{k_2}{2p_L}(1-\theta^2)\cos 2u$$

$$\Delta u = -\frac{k_2}{4{p_L}^2}(7\theta^2 - 1)\sin 2u$$

$$\Delta\Omega = \frac{3k_2\theta}{2{p_L}^2}\sin 2u$$

$$\Delta i = \frac{3k_2\theta}{2{p_L}^2}\sin i_o \cos 2u$$

$$\Delta\dot{r} = -\frac{k_2 n}{p_L}(1-\theta^2)\sin 2u$$

$$\Delta r\dot{f} = \frac{k_2 n}{p_L}\left[(1-\theta^2)\cos 2u - \frac{3}{2}(1-3\theta^2)\right]$$

The short-period periodics are added to give the osculating quantities

$$r_k = r\left[1 - \frac{3}{2}k_2\frac{\sqrt{1-{e_L}^2}}{{p_L}^2}(3\theta^2-1)\right] + \Delta r$$

$$u_k = u + \Delta u$$

$$\Omega_k = \Omega + \Delta\Omega$$

$$i_k = i_o + \Delta i$$

$$\dot{r}_k = \dot{r} + \Delta\dot{r}$$

$$r\dot{f}_k = r\dot{f} + \Delta r\dot{f}.$$

Then unit orientation vectors are calculated by

$$\mathbf{U} = \mathbf{M}\sin u_k + \mathbf{N}\cos u_k$$

$$\mathbf{V} = \mathbf{M}\cos u_k - \mathbf{N}\sin u_k$$

where

$$\mathbf{M} = \left\{ \begin{array}{l} M_x = -\sin\Omega_k \cos i_k \\ M_y = \cos\Omega_k \cos i_k \\ M_z = \sin i_k \end{array} \right\}$$

$$\mathbf{N} = \left\{ \begin{array}{l} N_x = \cos\Omega_k \\ N_y = \sin\Omega_k \\ N_z = 0 \end{array} \right\}.$$

Then position and velocity are given by

$$\mathbf{r} = r_k\mathbf{U}$$

and

$$\dot{\mathbf{r}} = \dot{r}_k\mathbf{U} + (r\dot{f})_k\mathbf{V}.$$

F.2 Users guide, constants and symbols

The values of the physical and mathematical constants used in the program are given below.

Variable name	Definition	Value
CK2	$\frac{1}{2}J_2{a_E}^2$	5.413080E-4
CK4	$-\frac{3}{8}J_4{a_E}^4$	.62098875E-6
E6A	10^{-6}	1.0 E-6
QOMS2T	$(q_o - s)^4\ (\mathrm{er})^4$	1.88027916E-9

S	s (er)	1.01222928
TOTHRD	$2/3$	.66666667
XJ3	J_3	-.253881E-5
XKE	$k_e \left(\frac{\text{er}}{\text{min}}\right)^{\frac{3}{2}}$	.743669161E-1
XKMPER	kilometers/Earth radii	6378.135
XMNPDA	time units/day	1440.0
AE	distance units/Earth radii	1.0
DE2RA	radians/degree	.174532925E-1
PI	π	3.14159265
PIO2	$\pi/2$	1.57079633
TWOPI	2π	6.2831853
X3PIO2	$3\pi/2$	4.71238898

where er = Earth radii. Following is a list of symbols commonly used in this mathematical model.

n_o = the SGP type "mean" mean motion at epoch

e_o = the "mean" eccentricity at epoch

i_o = the "mean" inclination at epoch

M_o = the "mean" mean anomaly at epoch

ω_o = the "mean" argument of perigee at epoch

Ω_o = the "mean" longitude of ascending node at epoch

$\dot{n}_o$ = the time rate of change of "mean" mean motion at epoch

$\ddot{n}_o$ = the second time rate of change of "mean" mean motion at epoch

B^* = the SGP4 type drag coefficient

$k_e = \sqrt{GM}$ where G is Newton's universal gravitational constant and M is the mass of the Earth

a_E = the equatorial radius of the Earth

J_2 = the second gravitational zonal harmonic of the Earth

J_3 = the third gravitational zonal harmonic of the Earth

J_4 = the fourth gravitational zonal harmonic of the Earth

$(t - t_o)$ = time since epoch

$$k_2 = \frac{1}{2} J_2 {a_E}^2$$

$$k_4 = -\frac{3}{8} J_4 {a_E}^4$$

$$A_{3,0} = -J_3 {a_E}^3$$

q_o = parameter for the SGP4 density function

s = parameter for the SGP4 density function

$B = \frac{1}{2} C_D \frac{A}{m}$, the ballistic coefficient where C_D is a dimensionless drag coefficient and A is the average cross-sectional area of the satellite of mass m

Appendix G

Orbital elements in practice

This chapter describes the classical, the 2-line elements, and the methods that are available for presenting the different sets of data. There exists a lot of confusion concerning the use of these orbital elements, the propagational accuracy which can be obtained and the propagational technique which should be used with each set of data. This chapter will attempt to remove some of the confusion summarizing the most important factors that have to be taken into account. Refer to appendix C for a detailed definition of the elements. The Celestrak website [104] and Vallado [35] have some useful hints on the correct use of orbital elements.

G.1 Orbital element formats

There is no uniform representation of the classical orbital elements. These elements and the 2-line elements are both based on the same principle defined by Kepler in that both represent the position of the satellite in the orbit. Depending on the source from which these elements are obtained, it is called ***two-body***, ***mean*** or ***osculating Keplerian elements***. The three versions are often considered equivalent, but there are some subtle differences in the way they are obtained and the way that they are used.

Two-body elements usually refer to those that are derived from and used with two-body equations of motion. When these elements are used to determine the position of a satellite, the propagation algorithm should be based on pure two-body orbital equations. It can be expected that this method will not deliver very high precision information about the position of the satellite. The initial position may be close to the true value of the satellite position, but because no perturbations are modelled, it will become inaccurate in a very short time. TS Kelso [104] made the following obser-

vation: *"When we combine all the effects in the SGP4 model and compare it to a simple two-body propagator, we find a position error of 150 km after only six hours and almost 400 km by the end of the day."*. This error of 400 km after one day consists predominantly of an in-line error and results in an angular displacement of 34° from the true position of the satellite after only one day for a satellite at a height of 600 km. An UHF yagi antenna has a typical -3dB beamwidth of 29° and a VHF yagi antenna has a typical -3dB beamwidth of 39°. This means that the signal coming from any source which is on a line of more than 19.5° from the centreline of the VHF yagi, will be attenuated by -3dB. The general case is that, the higher the frequency, the narrower the beamwidth of the antenna. It is clear that this error is unacceptable for the purpose of tracking a satellite with an antenna since the antenna can be a parabolic dish with a beamwidth of only a few degrees[1]. The two-body elements can be considered unsuitable for practical use.

Osculating elements are the instantaneous elements for a satellite under the influence of perturbations. It represents the true position of the satellite at a specific time. Osculating elements are usually provided along with the state vector since both represent the instantaneous position of the satellite, only in different formats. Satellite owners sometimes provide these sets of data together and launch companies provide the estimated initial condition of the satellite in this format. The osculating elements should be propagated with a propagation algorithm that requires osculating data as its input. Numerical integrators that are used to generate high-precision ephemeris data usually require osculating elements since algorithms with high precision output require high precision elements as inputs. A common use of the osculating elements is with NASA's Space Shuttle. It usually is the only near real-time ephemeris data available for the Space Shuttle directly after an orbit changing thruster burn. It usually takes a few hours (sometimes even days) for the new NORAD elements to be released and by that time the orbital elements could already be outdated due to subsequent thruster firings by the Shuttle. By using the osculating elements, an ephemeris of the highest possible accuracy can be generated.

Mean elements result from averaging the effect of perturbations over a specified interval of time. The averaging process results in an elimination of the short periodic effects of perturbations from the elsets. Where the osculating elements present the true position of the satellite, the mean elements have to be adjusted before the true position of the satellite can be found. This has to be done in an appropriate propagator. The U.S. Space

[1]For the SUNSAT groundstation a 4.5 m diameter parabolic dish with a S-band feed was used which resulted in a beamwidth of 1°.

Command (NORAD) provides mean elements in the 2-line element format. Elements generated by NORAD need to be propagated by means of one of the propagators in the SGP4 family of propagators (SGP, SGP4, SDP4) in order to reconstruct the short periodic variations which are needed for accurate predictions. Mean elements are updated every 5 to 7 days by NORAD. Because TLE's for almost any satellite can be obtained from the Internet so easily, it is the most commonly used representation of the satellite orbital state used today.

The confusion with the use of orbital elements often arises because the osculating elements describe the perturbed problem and are defined for a specific moment in time, but they are often used with simplified (a two-body propagator or one requiring mean elements as input) propagation schemes. Using the elements in this way nullifies the assumptions inherent to the osculating elements. It is not impossible to use it in this way, but it will result in predictions of poor accuracy. Mean elements are used in the same erroneous way. It is often used in a numerical integrator or simplified perturbation algorithm that requires osculating elements as input, resulting again in poor prediction accuracy. Another reason for poor prediction accuracy is that the wrong time-system is used or that the calculation of the rotational position of the Earth (sidereal time) is inaccurate. No matter how accurate the propagation technique, inaccurate calculation of sidereal time will always result in an inaccurate ephemeris[2].

G.2 Explanation of Two-line Elements

This section explains the format of the two-line elements (TLE's) that are commonly available on the Internet. The explanation presented here is a modified version of the explanation available on the website of the Radio Amateur Satellite Corporation (AMSAT)[3].

An example of a TLE-file is presented in table G.1. The file consists of

```
SUNSAT
1 25636U 99008C   99261.70472423  .00000371  00000-0  10947-3 0  1025
2 25636  96.4775 166.8279 0152478 320.7002  38.3229 14.40946227 29841
```

Table G.1: An examples of a TLE-file for SUNSAT.

[2]Refer to appendix B.2.3 for a discussion of the methods used to determine the sidereal time.

[3]http://www.amsat.org

three lines of data. The first line contains the satellite's name with the next two lines containing the actual orbital data in the format required for use with the SGP and SGP4 propagation algorithms. The different variables are presented in fixed positions within the file. The position of spaces within the file is significant. The last digit on each line is a modulo-10 check digit, which is used by most software to verify the validity of the data. The following key will explain the positions of the element-values within the TLE-file.

1. ***Line 1*** consists only of the name of the satellite. There is no checksum on this line.

2. ***Line 2*** is the first line of data. The format of the first line of data is presented in table G.2. The checksum is computed as follows:

Column	Description
01-01	Line Number of Element Data
03-07	Satellite Number
10-11	International Designator (Last two digits of launch year)
12-14	International Designator (Launch number of the year)
15-17	International Designator (Piece of launch)
19-20	Epoch Year (Last two digits of year)
21-32	Epoch (Day number and fractional portion of the day)
34-43	First Time Derivative of the Mean Motion divided by 2, or Ballistic Coefficient (depending on ephemeris type)
45-52	Second Time Derivative of Mean Motion divided by 6, (Blank if N/A).
54-61	B* drag term if SGP4 theory was used. Otherwise, radiation pressure coefficient.
63-63	Ephemeris type
65-68	Element number
69-69	Check Sum (Modulo 10)

Table G.2: The format of the second line of data in the two-line element file.

   (a) Start with zero.

   (b) For each digit in the line, add the value of the digit.

   (c) For each minus sign, add 1.

   (d) For each plus sign, add 2 (or maybe 0, depending on who created the element set and when)

   (e) For each letter, blank, or period, don't add anything.

(f) Take the last decimal digit of the result (that is, take the result modulo 10) as the check digit.

All other columns are blank or fixed. Note that the International Designator fields are usually blank, as issued in the NASA Prediction Bulletins.

3. ***Line 3*** is the second line of data. The format of this line of data is presented in table G.3. The same checksum algorithm is used as for the second line of data.

Column	Description
01-01	Line Number of Element Data
03-07	Satellite Number
09-16	Inclination (Degrees)
18-25	Right Ascension of the Ascending Node (Degrees)
27-33	Eccentricity (decimal point assumed)
35-42	Argument of Perigee (Degrees)
44-51	Mean Anomaly (Degrees)
53-63	Mean Motion (Revolutions per day)
64-68	Revolution number at epoch (Revolutions)
69-69	Check Sum (Modulo 10)

Table G.3: The format of the third line of data in the two-line element file.

G.3 Initial conditions of Orbital Elements

One of the most frequently asked questions related to orbital elements concerns the initial accuracy of the elements. To discuss the accuracy of the initial conditions, the method used to generate the initial conditions should be explained.

The initial conditions describing the updated orbital state of a satellite is determined through a process known as ***differential correction***. The process is described in Vallado [35] and Escobal [16] and consists of a least-squares approximation of the updated initial orbital state of the satellite by using current state vectors or element sets and measurements of the position of the satellite.

Measurements are made with a variety of sensor networks which include among others the Space Surveillance Network (SSN) of the US Department of Defence, the Russian Space Surveillance System (RSSS), the Deep Space

Network (DSN) managed by the Jet Propulsion Laboratory and the Satellite Laser Ranging (SLR) sites managed by NASA. These sites are spread all over the world and measure the satellite's position with a combination of radar, optical and laser sensors. The position of the satellite is usually presented in terms of the topocentric horizon coordinate system.

In order to calculate initial conditions for a particular epoch, measurements are combined with predictions. The orbital state of the satellite for the exact instant at which a measurement was made is determined by using the most recent orbital state description for the satellite in combination with a suitable propagation algorithm. The measurements contain errors due to errors in the sensors and for this reason, it cannot be considered as an exact description of the position of the satellite. The errors in the measurements can be described in terms of the statistical properties of the sensors. The difference between a group of measurements and the relevant predictions is determined and by considering the statistical error characteristics of the sensor systems, an updated initial position for the satellite at a new epoch is determined from a least squares approximation.

Two factors influence the accuracy of the initial conditions: the accuracy of and confidence in the measurements and the accuracy of the propagation algorithm. Higher accuracy measurements can be obtained by using better sensors and the confidence in the accuracy of the least squares approximation can be increased by increasing the number on observations used in the approximation. However, the most important limitation on the accuracy of the initial conditions is the accuracy of the propagation algorithm used to predict the position of the satellite. When the TLE-files are generated by NORAD, the SGP4 propagation algorithm is used to predict the position of the satellite. As the accuracy of this algorithm for a single step calculation is limited to approximately 1 km[4], it will result in the accuracy of the updated TLE's also being no better than 1 km, irrespective of the fact that measurements of higher accuracy was used in generating the updated TLE. In order to obtain high accuracy initial conditions for use in a propagational algorithm, a high accuracy propagation algorithm need to be combined with high accuracy measurements when the initial conditions are generated. When a high precision numerical propagator is combined with SLR or GPS measurements initial condition accuracies of a few metres are obtainable. Due to the influence that the propagator has on the accuracy of the initial conditions, these conditions are usually generated for use along with the particular propagator with which it was generated.

Data form the tracking network used by NORAD to generate the TLE-

[4]Refer to the work of Knowles [21] which was reinterpreted by Vallado [35].

files is not generally available to the public for generating orbital elements. The best substitute for the measurements made by the various tracking networks are GPS measurements made onboard a satellite. These measurements have a general accuracy of 50 m or better depending on the accuracy of the receiver, which can be improved by applying various correction techniques. According to Dawson [101] state vectors obtained from GPS measurements can be used as initial conditions for numerical propagation algorithms. It is preferable that the measurements should be used in a differential correction process to generate initial conditions for a particular propagator, but it can be used with reasonable success as initial conditions in any high accuracy numerical propagator.